JPL PUBLICATION 80-30

High Voltage Spark Carbon Fiber Detection System

Lien C. Yang

April 15, 1980

National Aeronautics and
Space Administration

Jet Propulsion Laboratory
California Institute of Technology
Pasadena, California

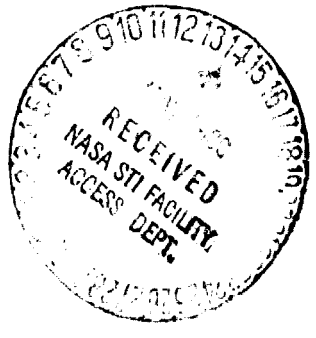

JPL PUBLICATION 80-30

High Voltage Spark Carbon Fiber Detection System

Lien C. Yang

April 15, 1980

National Aeronautics and
Space Administration

Jet Propulsion Laboratory
California Institute of Technology
Pasadena, California

The research described in this publication was carried out by the Jet Propulsion Laboratory, California Institute of Technology, under NASA Contract No. NAS7-100.

FOREWORD

The work described in this report was performed by personnel of the Physico-Chemical Systems Group, Chemical and Biological Processes Section, Energy and Control Division. Dr. L. C. Yang was the Principal Investigator, Dr. K. Ramohalli was the Task Manager. The pulse integrator circuit was designed by Mr. W. Wuest. The hardware fabrication and calibration were performed by Messrs. H. Burris and T. Vo. The data reduction program was written by Ms. C. Glazer.

For reviewing the report and for their helpful comments, the author thanks Mr. W. D. Dowler, Group Supervisor; Dr. G. Varsi, Section Manager and Dr. V. L. Bell of Langley Research Center, the technical monitor of the project.

ABSTRACT

This report summarizes the development by JPL of an efficient method of detecting carbon fibers released from a fire of carbon fiber composite material. The project was part of NASA's "Carbon Fiber Risk Analysis" program, which was initiated to study the risk of such electrically conductive fibers being released in a fire or aircraft crash situation, thereby posing a threat to electronic and electrical equipment.

In order to determine the density and length of carbon fibers released from such composites, a detection system is needed. The high voltage spark detection system reported here was developed by JPL for the NASA Langley Research Center between August 1978 and December 1979. It uses the ability of a carbon fiber to initiate spark discharge across a high voltage biased grid, to achieve accurate counting and sizing of fibers. The design of the system was optimized, and prototype hardware was proven satisfactory in laboratory and field tests.

TABLE OF CONTENTS

LIST OF FIGURES

LIST OF FIGURES (continued)

LIST OF TABLES

I. BACKGROUND

Graphite or carbon fiber in an epoxy matrix provides a composite material having a high strength and stiffness relative to weight. It has potential widespread use in aerospace applications. In fact, certain commercial and military aircraft already carry a significant amount of the material in various components. However, since the fibers are light in weight and electrically conductive, they pose a potential hazard in the event they should be released from the composite during an aircraft crash or fire situation. Currently, NASA is carrying out a "Carbon Fiber Risk Analysis" program to evaluate this potential problem (References 1 and 2). The detailed study covers every aspect of the problem related to the use of carbon composites in aircraft, such as the release of fiber in the aircraft crash or fire, fiber length distribution, fiber fragment migration, economic and environmental impacts on industry and population, dust filter design, and the effects of fiber fragments on electrical equipment, instrumentation, facilities and household appliances.

In this NASA task, a large number of experiments and field tests are being conducted to establish the technical basis for mathematical analyses. Carbon fiber composites are combusted, and the number of fibers as a function of fiber length are then determined. During this study, various types of fiber detection techniques and instruments have been developed for use in the tests. These include the sticky tape technique and prototype high voltage fiber detection system, developed by JPL for NASA LaRC under this project between August 1978 and December 1979.

Independently NASA is also studying methods to alleviate or eliminate the fiber emission problems from the combusting fiber composite. Approaches used include coating the fiber with an electrically insulating layer, using epoxy which forms a strong char residue during combustion to physically retain the fiber from being released, and adding catalysts to the composites to achieve fiber gasification during the fire. For all these experiments a fiber detection system is needed to determine the quantitative reduction in fiber emission. The high voltage fiber detection system has been used successfully in the fiber gasification study conducted at JPL.

The NASA studies, which include fiber detection, have been successful. The emphasis was on aircraft-related problems. In the simulated fire situation, the fiber fragments emitted by the composite and subsequently transferred into the atmosphere ranged in length mainly (about 90% or more) between 1 mm and 4 mm (Reference 3). The instruments for monitoring these fibers were developed for optimized performance in this fiber length region. The fiber density dealt with in these studies was relatively low due to very limited amounts of carbon fiber composites that were tested and the large distance between the fiber release source and the sensing device.

The following is a brief discussion of the instruments and techniques used or explored in the NASA "Carbon Fiber Risk Analysis" program. The instruments fall into the two categories of active and passive methods. The instruments are inserted into an air stream which carries the carbon fiber fragments from the source of fiber, i.e., a burning carbon fiber composite. The active instruments can provide a live signal to indicate the relevant information on the fiber concentration and length distribution, while the passive instruments can collect the fibers for post-test examination and analysis. The active methods are:

1. Brass-Ball Technique

This technique was developed by the U.S. Army at Aberdeen Proving Ground (Reference 4). It consists of a 3.8 cm (1.5 in) diameter brass ball supported by a plastic insulated rod-electrode. The ball is charged by a high voltage power supply to about 1 to 2 kV through a high-impedance current limiting resistor, and it is connected in parallel to a small capacitor. The ball thus attracts the fiber fragments, in a flow stream. Upon contact with the fiber, the capacitance of the ball is changed, thereby introducing electrical signals. Analysis has shown that the amplitude of this signal is correlatable to the fiber length. The disadvantages of the system are:

a) The signal is weak, in the millivolts region; therefore amplification by sophisticated electronics is needed. The equipment required for such amplification and signal processing limits portability for field tests.

b) The system is influenced by strong electrical noises of unknown origin, thereby making difficult the detection of the short fiber fragments with lengths below 2 mm.

c) The fiber capture efficiency of the device is low, and it may be dependent upon the flow velocity of the air.

d) The system is sensitive to moisture and soot.

These problems make the system relatively inconvenient for field tests and for many laboratories.

2. Low Voltage Grid System

This approach was explored at JPL in the early stages of the fiber gasification development program. It was soon abandoned due to a variety of problems. The system used parallel brass-rod grids supported in an insulation frame. The adjacent rods were biased by low voltage DC up to 15 volts. When fiber was collected in the grid, it drew electrical current, thereby producing an electrical signal. The serious problems were:

a) Loss of sensitivity due to fiber accumulation on the grid.

b) Multiple irregular signals produced when a single fiber made multiple contacts with the grid.

c) Low count efficiency due to: 1) fibers passing through grid, and 2) the variable high value of contact resistances which existed between the fiber and brass-rod electrodes.

The attractive features of the system were its simplicity and the safety of operation because of the low bias voltage used.

3. Continuous Optical Counter

This instrument is similar to a commercial aerosol optical counter. A light source such as a LED or laser beam is incident on a photodiode device. When the air flow carrying fiber fragments is passing between them, the shadow of the fiber generates an electrical signal. The major advantage of the system is its

high counting rate capability. It has several serious problems when applied to fiber monitoring.

a) It cannot differentiate fiber from the soot in the flame or dust particles in the air.

b) The signal response (shape) as well as sensitivity is very dependent on the flow rate and optical design.

c) Fiber length is not easily determined.

4. LADAR

This system detects the back scattering of a laser beam by the fibers (or any other particulates), and is in principle similar to a RADAR. The sensitivity attainable with the system probably limits its application to a dense cloud of fibers. Even in that case, the noise generated by the soot also poses a serious problem.

5. Microwave

This technique is being pioneered by TRW Systems, Inc., under the sponsorship of NASA and USAF, and currently technical details are not available. It is believed to be based upon a common microwave approach, and the system presumably uses a microwave waveguide. The fibers flowing in the air across the waveguide will attenuate the transmission and induce reflections of the electromagnetic waves propagating in the guide. By monitoring these parameters, gross fiber concentration information could be obtained. Thus, the technique cannot measure the length of individual fibers, and the sensitivity is questionable because the cross-section of a microwave waveguide cannot be made arbitrarily small.

A brief discussion of two relevant passive fiber detection techniques follows.

6. Sticky Tape

This is a convenient and economical means of collecting fiber fragments and storing fiber information. It is worthy of mention because so far it is the most used technique in a field test. Needless to say, the readout of the fiber under an optical microscope is a very tedious procedure and therefore limits its effectiveness. Two automated readout techniques, both being investigated at JPL, may bring a solution to this problem.

The first one uses photographic film and a microdensitometer to digitize the fiber image and subsequently process it by a digital computer system (Reference 5). The second technique for counting the fibers collected on the sticky tape, which to date is a very promising one, uses a set of high voltage plate electrodes (similar to the high voltage grid technique). Under a proper high voltage bias, the device generates sparks as guided by the fibers collected on the tape when the tape is in contact with the electrodes. The spark destroys the fiber and generates an electrical signal. In this way, high counting rate of the fibers previously collected on the tape can be accomplished. So far, there is no reliable calibration data for the tape. The accurate interpretation of the

sticky tape data, just as for any other fiber detection instrument, is dependent on a variety of parameters such as air flow rate, angle of coincidence, shape of the tape, temperature, soot interference, etc. Recently, preliminary tests at JPL have shown the capture efficiency of the tape to be quite poor. The efficiency ranged between 5% and 10% for a nominal wind speed of 0.5 to 2.0 m/s.

7) Filter Technique

In the NASA field tests, bridal veil screens of different mesh were used in a variety of geometrical configurations to collect fibers. This is a most effective way to collect fiber clusters. For a single fiber fragment the fiber capture efficiency is uncertain.

The system to be discussed in this report, in the active category, uses a high voltage grid to detect carbon fibers.

II. PRINCIPLE OF OPERATION

Carbon fibers released from the fire of carbon fiber composites may be coated with epoxy resin residues. In most cases, unprocessed raw carbon fibers are also precoated. Therefore there is considerable difficulty in establishing electrical contact between a fiber and an electrode. Careful tests have shown that, in the most cases, a carbon fiber laid carefully across a pair of electrodes shows no electrical conductivity if the bias voltage between the electrodes is less than 400 V. Beyond 400-500 V of bias voltage, arcing starts to occur at the contact points so that there is electrical conduction through the fiber. Therefore, the reliability of a grid carbon fiber counting system is higher when using a high voltage bias than when using a low voltage bias.

Because of the high resistance of the fiber ($\sim$3000 Ω/cm), under a moderate high voltage bias (0.5 kV to 2.0 kV), a carbon fiber draws very small current between a pair of grid electrodes. It can be heated red hot, but rapid burnout does not readily occur. Thus, most problems associated with a low voltage biased grid fiber detector remain under high bias voltage. That is, the decrease of sensitivity as fibers accumulated on the grid, and the creation of multiple irregular signals as a single fiber is bouncing around the electrodes of the grid. To quickly burn out a fiber by electrical heating takes considerable electrical power and may be impractical.

Our concept was to achieve individual fiber counting by using a pulse discharge technique which is schematically shown in Figure 1. The electrical energy is stored in a small capacitor C. The high voltage leads of the capacitor are directly connected to the grid wherein alternate electrodes of the grid are biased positive and negative. Upon conductivity being established by a carbon fiber, a discharge phenomenon occurs in a typical manner of an RLC circuit. The inductance L comes from the self-inductance of the grid lead wires. It can be minimized by shortening the lead wires but it cannot be completely eliminated. The value of the inductance L with about 7.6 cm (3 in) long lead wires was about 0.5 μh.

A typical discharge current waveform is shown in the Figure 2. By using this approach, a number of advantages are apparent:

1) The signals for fiber counts are prominent and reproducible.

2) The short duration of the signal, 0.5 to 1.0 μs, is favorable for high counting rate operation. In fact, this rate is mainly limited by the recharging time of the capacitor C.

3) The contact resistance problem is eliminated by the high voltage.

4) The grid is self-cleaning, i.e., fibers do not accumulate on the grid. Therefore the problem of decrease in sensitivity due to more than one fiber across the grid electrodes is eliminated. Also, since the fiber does not stay long on the grid, repetitive irregular arc signals produced by a single fiber are avoided.

5) Strong evidence indicates that the use of a high voltage bias increases the fiber counting efficiency. The fiber fragments, being conductors, polarize under an electrical field and thus are attracted to the grid.

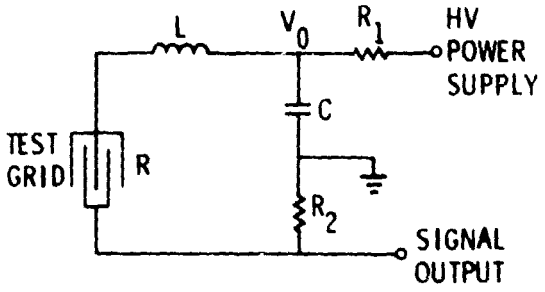

$R^2 > \frac{4L}{C}$ EXPONENTIAL

$R^2 = \frac{4L}{C}$ CRITICAL DAMPED

$R^2 < \frac{4L}{C}$ OSCILLATORY

R_1 = CURRENT LIMITING RESISTOR

$\simeq$ 1 kΩ

R_2 = CURRENT SHUNT

$\simeq$ 0.005 TO 0.1 Ω

C $\simeq$ 0.05 μF

L = CIRCUIT INDUCTANCE

$\simeq$ 0.5 μH

R = SPARK RESISTANCE

$\simeq$ 0.5-10 Ω

NOTE: R IS VOLTAGE DEPENDENT

Fig. 1. Discharge Circuit Schematic Diagram

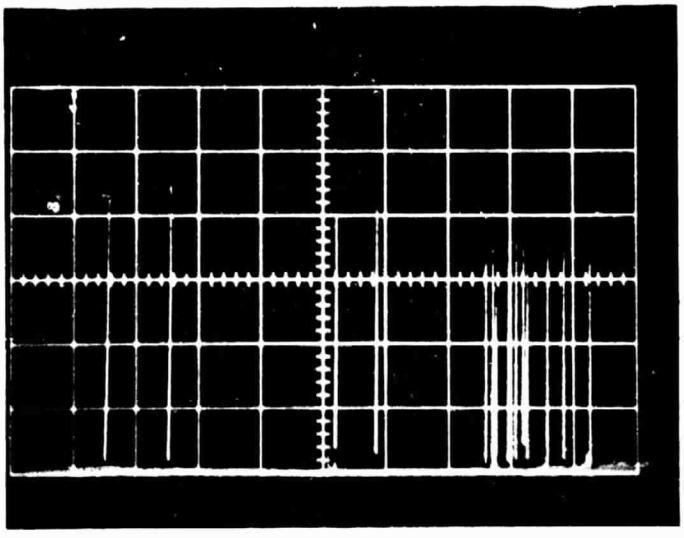

2 V/DIV

5 s/DIV

V_0 = 1 kV

GRID SPACING ≈ 4 mm

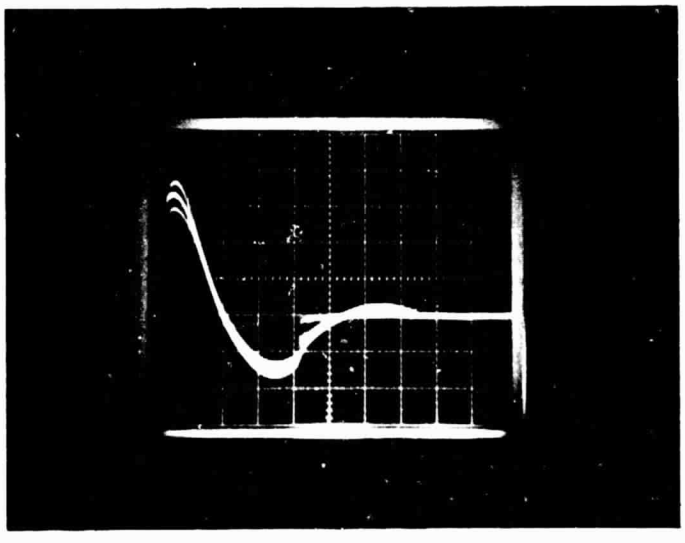

1 V/DIV

0.2 μs/DIV

V_0 = 1 kV

GRID SPACING ≈ 7.5 mm

Fig. 2. Typical Discharge Current Waveform as Recorded by an Oscilloscope

Under a moderately high voltage, the electrical field is strong enough to overcome the air flow pattern. It aligns the fiber perpendicular to the axes of the electrodes (grid) and the plane of the grid. Therefore the probability of fiber contact is high, and is efficient to generate the spark count. In the absence of the electrical field, the fiber fragments presumably will align with the stream lines of the air flow which is parallel to the axis of the grid plane. One can envision, in this case, that it is easy for fibers to flow through the grid without contacting the grid electrodes.

III. GENERAL DESCRIPTIONS AND SPECIFICATIONS

The JPL high voltage (H.V.) spark carbon fiber detection system was developed to monitor carbon fiber fragments in the length range of 1 to 5 mm. It consists of the following sub-assemblies.

1) Five independent grid-windbox assemblies (Figure 3) each of which contains:

   a) A grid made of a number of equally spaced, parallel copper blade electrodes secured in a frame made from electrically insulated material. The electrodes are biased by a high voltage circuit.

   b) A pre-screen (a stainless-steel screen with square meshes), to prevent fiber clusters from short-circuiting the grid-bias circuitry (Figure 4).

   c) An AC voltage-driven fan.

   d) A windbox, which works in conjunction with the fan to sample the air.

   e) High voltage discharge circuit (H.V. Pulser, Figure 5), to store electrical energy and provide the high voltage bias for the grid. It sends out a prominent pulse signal, which is subsequently counted when the spark is initiated by a fiber in contact with the grid.

2) Five independent pulse integrator electronic packages (Figures 6, 7 and 8). These provide the pulse-shaping function for the input spark signal and integrate these pulses so that a DC voltage output is provided which corresponds to the total number of fiber counts; this signal is generated for recording purposes on a strip chart recorder.

The following lists the general specifications for the system.

1) Fiber length detection range: 1-2 mm, 2-3 mm, 3-4 mm, 4-5 mm, 5-10 mm.

2) Counting rate = $I/CV = 6.6 \times 10^3 \frac{I}{V}$

   where I = H.V. power supply current in mA
   V = H.V. power supply voltage in volts
   C = Capacitance of the discharge capacitor in Farads
   = 0.14 μF

For safety of operation, a low current H.V. power supply should be used for most tests which have a low fiber-counting rate. A dry battery pack made of Eveready No. 497 batteries was designed and supplied for the prototype tests (Figure 9). It is suitable for use in most carbon fiber tests.

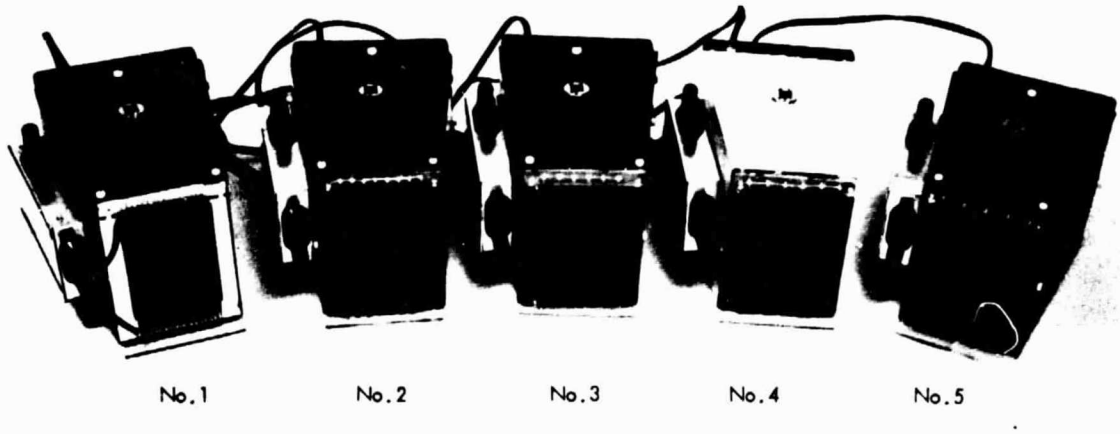

Fig. 3. Full View of 5 Independent Channels of Grid-Windbox Assemblies

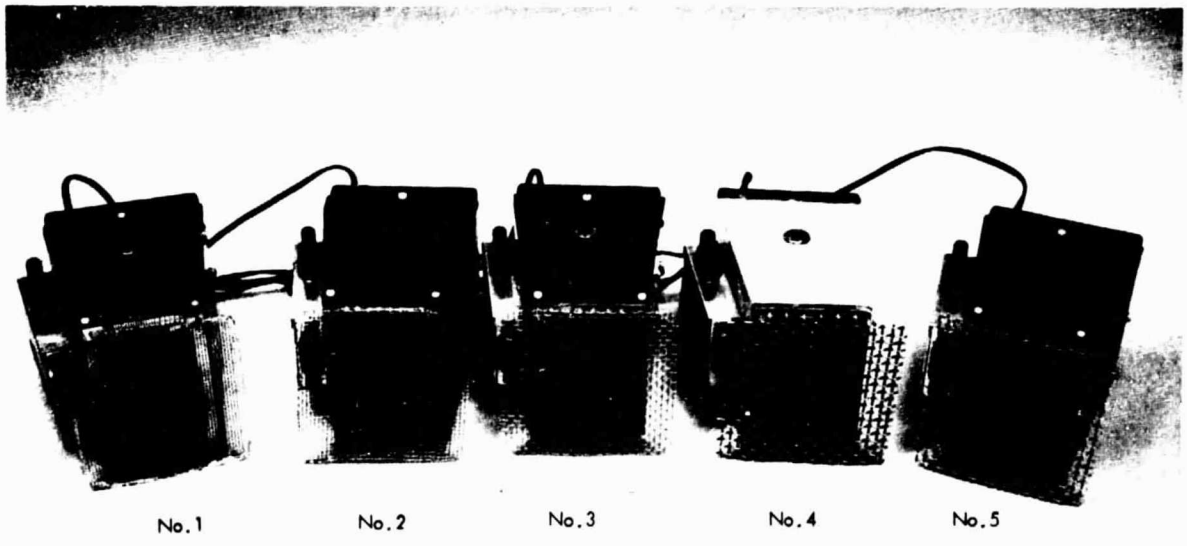

Fig. 4. Grid-Windbox Assemblies Equipped with Prescreens

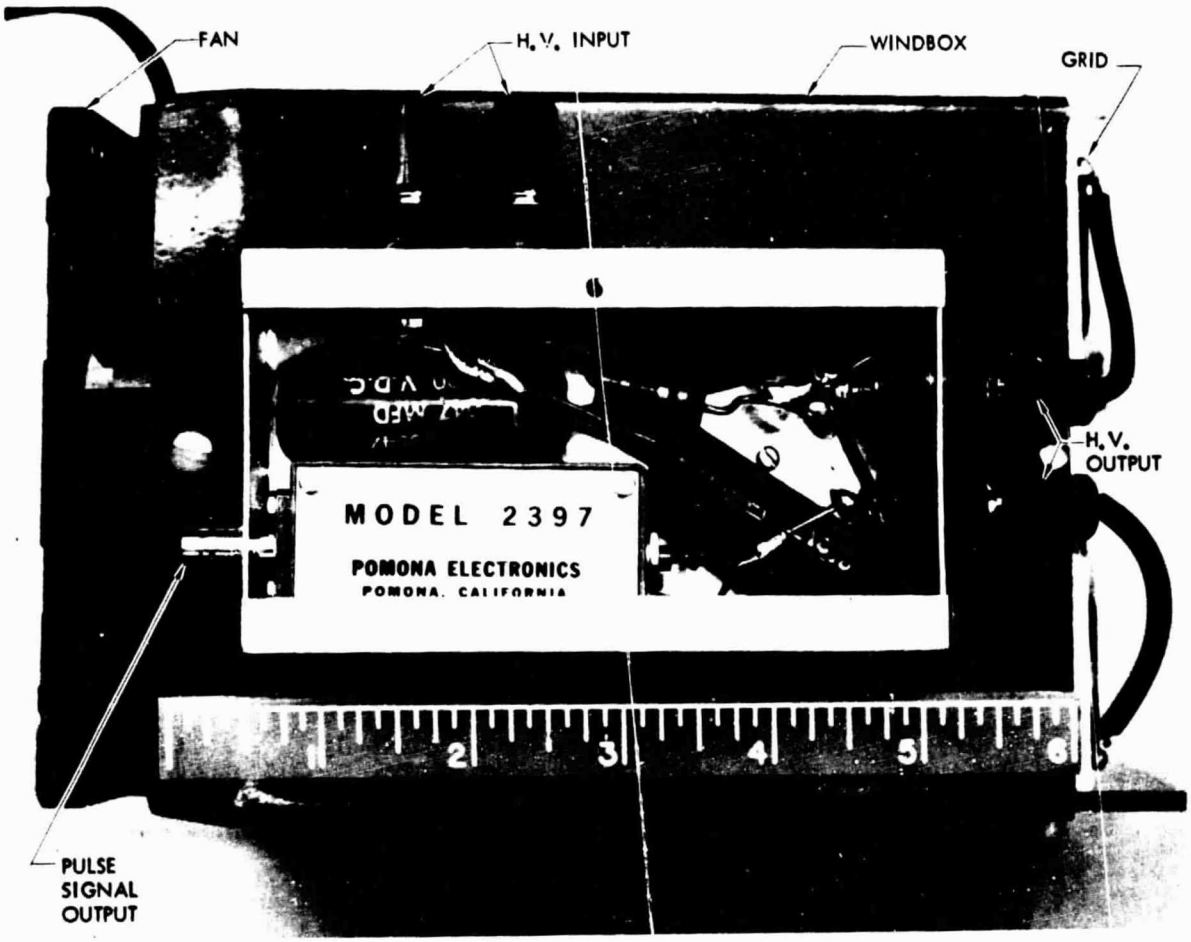

Fig. 5. Construction of the H.V. Discharge Circuit

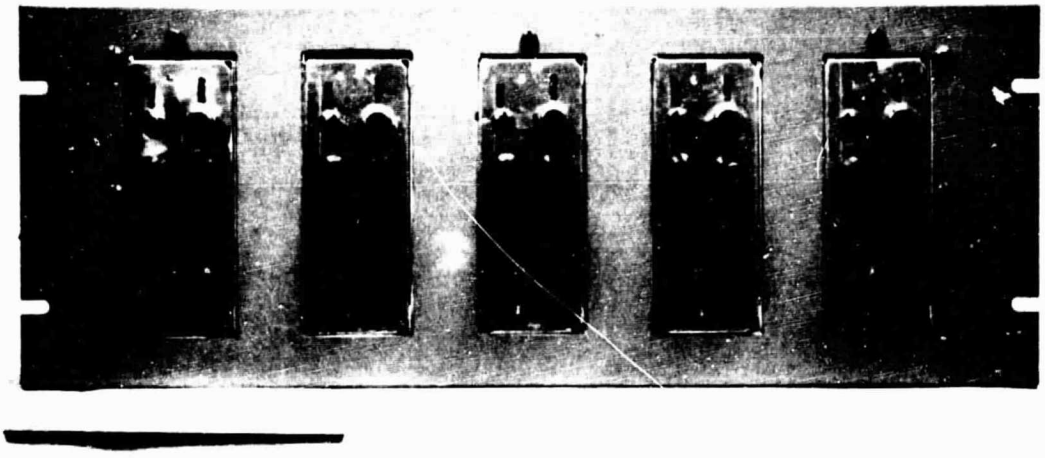

Fig. 6. Front View of 5 Independent Channels of Pulse Integrators, mounted on an Instrumentation Panel

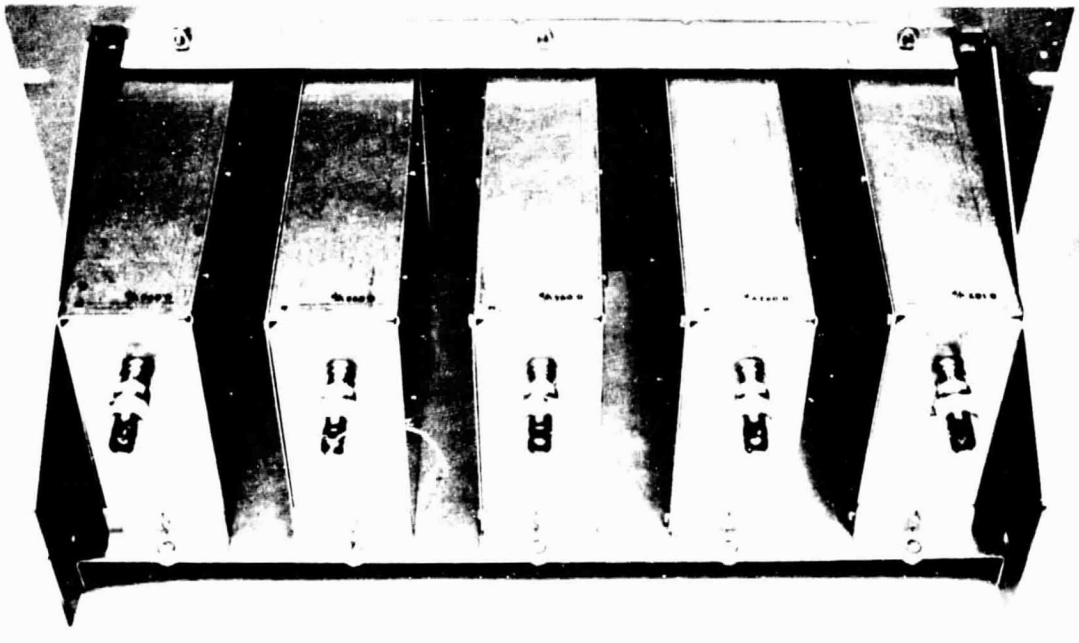

Fig. 7. Back View of the Pulse Integrators

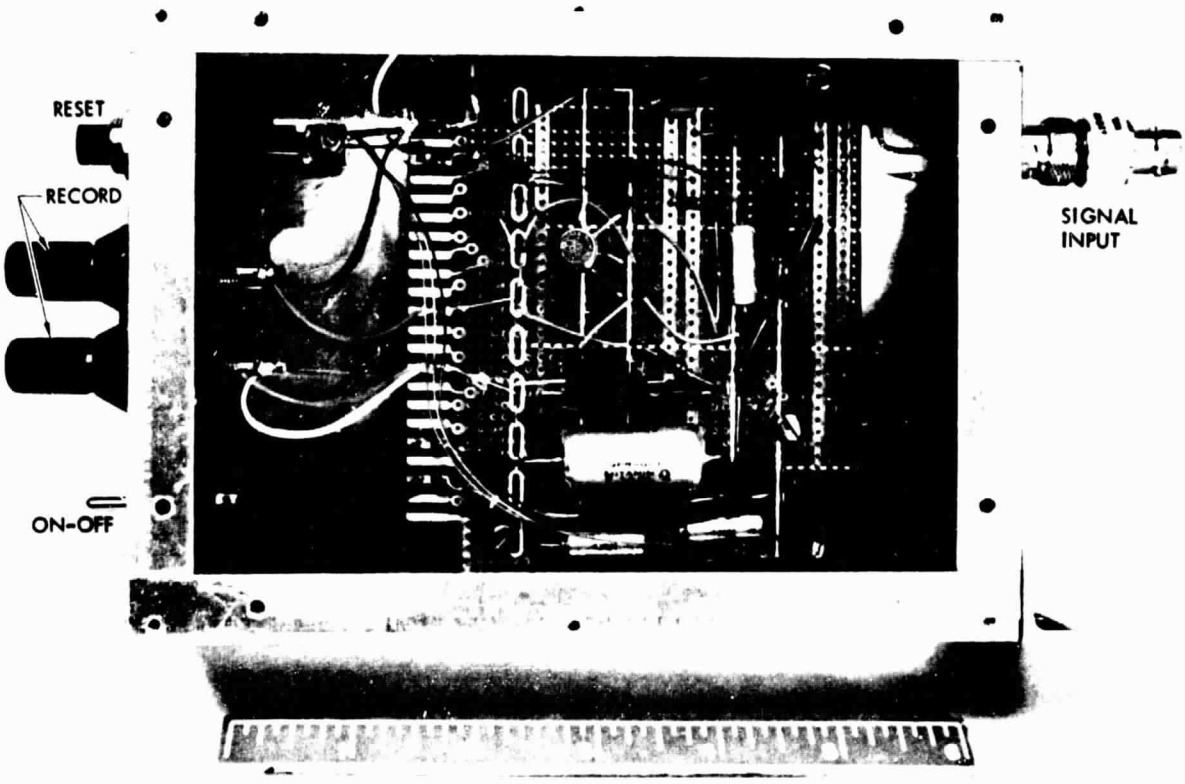

Fig. 8. Layout of Components of Pulse Integrator

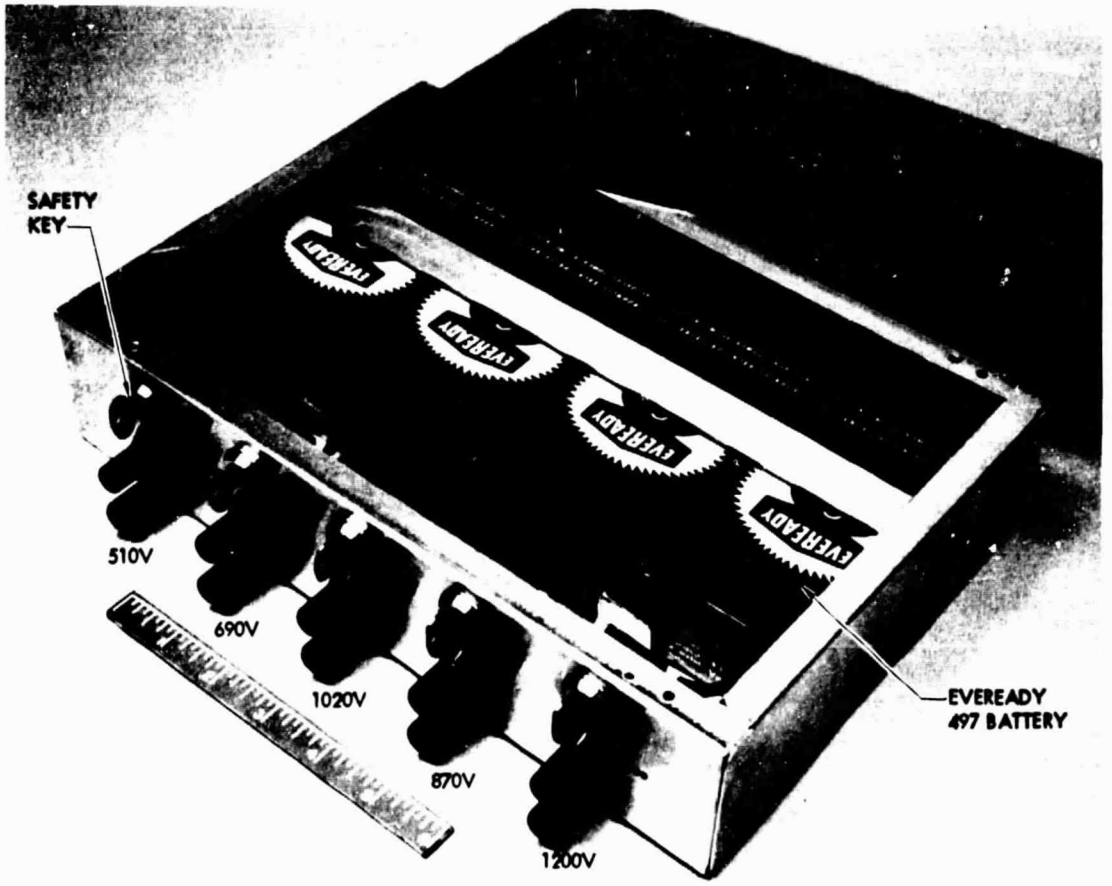

Fig. 9. Construction of the 5-Channel-Output H.V. Battery-pack

3) H.V. pulse discharge circuitry (Figure 5)

Capacitor bank = 0.14 μF
Current limiting resistor = 1 W 1 KΩ
Signal output amplitude ≅ -5 V
Signal output duration = ∿0.5 μs

4) Nominal operation AC voltage for fans = 50 V rms

5) Pulse integrator

DC input = 40 V
Signal input = -5 V nominal
10 ns to 5 μs rise time
Signal output = 0 to -10 V, automatically reset at -10 V
Sensitivity = ∿10 pulse/volt

6) Mechanical

Grid-windbox assembly = 10.7 x 12.1 x 17.0 cm
1.3 kg
Pulse integrator = 5.1 x 12.7 x 17.8 cm
0.39 kg

7) Other relevant physical parameters (see Table 1)

TABLE 1. Relevant Physical and Operational Parameters

CHANNEL NO.	1	2	3	4	5
Grid gap, mm	1.19	2.38	3.58	4.77	5.97
Bias Voltage, Volts	510	690	870	1020	1200
Threshold Fiber Length, mm	1.0	2.0	3.0	4.0	5.0
Prescreen Mesh Size, mm	1.50	2.44	3.43	4.69	5.46
A, Total Aperture x $10^{-3} m^2$	4.80	4.80	5.00	5.56	5.36
V, Wind Speed at 50 V Variac, m/s	1.40	1.52	1.78	1.98	2.41
Color Code, Windbox	Brown	Red	Orange	Yellow	Green

8) Input, output and control elements of the system:

GRID-WINDBOX

H.V. INPUT: banana posts
red: + black: -
Connect directly to H.V. power supply for charging of the 0.14 μF capacitor bank.

H.V. OUTPUT: banana posts
red: + black: -
Connect to the grid for H.V. bias.

PULSE SIGNAL:

Output: BNC terminal for 50 Ω impedance BNC cable (RG58C), connect to the Signal Input BNC terminal on the Pulse Integrator

Wind Monitor

Port (Figure 10): on top of the windbox for insertion of air flow probe such as the Hastings-Raydist Model AB-27.

PULSE INTEGRATOR

SIGNAL INPUT: receptacle BNC terminal for receiving the PULSE SIGNAL OUTPUT from the H.V. pulser circuit. It is equipped with a 50 Ω terminal load for a better noise rejection.

Power Supply

Input: banana posts, input for 40 VDC
red: + black: -

ON-OFF: miniature toggle switch to control the application of the 40 VDC to the electronics.

RESET: momentary push-button switch to achieve zero voltage at RECORD voltage.

RECORD: banana posts, connect DC output to the recording system with typical input impedance of 1 MΩ

ZERO: miniature potentiometer, adjust to minimize the drift of the RECORD output.

Detailed operating procedures may be found in Appendix A.

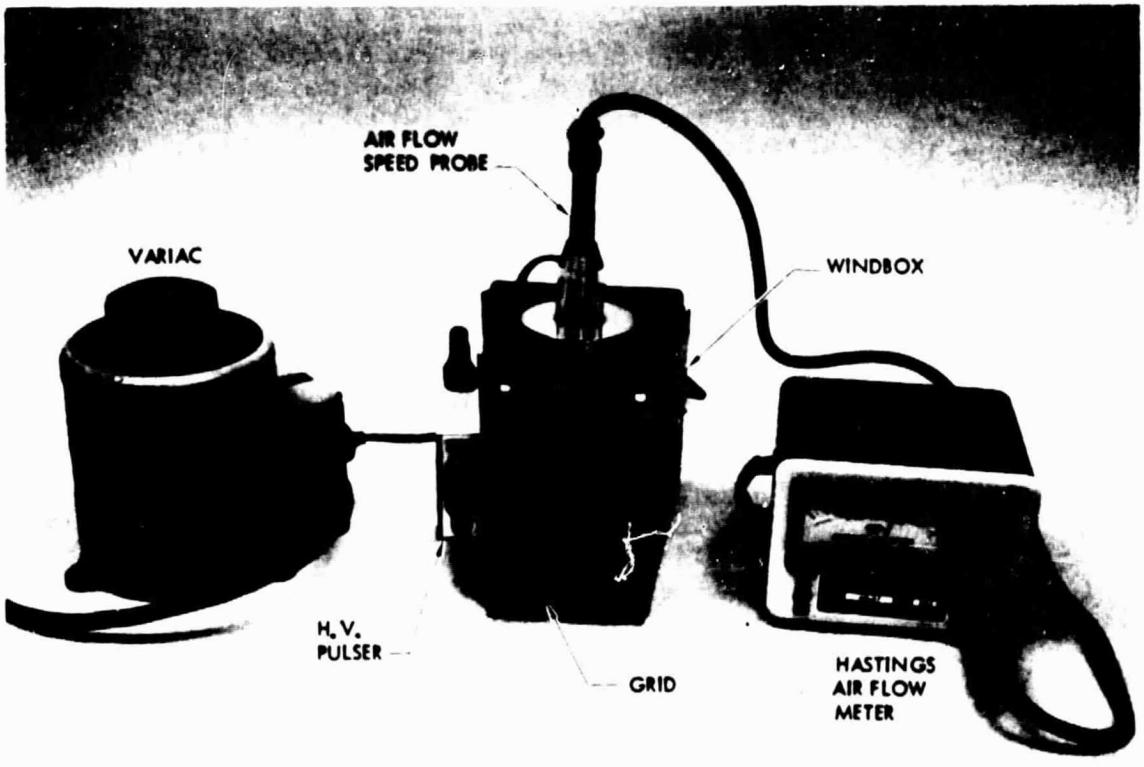

Fig. 10. Measuring Air Flow Speed in the Windbox

IV. EARLY EXPERIMENTS

1. Dynamic Test

At the beginning, grids were made from gold-plated round brass rods secured in a Micarta frame. They were originally designed and fabricated for use as low voltage biased grids for carbon fiber counting. The frame was about 10.2 cm x 10.2 cm (4 in. x 4 in.) in size and had a grid aperture of 7.5 cm x 7.5 cm (3 in. x 3 in.). The brass rods were 2.3 mm (0.090 in.) in diameter and arranged in parallel to the face of the frame. Typical spacings between the centers of these rod electrodes were 3.8 mm and 7.6 mm. Each frame had two layers of grids. The axes of the rod electrodes in the two layers were perpendicular to each other. The separation of the layers was about the same as that of the adjacent rods.

The grid with the H.V. discharge circuit was then mounted on top of a small glass chimney (Figure 11). The lower end of the chimney had a funnel shape in which a small amount of carbon fiber composite was burned with the aid of a propane flame, so that the fiber fragments were released. The convection of hot air surrounding the fire carried the fiber fragments upward to reach the grid so that they could initiate sparks in the grid and thus be counted.

Figure 12 shows some test results obtained in this manner. The peak current of the spark as monitored by the current shunt is plotted as a function of the grid bias voltage. It can be seen that a linear relationship holds for both grids. The extrapolated zero current bias voltages were about 300 to 400 V due to the contact resistance problem as discussed previously. Later, small-spacing (1 mm to 2 mm) grids made from small metal wires (diameters 0.25 mm and 0.51 mm) were tested in a similar manner and the results are shown in Figure 13. In these cases, the linear relationship between the peak current and bias voltage remained. However, the extrapolated zero current grid bias voltages were lower, of the order of 100 V to 200 V. This was due to the fact that larger electrical fields were achievable at a relatively low bias voltage for small diameter electrodes.

In the above tests, the air flow rate was not precisely controlled; neither was the length of the fiber fragments. As a result, for a fixed grid bias voltage, the peak spark current followed a wide distribution. This result was anticipated because if a fiber was not landed perpendicular to the electrode axes, a longer fiber length across a given pair of electrodes would occur. The larger resistance of the long fiber would result in a lower peak current. In Figures 12 and 13, the highest peak current for a given bias voltage was used in the plot. It is assured this current corresponded to the fiber which bridged a pair of electrodes in the shortest possible distance, i.e., perpendicular to them.

2. Static Tests

In order to obtain more controlled experimental results, expecially in regard to the fiber length effect and the cases when the fibers were landed obliquely across the electrodes, a static test was necessary. The fiber segments were manually placed on an extension card which is normally used for electronic test and service and covered by a microscope slide. The parallel metal strips on the card which were 2.3 mm wide and 1.5 mm apart served as electrodes for the discharge. In this way, fiber segments could be oriented at any angle oblique to

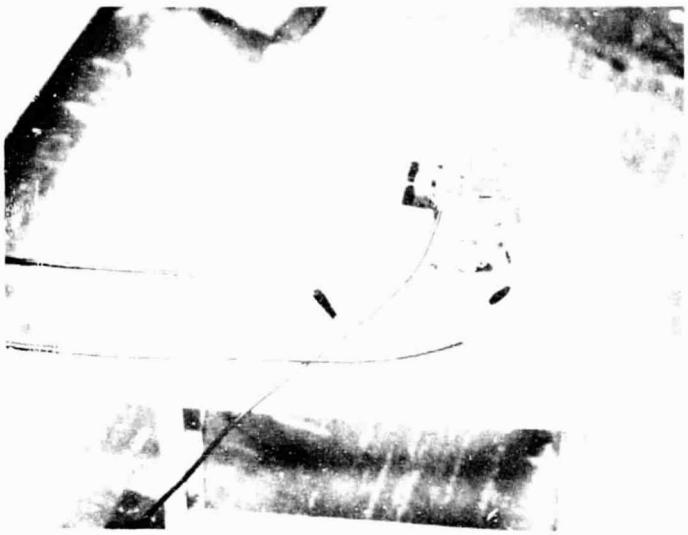

DYNAMIC TEST
TEST CIRCUIT

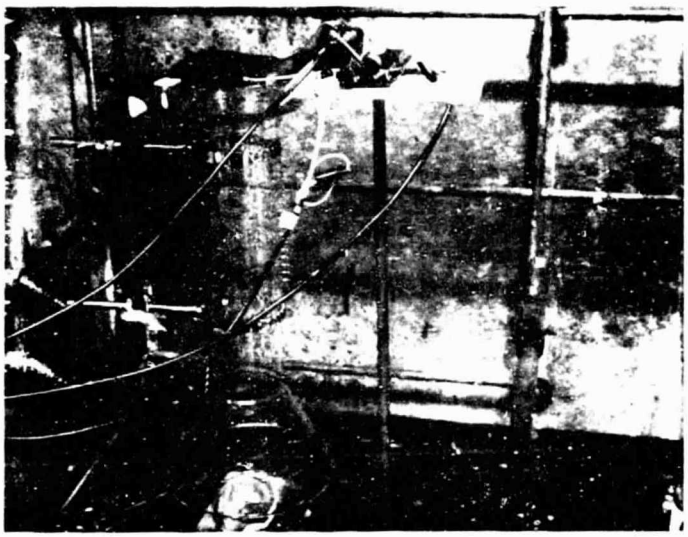

DYNAMIC TEST
TEST SETUP

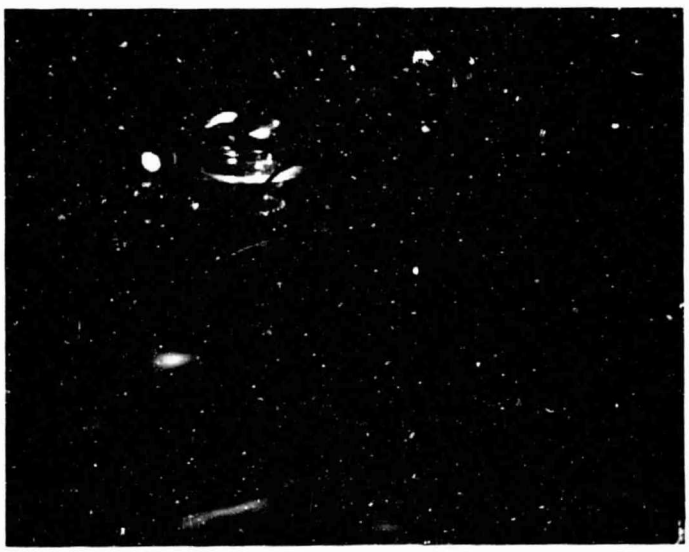

HIGH-VOLTAGE,
HIGH-CURRENT
SPARK PRODUCED
BY FIBERS

Fig. 11. Setup of the Dynamic Test

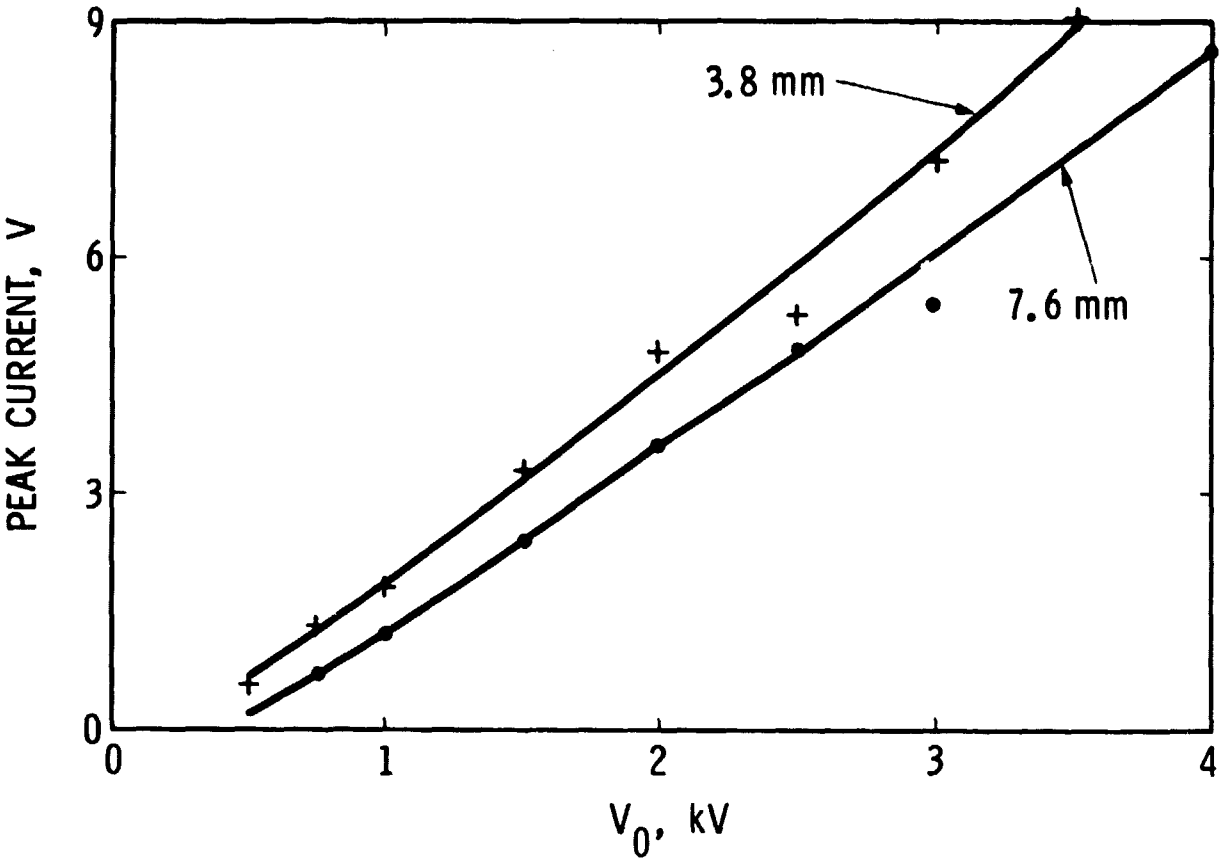

Fig. 12. Typical Dynamic Test Result, Peak Current (Measured by Oscilloscope Voltage V, where 1 V = 115.5 amps) as a Function of Grid Bias Voltage, V_0

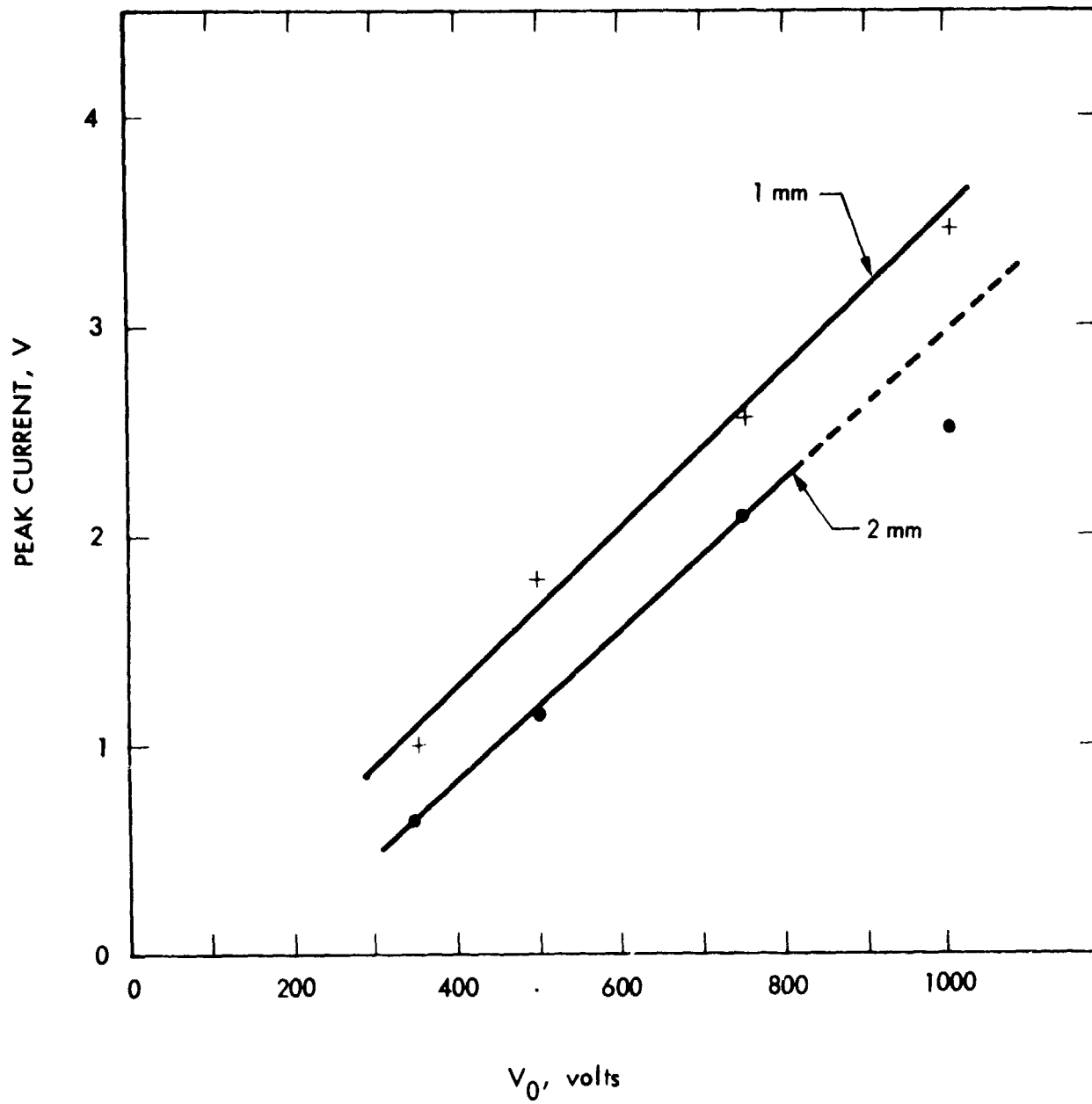

Fig. 13. Dynamic Test Results of Small Spacing Grids, Peak Current (Measured by Oscilloscope Voltage V, where 1 V = 115.5 amps) as a Function of Grid Bias Voltage, V_o

the strip electrodes. A different fiber length under discharge could be selected by selecting any pair of strips on the card as the discharging electrodes (Figure 14).

The electrodes, in this case, could not be directly connected to the energy storage capacitor; the discharge through the fibers would prevent the electrical charge from accumulating in the capacitor. A spark gap was needed to allow the capacitor to charge up. Subsequently one could dump the energy into the grid by sending an external trigger command to the spark gap.

A circuit based upon a EG & G KN-22 krytron is shown in Figure 15. The 30 kV trigger pulse can be supplied by a trigger module such as the EG & G TM-11. The current trace of the discharge, shown in Figure 15, was essentially similar to those obtained in the dynamic test. However, some features, especially the turnoff of the discharge, were affected by the characteristics of the krytron.

Figure 16 shows the peak current of the discharge as a function of the discharge voltage, with the fiber length as a study parameter. For short fiber lengths of 3.86 mm and 7.72 mm, the results were similar to those obtained in the dynamic test. For longer fibers, the responses were very different in the lower voltage region. Figure 17 shows the peak current as a function of the fiber length for a fixed discharge voltage of 1 kV. A distinct functional relationship is established. Therefore it appears feasible to distinguish the fiber length by its corresponding peak current in the spark. A commercial multichannel-pulse-height-analyzer can be used to measure the fiber length distribution.

However, the H.V. electrical field is capable of orienting the fiber fragment; thus, at an optimized bias voltage on the grid, one can minimize the oblique incidence of the fibers on the grid. Therefore, the pulse height analyzer approach, which is more complicated, was not considered absolutely necessary. For fiber fragment size measurement, one can use grids of different spacings. This was the design philosophy adopted for the JPL H.V. grid spark carbon fiber detection system.

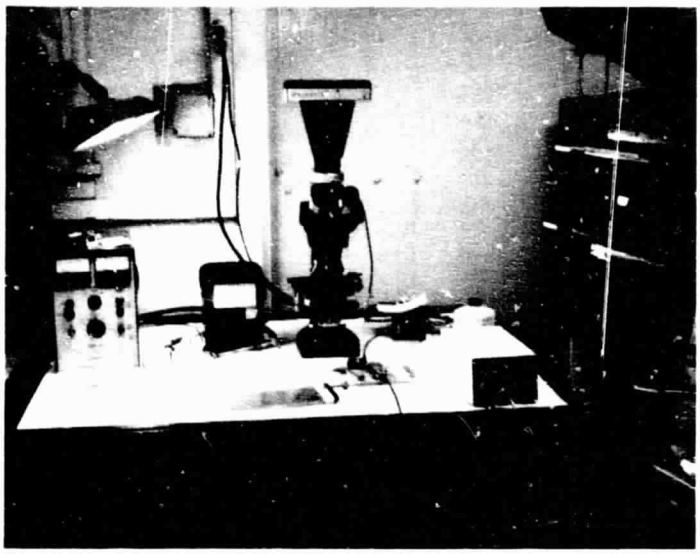

TEST SETUP

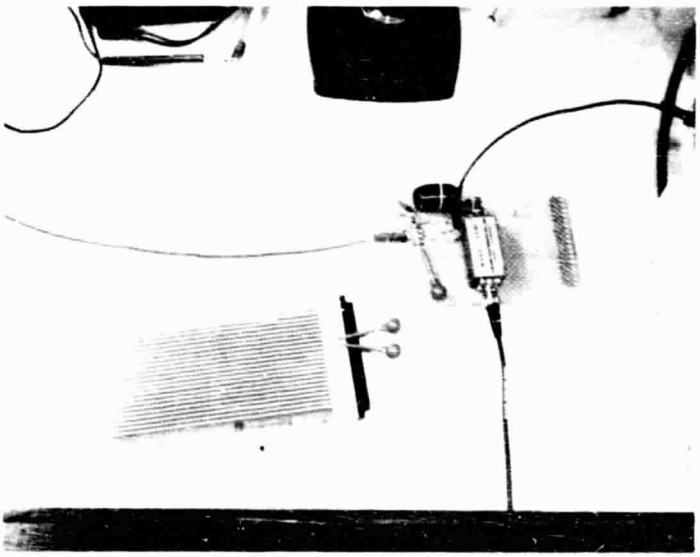

TEST CIRCUIT

Fig. 14. Setup of the Stationary Test

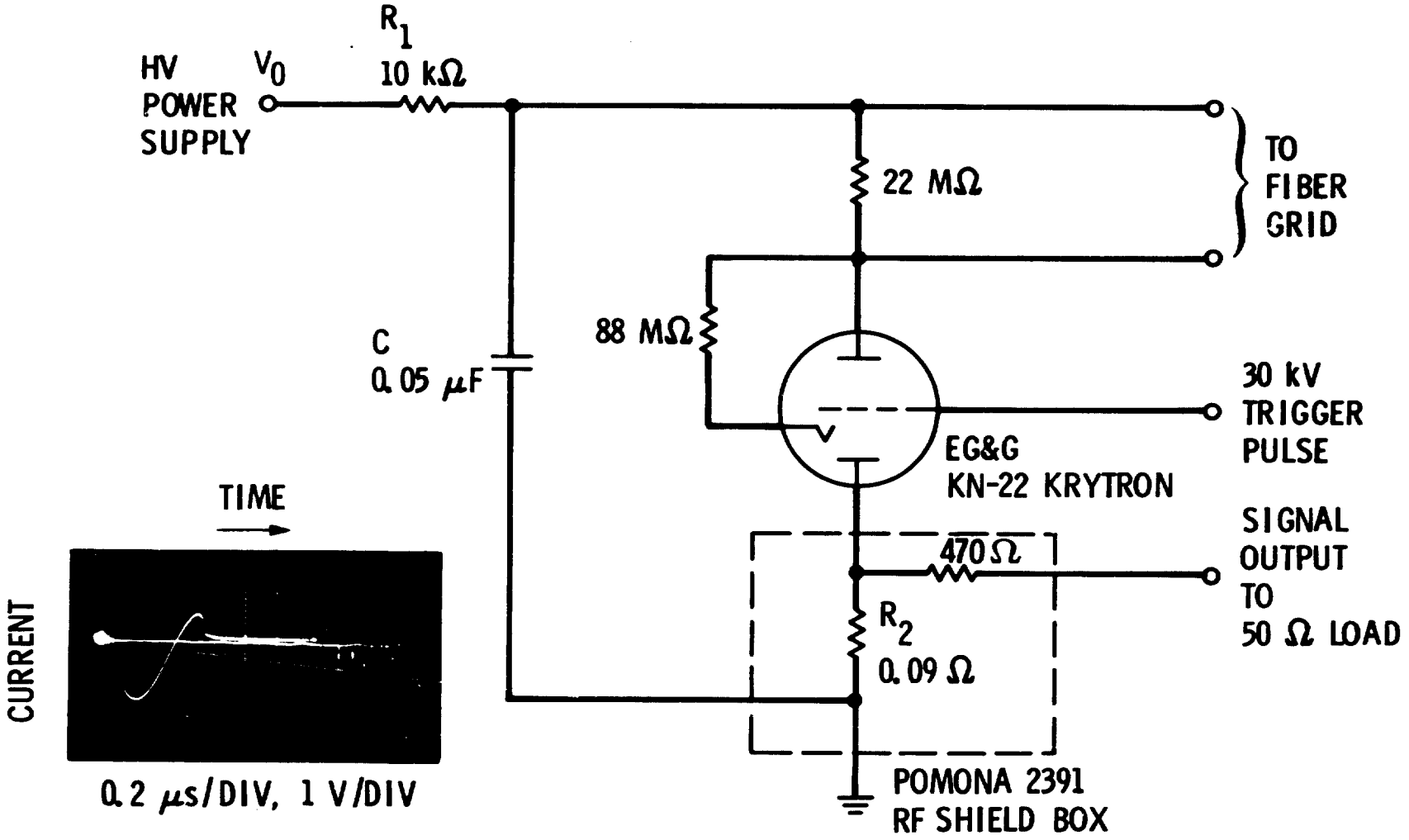

Fig. 15. Test Circuit for the Stationary Discharge Test

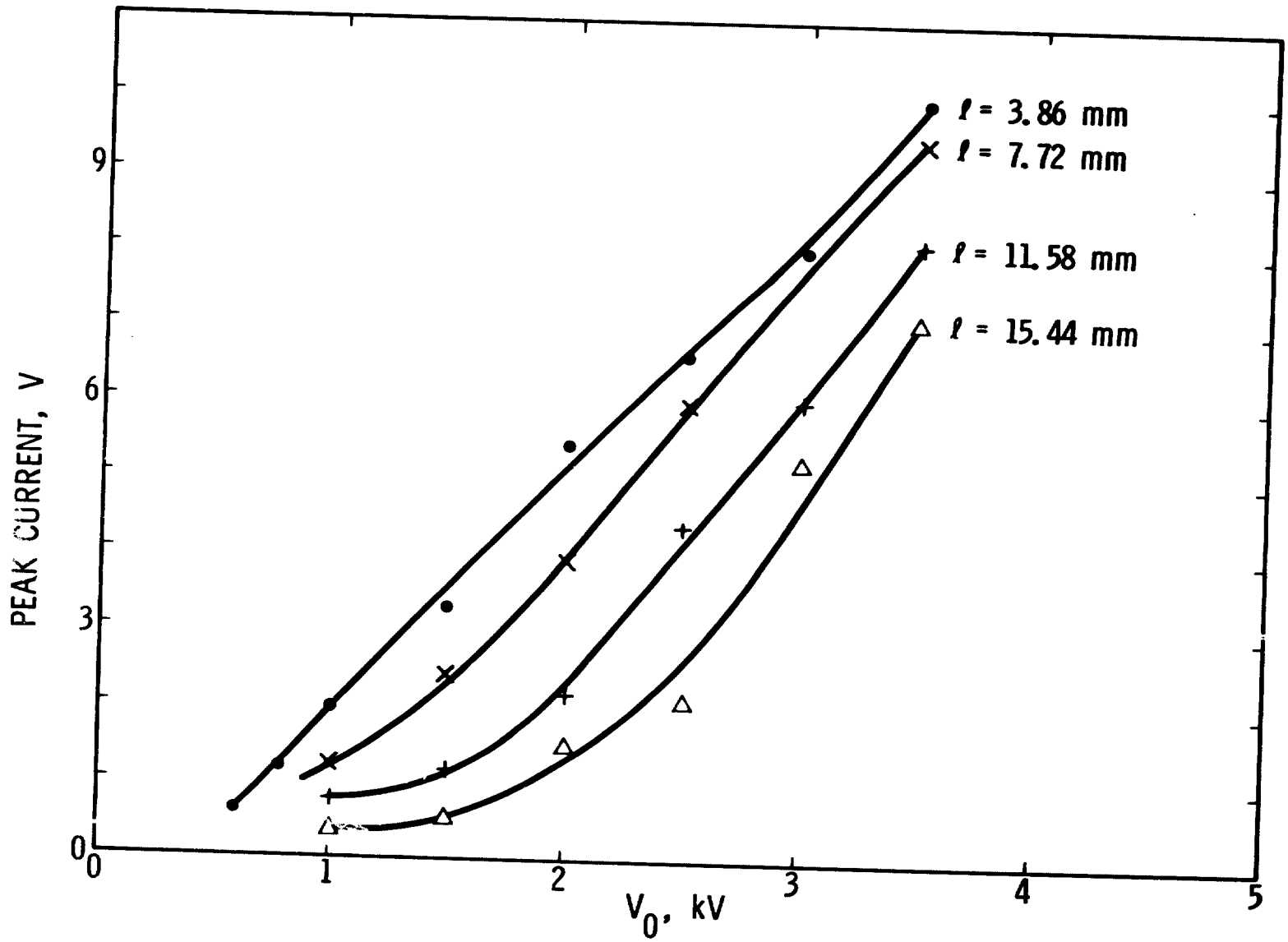

Fig. 16. Stationary Test Results, Peak Current (Measured by Oscilloscope Voltage V, where 1 V = 115.5 amps) as a Function of Grid Bias Voltage, V_0

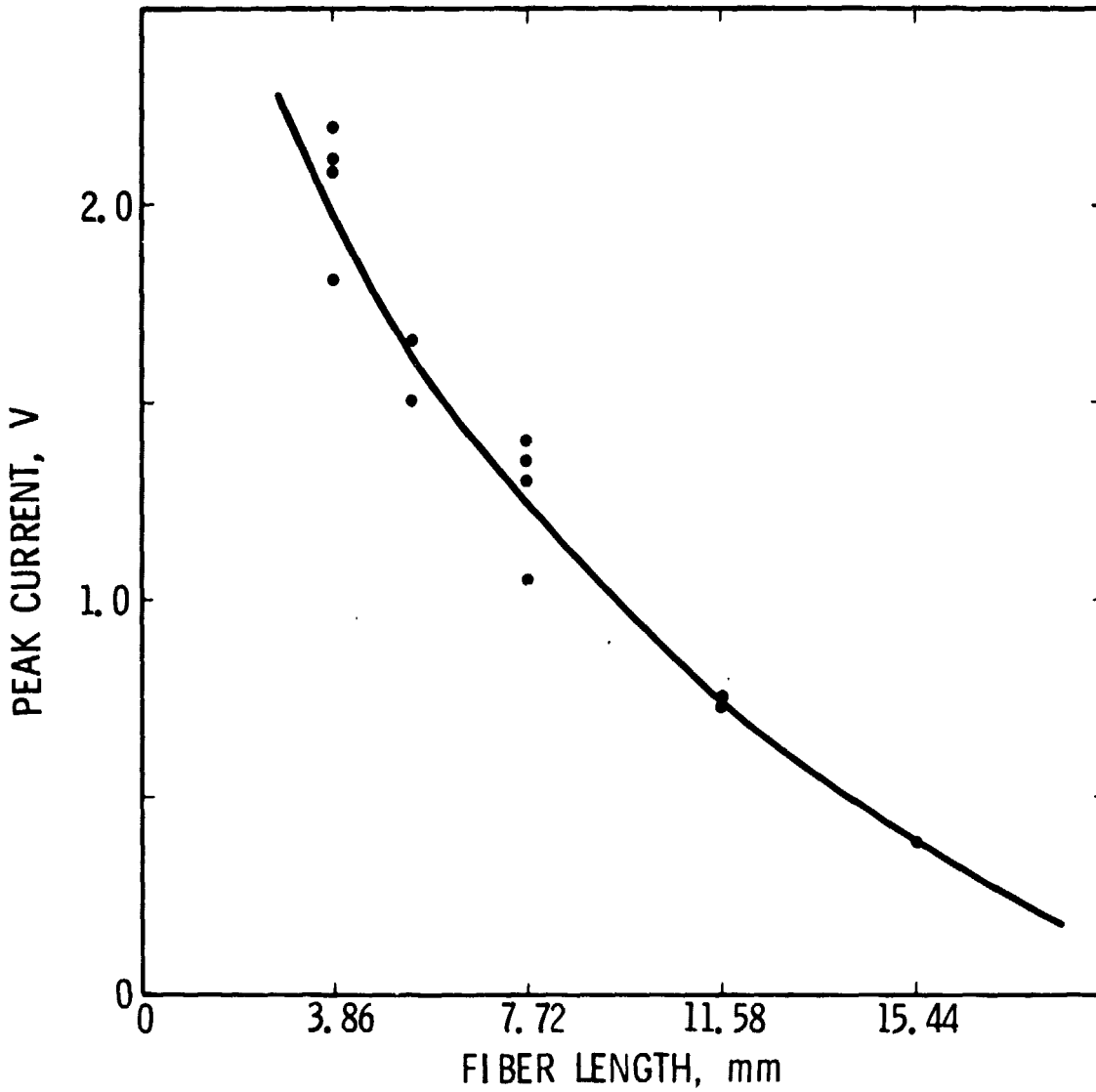

Fig. 17. Stationary Test Results, Peak Current (Measured by Oscilloscope Voltage V, where 1 V = 115.5 amps) as a Function of Fiber Length, at Discharge Voltage of 1 kV

V. PHYSICAL DESCRIPTION OF THE SPARK PHENOMENON

The peak currents observed in the fiber-induced spark discharge were of the order of several hundred amperes. They were definitely too high to be accounted for by a current flowing through the fiber under the grid bias voltage. As mentioned previously, the resistance of a carbon fiber is typically 3000 Ω/cm. Therefore, at the test voltage in the kilovolts region, current should be only several amperes. Some other mechanisms were believed to exist to carry these abnormally high currents. After careful examination, the phenomenon manifests itself as follows:

1) When the fiber makes initial contact with a pair of electrodes in the grid, the high voltage imposed on the grid will overcome the contact resistance by forming arcs around the points of contact. There are then currents flowing through the fiber. Supposedly if the high voltage was current limited this would be the complete story of the discharge.

2) The arc resistance of the air between two electrodes under a high voltage is much smaller than that of a fiber laid between the electrodes. Therefore the initial arc at the contact points tends to grow along the surface of the fiber until it has completely bridged the space between the two electrodes along the direction of the fiber when a high current condition is allowed by the discharge circuit. This is a transient process in which the arc resistance is not constant as indicated by the slow rise time of the current pulse (Figure 2). According to a simple RLC discharge in which R is constant, this rise time should be much shorter in duration. The peak arc resistance of the spark was several ohms.

Some visual features of the spark are shown in the photographs in Figures 18 and 19. They were taken under a microscope as described in the static tests. The broad but relative faint light was emitted by the plasma in the spark. The bright filaments were the light emitted by the fiber. Indeed, prior to and immediately after the spark, low currents were flowing in the fiber. Therefore it was heated up to incandescence. Even though it had much lower light intensity as compared to the spark plasma, it had a much longer duration. Under the long integration time of the camera film, it appeared to be brighter. It is apparent in these photographs that the position of the fiber changed a number of times, presumably due to the disturbance caused by the spark.

It is also apparent that the direction of the spark followed that of the fiber. The fiber was a spark initiator as well as a guide for the spark. Because there are no detailed previous studies on the spark phenomenon, theoretical predictions of more fundamental aspects of the plasma are not available. The plasma is not confined. The variable dimension of the spark made it difficult to estimate the plasma's specific resistance as a function of voltage. Relationships of this kind are usually complicated and depend upon a variety of parameters. Therefore, it is not surprising that the peak current (arc resistance) is a nonlinear function of the fiber length (arc length) as shown in Figure 17.

Upon the polarity reversal in the capacitor, the spark discharge died out rapidly. Due to the short duration of the phenomenon, a shock wave was produced

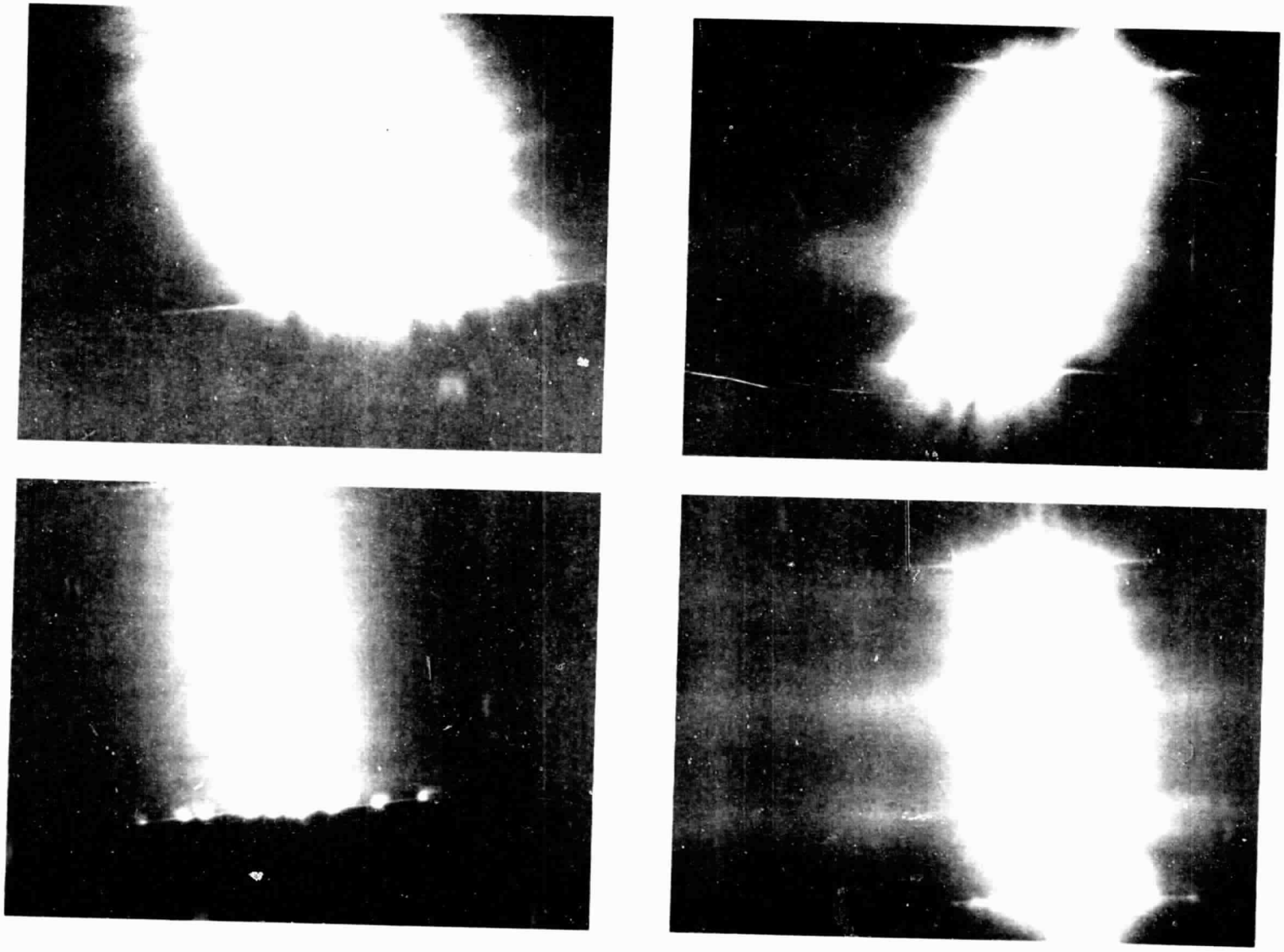

Fig. 18. Microscope Photographs of the H.V. Spark Phenomenon

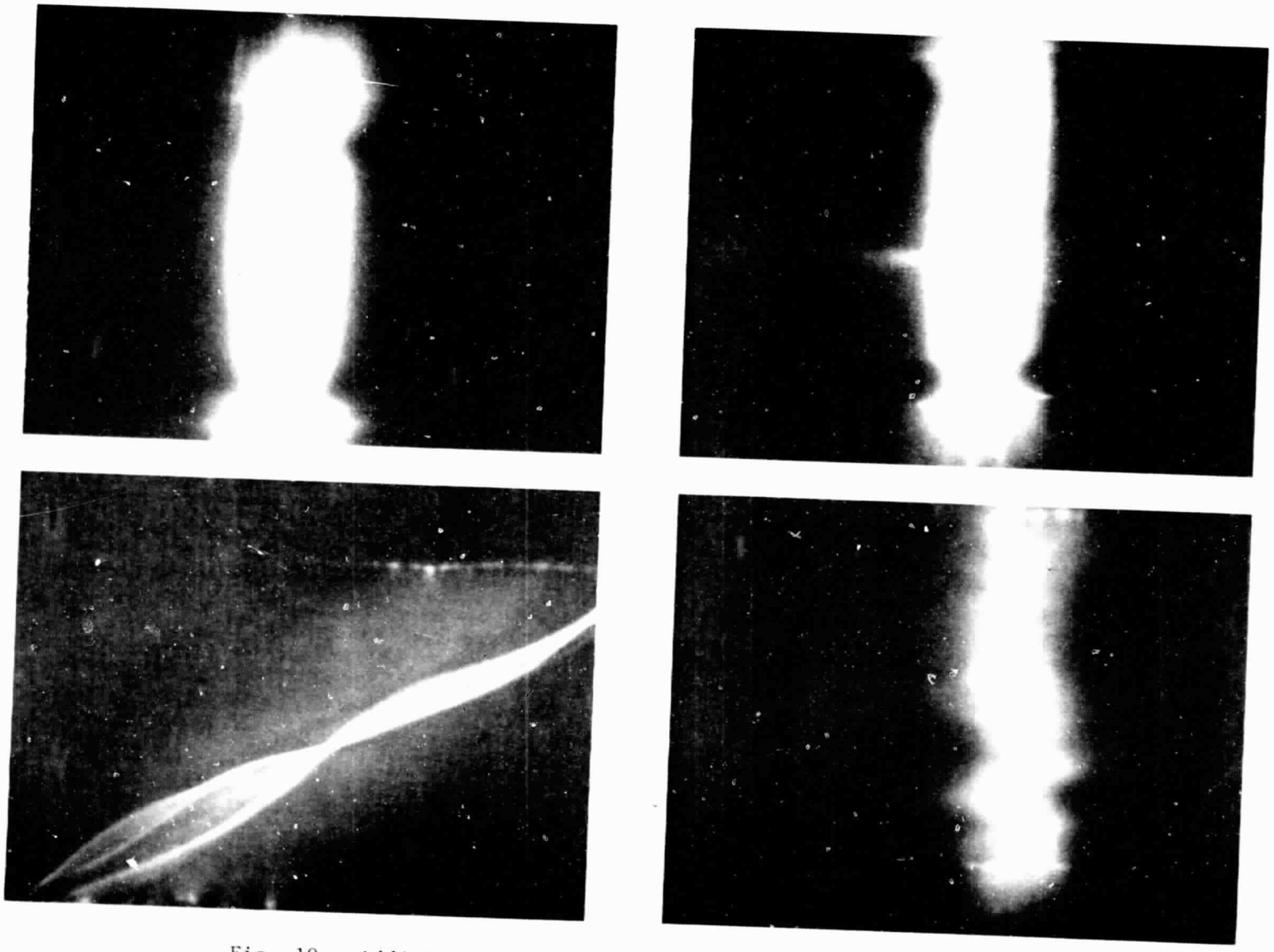

Fig. 19. Additional Aspects of the H.V. Spark Phenomenon as shown in Microscope Photographs

in the air at the end of the spark. This disturbance was strong enough to release the fiber from the grid electrodes, the fiber debris being carried away by the air flow. Self cleaning of the grid was thus accomplished.

VI. PHYSICAL DESTRUCTION OF THE CARBON FIBER

There is significant graphitization in a carbon fiber. Thus the combustion of a carbon fiber requires a high temperature, a long time of reaction and sufficient oxygen background. When a carbon fiber composite is being combusted, the relatively low temperature generated by the epoxy combustion and the depleted oxygen background prevent the complete oxidation of the fiber. Therefore carbon fiber fragments are released from the fire and can cause carbon fiber pollution problems. Heating of the fiber can be done in the laboratory either by passing electrical current through it or by placing it into a high temperature oven. It was found that the complete consumption of the fiber usually took minutes to accomplish under these circumstances.

Severe damage and consumption of carbon fibers by the high voltage spark discharge across a grid have been observed. Figure 20 shows a number of post-spark examinations of carbon fiber segments after the static discharge tests. The fibers were laid across the metal strip electrodes on the extension card and covered by a microscope slide as previously described. The pulse discharge circuit had a 0.05 μF discharge capacitor, and bias voltages ranging from 0.5 to 1.0 kV were used.

Figure 20 a) shows a fiber after the first pulse discharge. The fiber appeared to be intact physically. The discoloration on the glass slide was probably caused by the vaporization of impurities on the fiber surface. Figure 20 b) shows the same fiber after the second pulse discharge. The fiber had broken open and a burn mark on the fiberglass board of the extension card was visible. Because the gap at the break point was small, a third spark discharge still could be initiated by the fiber but a considerably higher voltage across the grid was necessary to achieve the spark. After the third discharge, as shown in Figure 20 c), the fiber was severely damaged. It showed large curvature and broke widely open due to the mechanical shock produced by the spark. Figure 20 d) shows the post spark examination of a longer fiber laid across the electrodes obliquely.

Serious physical change had taken place in the curly shape fibers produced after several discharges. They become less conductive and their ability to initiate a spark across the grid was apparently reduced. The interpretations are as follows: Currently, it is understood that carbon fibers have a graphite-type structure on their exterior surface. This is the main reason why the fiber is electrically conductive. The inner part of the fiber consists more or less of amorphous carbon materials which are not conductive. The low current but long duration discharge through the fiber, which occurs at the beginning and the end of the spark, can heat up the fiber but probably will not damage the fiber. The real damage is due to two mechanisms related to the spark in the air. First, the plasma of the spark has a high temperature (>5000 K). Therefore it can heat up the fiber surface to a much higher temperature than that done by a fire or low current discharge. The estimated thermal penetration depth in the fiber surface is of the order of one micrometer for the duration of the spark ($\sim$1.0 μs). It is felt this may be sufficient to accelerate the oxidation and gasification of the exterior graphitized structure of the fiber.

The second possible damage mechanism is that of plasma etching. The high energy ions and electrons in the plasma are capable of bombarding a solid surface in contact with it and eroding it away. This process can take off a

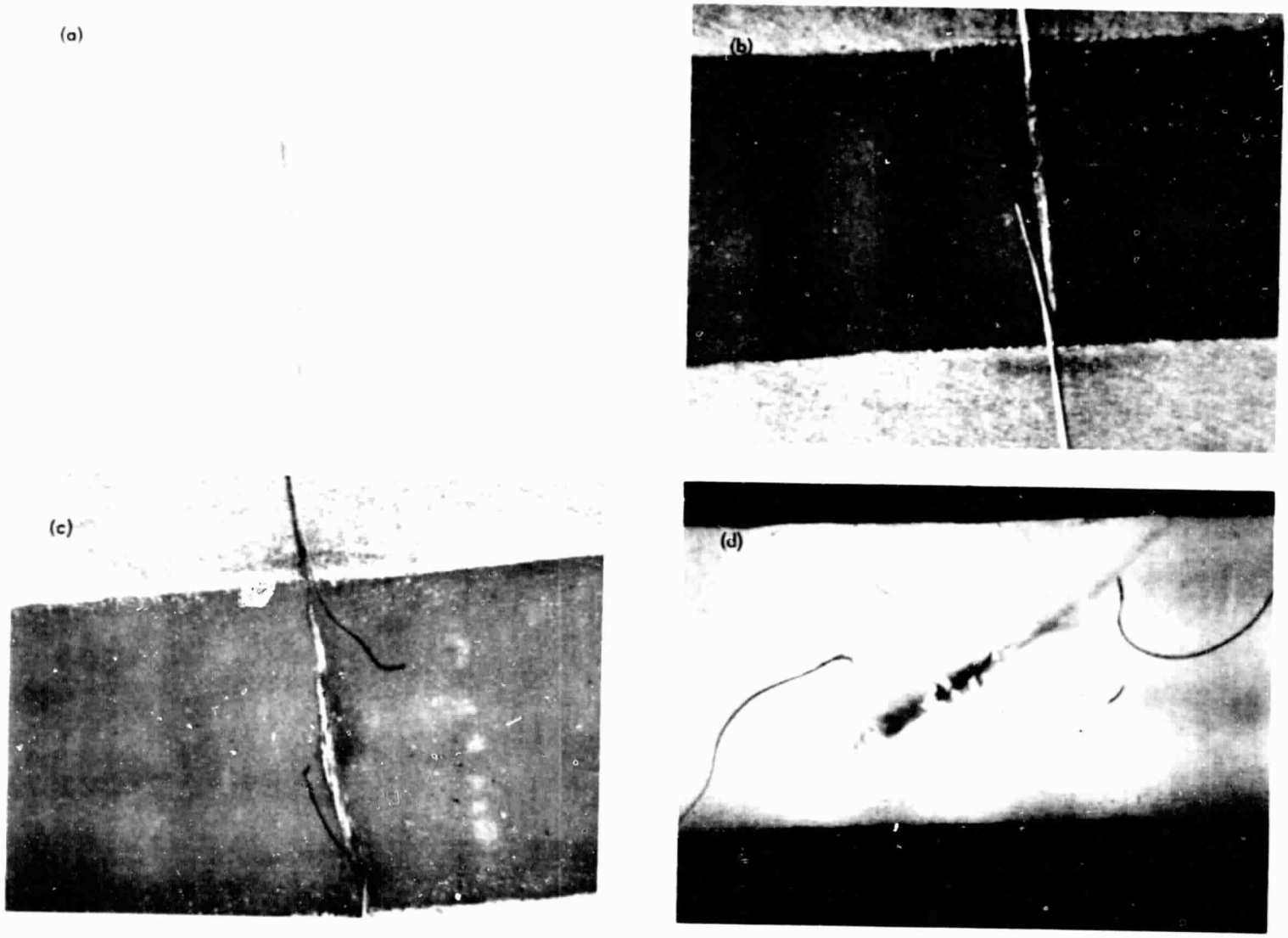

Fig. 20. Post-spark Examinations of the Carbon Fiber

significantly thick layer of material from the surface, especially if the plasma of a spark possesses a high current and high density.

The rate and degree of the damage of the fiber can be accelerated if higher discharge energy and/or voltage were used in the discharge. In the former case, due to the inductance in the discharge circuit, a large capacitance was used to store more electrical energy so as to introduce more current oscillations into the discharge. This, in fact, is equivalent to multiple pulsing of the fiber except that it occurred in a much faster sequence than in the manually triggered operations (these results were shown in Figure 20).

For the carbon fiber detection system development, the objective was the accuracy of counting of fiber fragments. Fiber destruction was an important parameter for the trade-off in the system design. The phenomenon was not studied in great detail due to the complicated nature of the process. As a result, the detection system was designed to have independent grids to detect different sizes of the fibers. The idea of assembling different size grids in series flow was not pursued further. In order to make that approach work, one would have to make sure that a fiber fragment was completely destroyed after it had been sparked and counted by a given grid in the stack of grids.

VII. DESIGN CONSIDERATIONS

A. System Level

The following is a complete list of physical parameters which need to be optimized in order to complete the design of the H.V. grid spark carbon fiber detection system. Many of them have been discussed previously.

1) Major Parameters

a) Voltage of the H.V. discharge circuit.
b) Energy storage (capacitance) of the discharge unit.
c) Sampling air flow rate.
d) Depth of the grid electrode.
e) Length of the fiber fragments.
f) Repetition rate and the effect of fiber clusters.

2) Minor Parameters

a) Width of the electrode.
b) Size of the grid aperture.

As has been discussed previously, in order to overcome the contact resistance problem, one has to use a bias voltage higher than 400 V. A higher voltage tends to increase the counting efficiency as it is more effective in orienting the fiber fragment relative to the grid electrodes. However, too high a grid bias voltage will introduce the self-discharge of the grid, i.e., sparks will be initiated even though the fiber is shorter than the grid spacing. The spark will first form between the ends of the fiber and the electrodes; subsequently it will grow across the entire fiber.

A larger capacitance in the discharge circuit tends to reduce the risk of multiple counting of a single fiber segment. The higher electrical energy will damage the fiber and cause it to lose its ability to initiate the spark as has been discussed previously. However, too large a capacitance will result in a too long capactor recharging time and, as a result, an unsatisfactorily low counting rate capability. It will force one to use a higher current H.V. power supply which could increase the operational safety risk.

The air flow rate and the depth of the electrode are working together. The real physical parameter here is the residence time of the fiber in the electrical field of the grid. This time is approximately equal to the ratio of the grid depth D to the air flow velocity v through the grid ($t = D/v$). For a given grid bias voltage, the longer the residence time, the more effective will be the electrical field in orienting the fiber fragments toward the electrodes to achieve a better fiber counting efficiency.

The length of the fiber fragment is important. If it is very long as compared to the grid spacing, it will run across multiple pairs of electrodes in the grid. Multiple counting from one single long fiber will be the result. The fibers in a fiber cluster tend to arrive at the grid at the same time. A short-circuit of the system could occur which can prevent the successful recharge of the capacitor in the discharge circuit. Both problems can be minimized by installing a prescreen in front of the grid. The mesh size of the screen should

be comparable to the grid spacing. The effect of the electrode width is that a thick electrode tends to restrict the air flow through the grid. On the other hand, for a better mechanical stability of the electrode spacing, a larger grid width is desirable. The size of the grid aperture will have some minor effect on the counting rate of the system. All the electrodes are connected in parallel electrically, and for a given fiber exposure rate the larger the aperture the greater will be the number of counts registered.

B. Electronics Design

Two prominent problems affect the design:

1) The pulse signal from the spark may have several peaks. By using a conventional high frequency digital counter, several counts may be recorded for a single discharge pulse produced by a single fiber. Therefore a signal conditioner is needed, i.e., a technique which counts the first peak of the signal; then it is blanked-out for a brief period of time to discount the immediately following peaks from the same spark signal.

2) The exposure rate of fibers in most tests is low, of the order of several pulses per minute. Therefore counting in the frequency mode is not very useful. It is preferable to sum the total fiber counts over a prolonged period of time (hours). In this case, it is difficult to obtain a straightforward analog signal for recording and visual display. Conventional laboratory electronic instruments are too cumbersome and inconvenient for use in field tests. An analog pulse integrator of high stability and portability is needed.

An electronic system with these features was successfully developed and fabricated during this project. It will be described in detail in a later section (Section IX D).

VIII. COUNT EFFICIENCY

A. Test Technique

The principle of the test is simple. One has to inject a known number of fiber segments into the grid-windbox assembly and compare it with the counts registered by the electronics. A percentage count efficiency figure can thus be obtained. In practice, it is very difficult to perform such a test. If a massive number of fibers is being used at one time and the total number of fibers is known beforehand (e.g., chop a section of a standard fiber bundle which contains 3000 individual fibers), one has to control the injection rate and efficiency, and prevent fiber conglomeration from occurring. If the total number is not known beforehand, one has to collect the fibers after they have passed through the grid and perform elaborate visual counting. Both procedures are formidable and difficult; besides, in the latter case, there are complications due to possible fiber breakages induced by the spark as have been discussed previously.

For this project, we adopted a relatively simple calibration technique. We injected the fibers into the grid-windbox assembly one at a time under controlled conditions. A single-fiber segment handler was constructed (Figure 21). It consisted of a vacuum lead to a suction jet which can pick up, transport and release a single fiber. The test procedure was:

1) Using set of razor blades that are carefully mounted in pairs with prescribed spacer width, cut out a length segment of a fiber bundle.

2) Spread the fibers on a tray with proper color background to enhance the visibility of the fibers.

3) Pick out a single fiber under a magnifier using the fiber handler.

4) Align and release the fiber into the grid-windbox assembly. The last two steps are illustrated in Figure 22.

5) Observe the indication of the fiber being counted by the occurrence of the spark.

The need of a windbox became evident in an early stage of the calibration. The air currents in the laboratory due to the room air conditions were considerable, of the order of 0.1 to 0.22 m/s (20 to 40 ft/min.). In a large scale fiber test such as the NSWC Dahlgren shock tube test or small-scale tests such as the JPL glass chimney burn test and Ames box burn test, the air flow rates were higher and variable with time. In order to minimize the effects of uncontrollable air flow rates and direction, a fan was used to provide a controlled and known air flow rate through the grid. An AC-operated fan commonly used for instrument cooling and controlled by a Variac autotransformer was used for this purpose. The windbox was 15.2 cm long with one end to accept the 11.9 cm x 11.9 cm fan and the other end to accept the grids which were 8.9 cm x 12.1 cm in size. The air flow speed between the fan and the grid was measured by a commercial air flow meter, Hastings-Raydist Model AB-27. It was inserted in the windbox through an uncoverable port on the top of the box.

Figure 23 shows typical air flow speed measurements for three brass-rod (diameter 2.3 mm) grids. The grid No. 1 was a double-layer grid with 3.82 mm

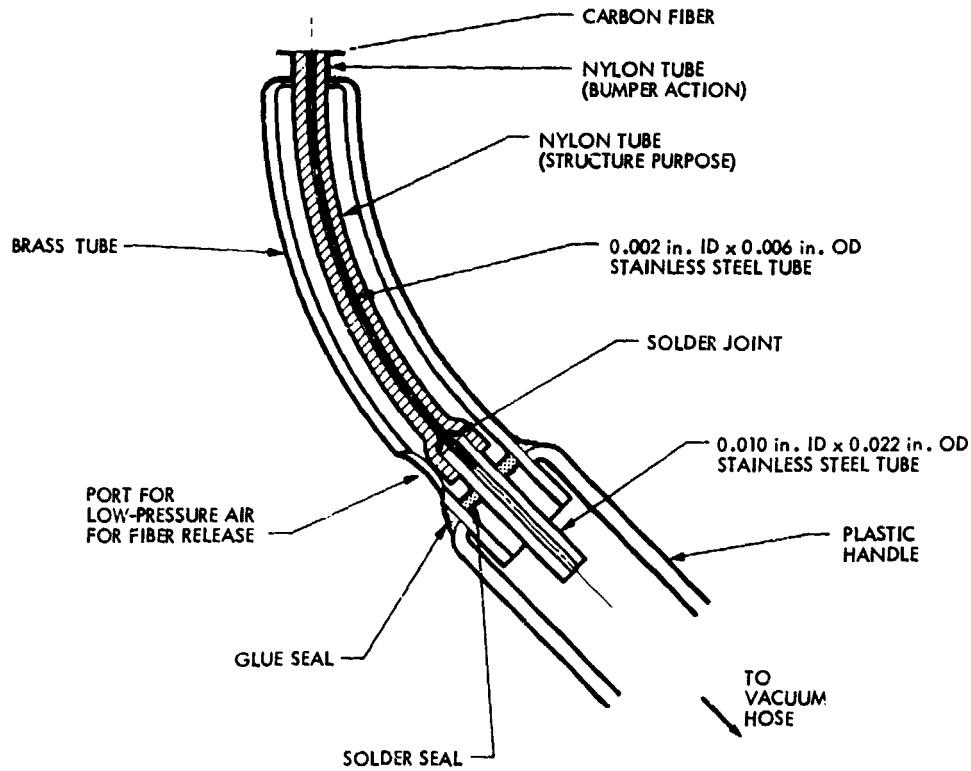

Fig. 21. Construction of the Single-Fiber Segment Handler

PICK UP SINGLE FIBER UNDER MAGNIFIER

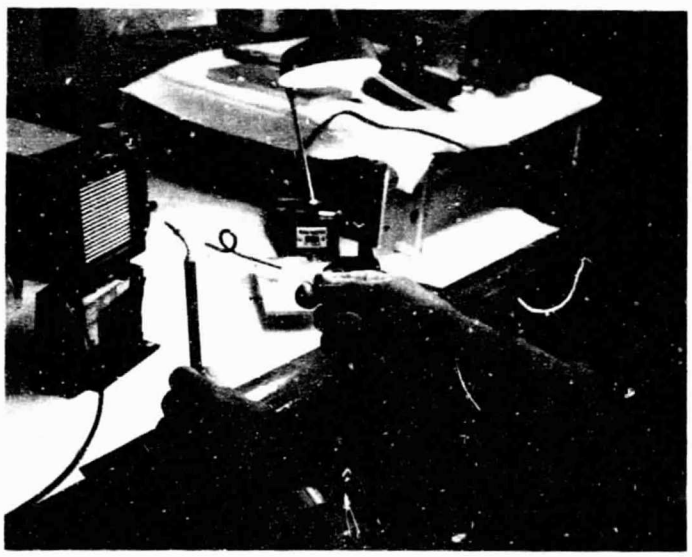

ALIGN AND RELEASE FIBER INTO GRID AND WINDBOX

Fig. 22. Calibration Procedure for Measuring H.V. Grid Carbon Fiber Counting Efficiency

separation distance between the central axes of the rods. The grid No. 2 was also a double-layer grid and had 7.6 mm grid spacing. Grid No. 3 was the same as grid No. 1 except that it had only one layer of electrodes. The measured air flow speeds inside the windbox did not vary significantly among these three grids. This indicated that their impedance loadings to the air flow were small.

B. Results for the Round-Electrode Grids

The tests were normally performed by varying the bias voltage on the discharge circuit. For a given grid and voltage, fibers of different sizes were tested. Figure 24 shows the smoothed-out results for the round-electrode grid No. 1. Each curve consists of at least five data points and each data point represents the results of 20 tests at the fixed experimental conditions, i.e., the same grid, same bias voltage, same fiber length and same air flow speed. Similarly, Figure 25 shows the results for the round-electrode grid No. 2.

As has been mentioned previously, it is evident from these figures that the sparks could be initiated by fiber segments shorter than the grid spacing if the bias voltage was sufficiently high. The results indicated that the count efficiency was poor for these grids. There existed no optimized bias voltage to provide the fiber length discrimination, i.e., at any bias voltage, significant counts of fibers of all different lengths were registered. Ideally, one wishes that at an optimized bias voltage, the grid will count all fibers that exceed a certain length and will not count fibers shorter than this length.

It was reasoned that this inefficiency was possibly caused by the limited grid depth, since the diameter of the round electrodes was small. In order to increase this parameter to achieve a better counting efficiency through a longer fiber residence time in the grid, metal-strip electrodes of proper width could be used to construct the grid. This approach has proven to be a solution to the problem.

C. Results for the Strip-Electrode Grids

Four experimental grids with straight metal strip electrodes were constructed. The electrodes were made from 1.6 mm (0.065 in.) thick copper plates. They were machined to about 9.3 cm (3.65 in.) long and 1.9 cm (0.75 in.) wide. They were secured in Micarta frames 8.9 cm x 12.1 cm (3.5 x 4.75 in.). The air gap spacings between the electrode pairs were 1.52 mm (0.06 in.), 2.28 mm (0.09 in.), 3.17 mm (0.125 in.) and 4.44 mm (0.175 in.), respectively.

Figures 26 to 29 show the test results presented with the count efficiency as a function of the grid bias voltage and using the fiber length as a study parameter. The tests were performed in the same way as in the round electrode grid tests. As in those cases, fibers shorter than the grid spacing could introduce spark counts. However, the count efficiency had been drastically improved. Optimized bias voltage to achieve the desirable fiber length discrimination did exist for each grid. For instance, if one biased the 1.52 mm (0.06 in.) grid at 600 V, it would count fibers longer than 1.25 mm (0.050 in.) and would not count fibers shorter than this length. Similarly, optimized bias

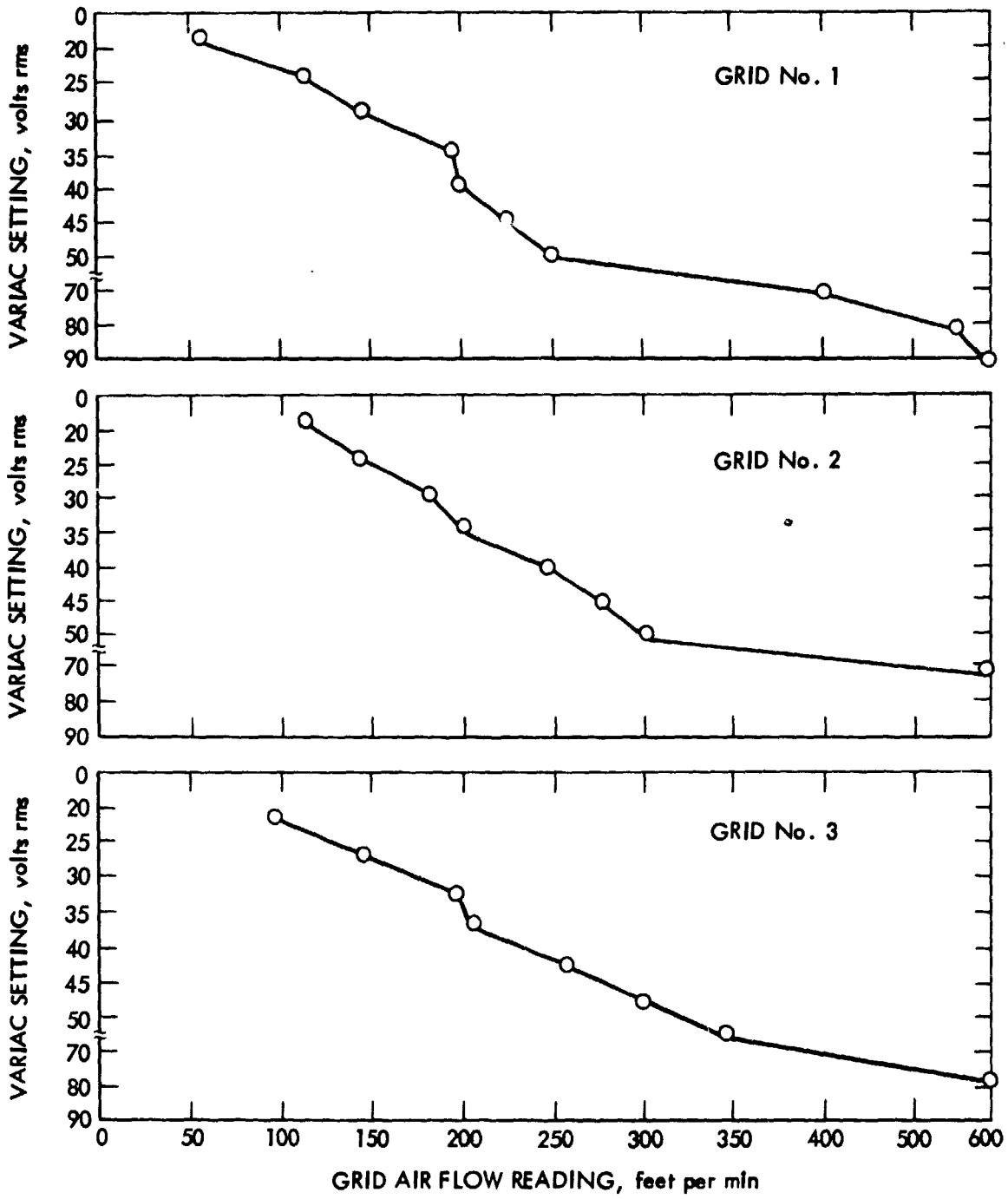

Fig. 23. Typical Air Flow Speeds in the Windbox for Round-Electrode Grids as a Function of Variac Setting for the Fan

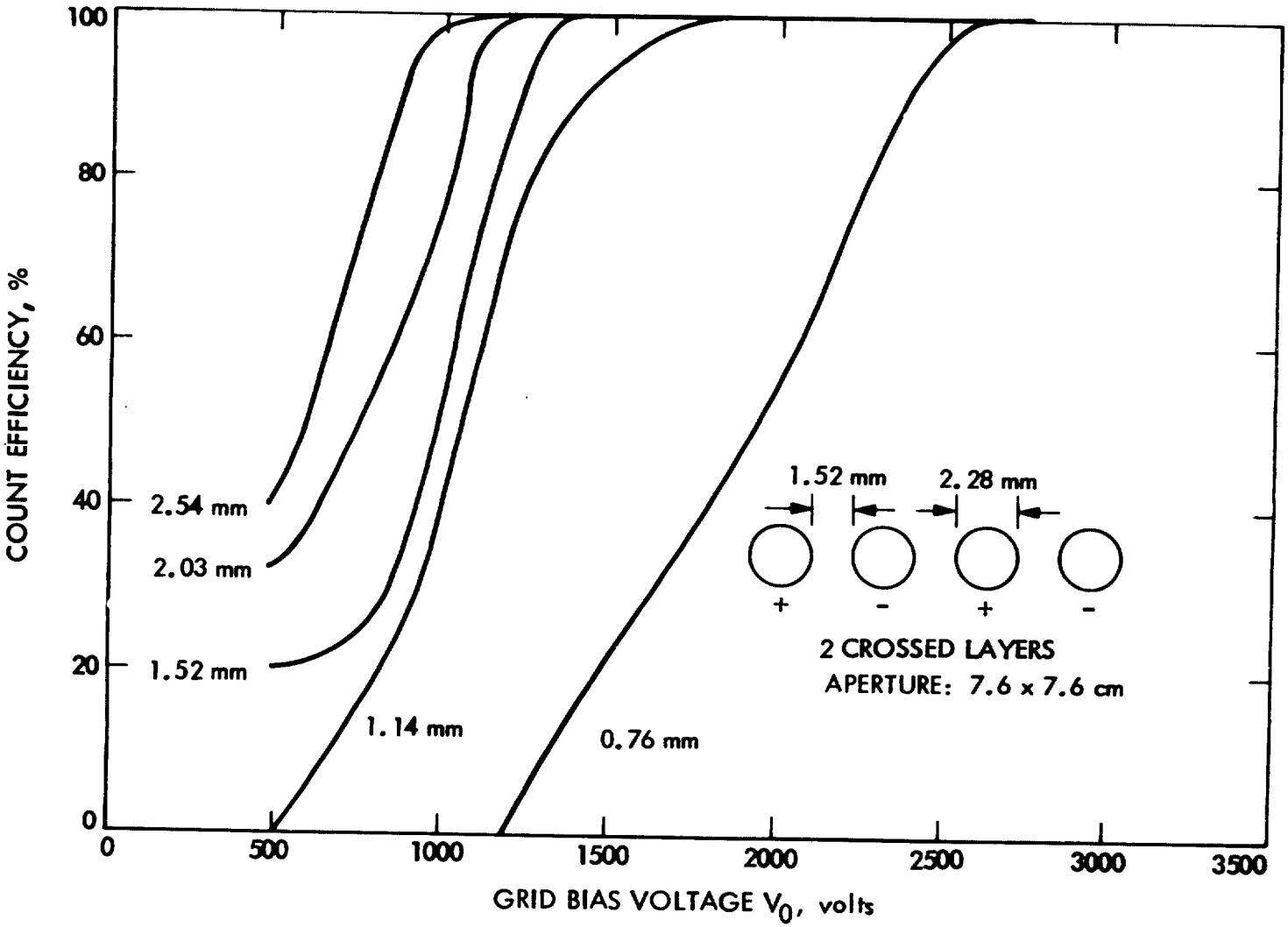

Fig. 24. Count Efficiency as a Function of Grid Bias Voltage with Fiber Length as Parameter for Round-Electrode Grid No. 1 (Variac Setting = 50 V rms)

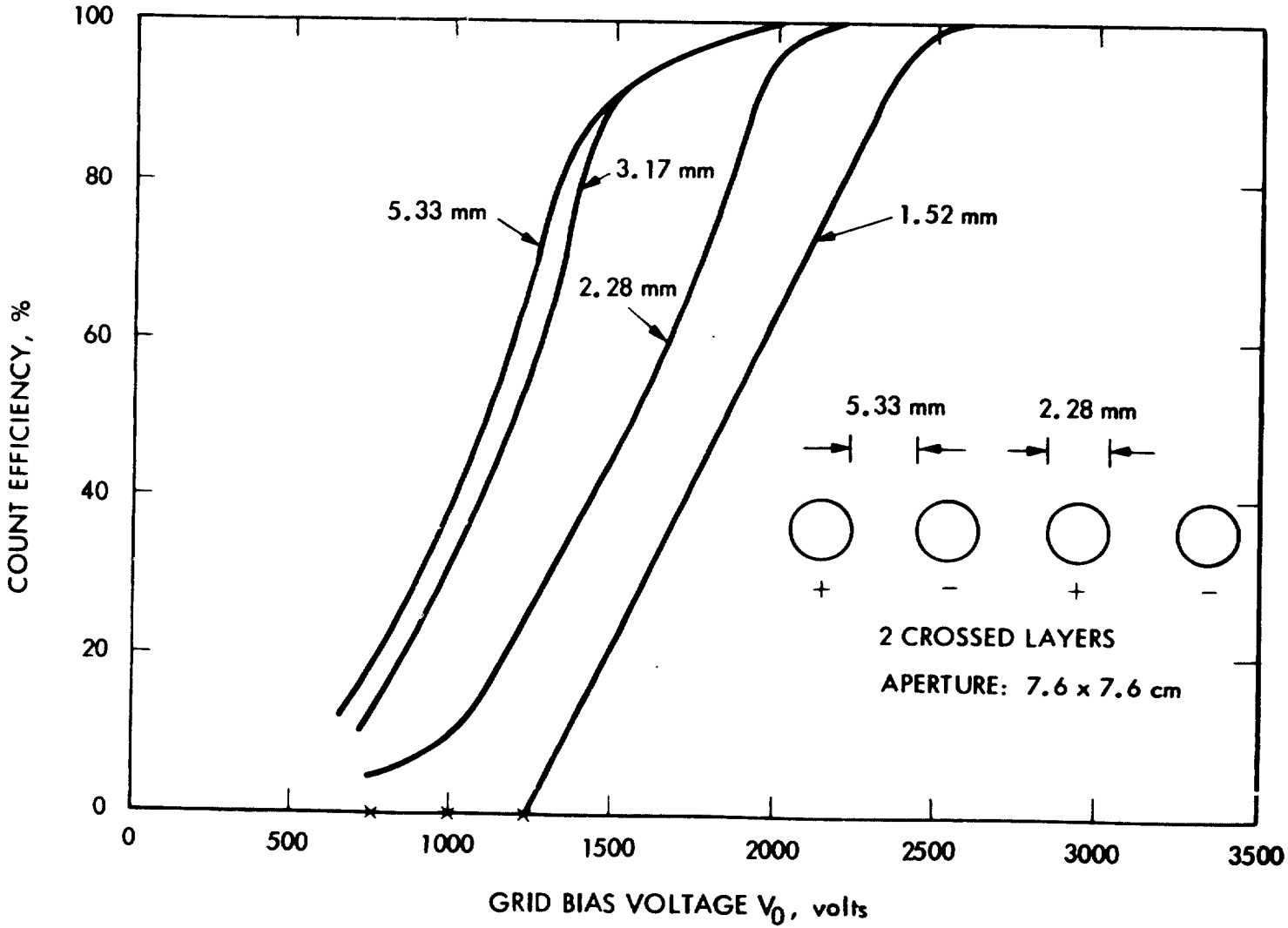

Fig. 25. Count Efficiency as a Function of Grid Bias Voltage with Fiber Length as Parameter for Round-Electrode Grid No. 2 (Variac Setting = 50 V rms)

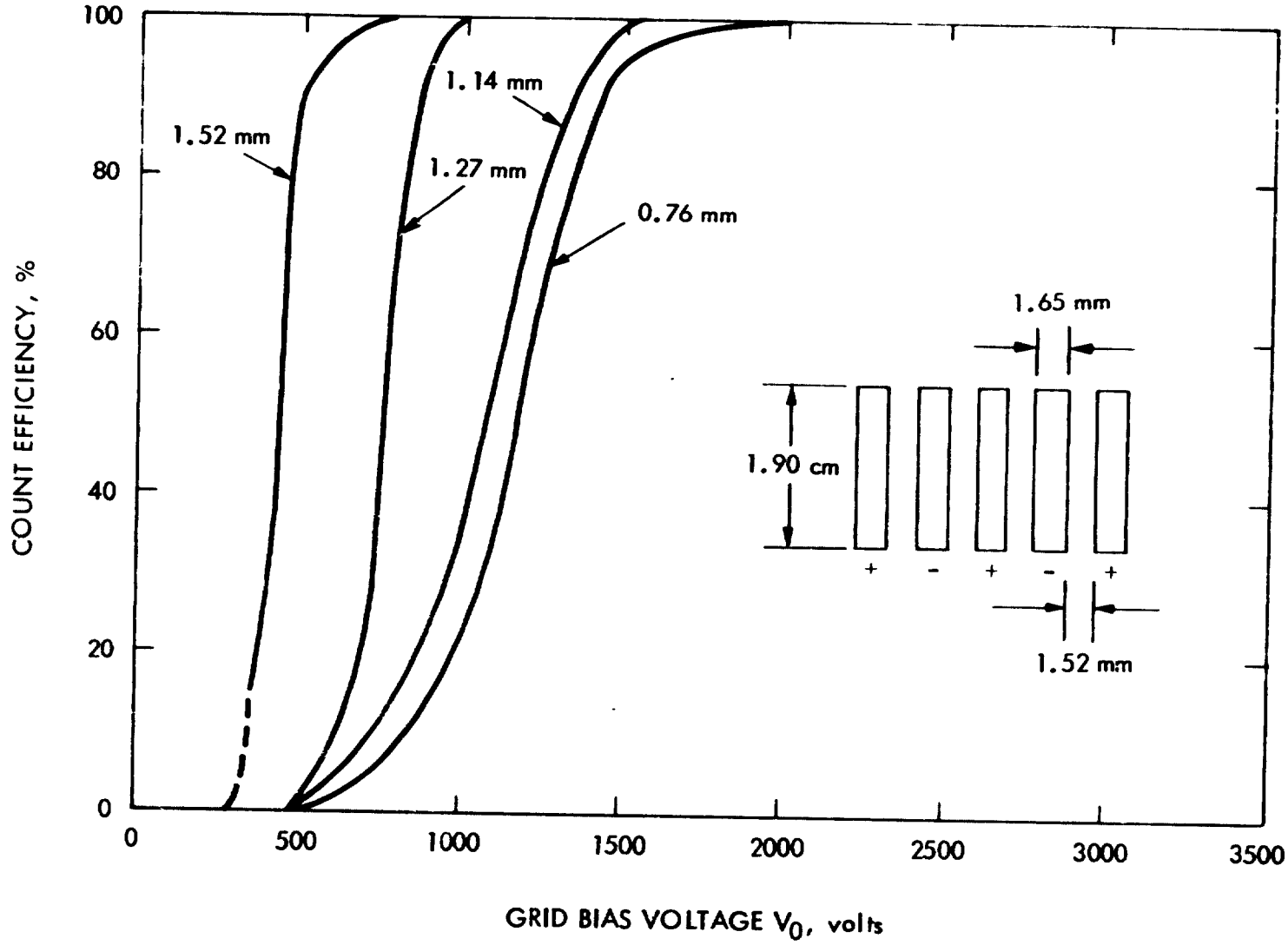

Fig. 26. Count Efficiency as a Function of Grid Bias Voltage with Fiber Length as Parameter for Strip-Electrode Experimental Grid No. 1 (1.52 mm grid spacing) (Variac Setting = 50 V rms)

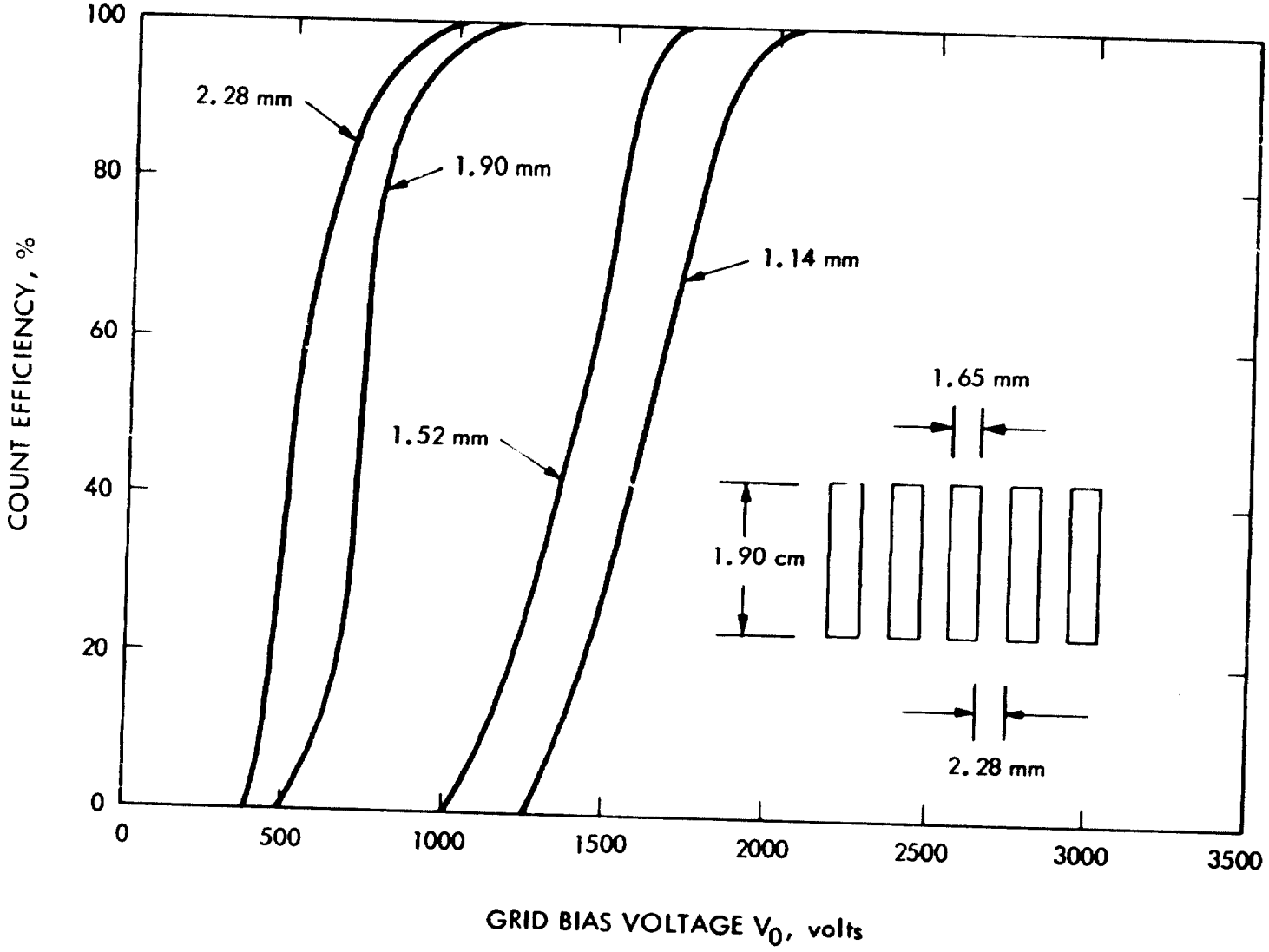

Fig. 27. Count Efficiency as a Function of Grid Bias Voltage with Fiber Length as Parameter for Strip-Electrode Experimental Grid No. 2 (2.28 mm grid spacing) (Variac Setting = 50 V rms)

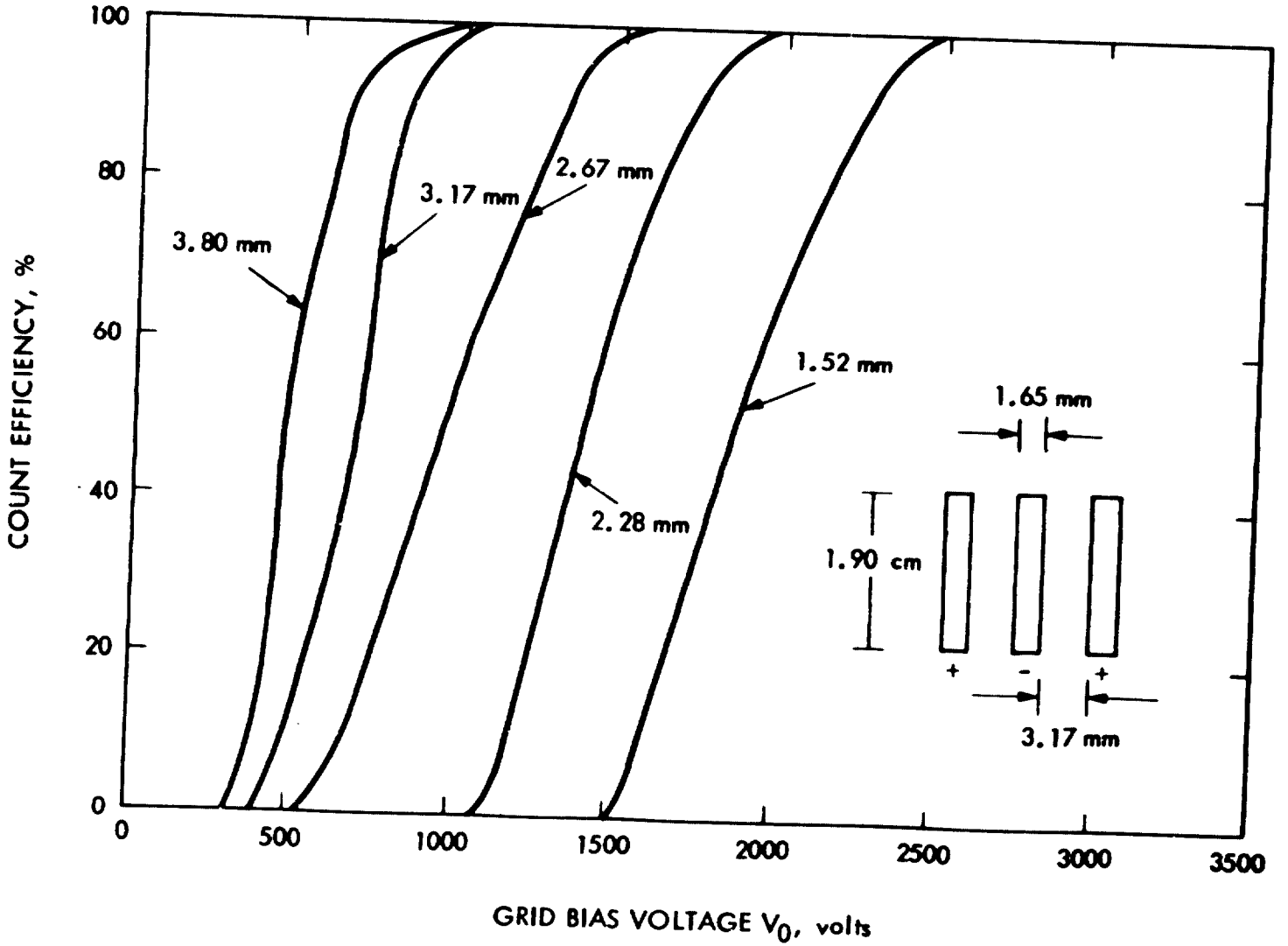

Fig. 28. Count Efficiency as a Function of Grid Bias Voltage with Fiber Length as Parameter for Strip-Electrode Experimental Grid No. 3 (3.17 mm grid spacing) (Variac Setting = 50 V rms)

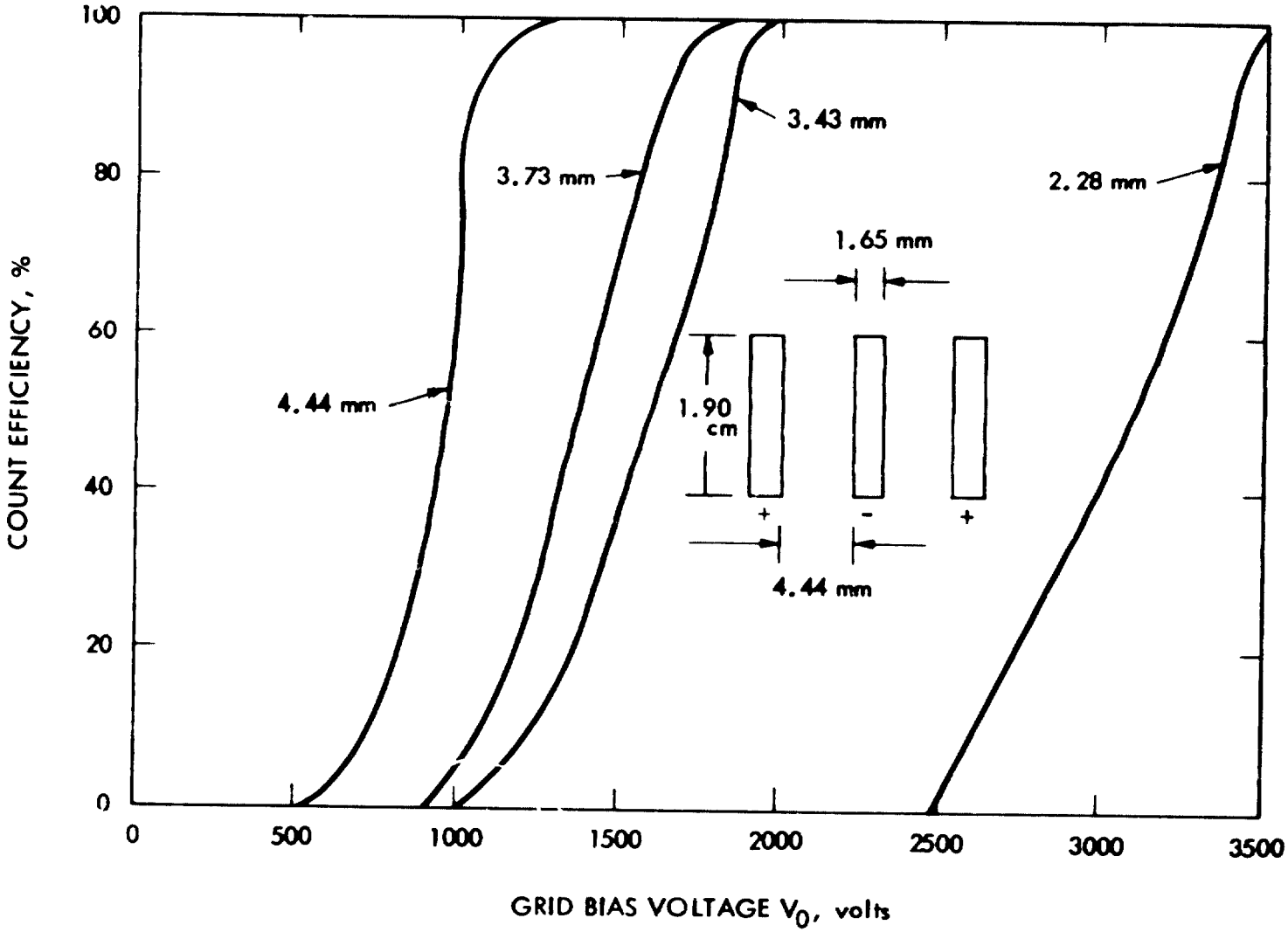

Fig. 29. Count Efficiency as a Function of Grid Bias Voltage with Fiber Length as Parameter for Strip-Electrode Experimental Grid No. 4 (4.44 mm grid spacing) (Variac Setting = 50 V rms)

voltages that can count fibers longer than 0.84 times the grid air gap spacing exist for the other three grids.

Figure 30 shows a plot of these optimized bias voltages as a function of the grid air gap spacing for the strip electrode grids. A straight-line curve was thus established for the design of grids used for fiber sizing measurements. From these data, the optimized grid spacing and bias voltage for detecting fiber fragments with lengths exceeding 1 mm, 2 mm, 3 mm, 4 mm and 5 mm are 1.19 mm, 2.38 mm, 3.58 mm, 4.77 mm and 5.97 mm; 510 V, 690 V, 870 V, 1020 V and 1200 V (as listed in Table 1). The grids were constructed according to these design parameters for field tests and delivered to the NASA LaRC.

These test results were obtained with the Variac setting of 50 V rms. This corresponded to air flow speeds of 1.52 m/s to 2.41 m/s (300 ft/min to 475 ft/min.) in the windboxes, depending upon the grid spacing. Limited tests at other Variac settings and air flow speeds were performed. The results showed that for a Variac setting between 40 to 60 V rms, the changes in flow rate in the windboxes were small and the counting efficiencies remained constant. Significant changes in these quantities started to occur when the Variac setting reached 75 V rms (air flow speed 4.1 m/s or 800 ft/min). Drastically changed counting efficiencies were observed when the Variac setting reached 90 V rms (air flow speed 4.5 m/s or 1100 ft/min).

The reason for this insensitivity of count efficiency to the air flow speed was due to the large depth of the grids, i.e., electrode depth of 1.9 cm (0.75 in.). A long electrode depth tends to offset the effect of high air flow speed so that a sufficiently long residence time to obtain a fiber count in the grid was always achievable.

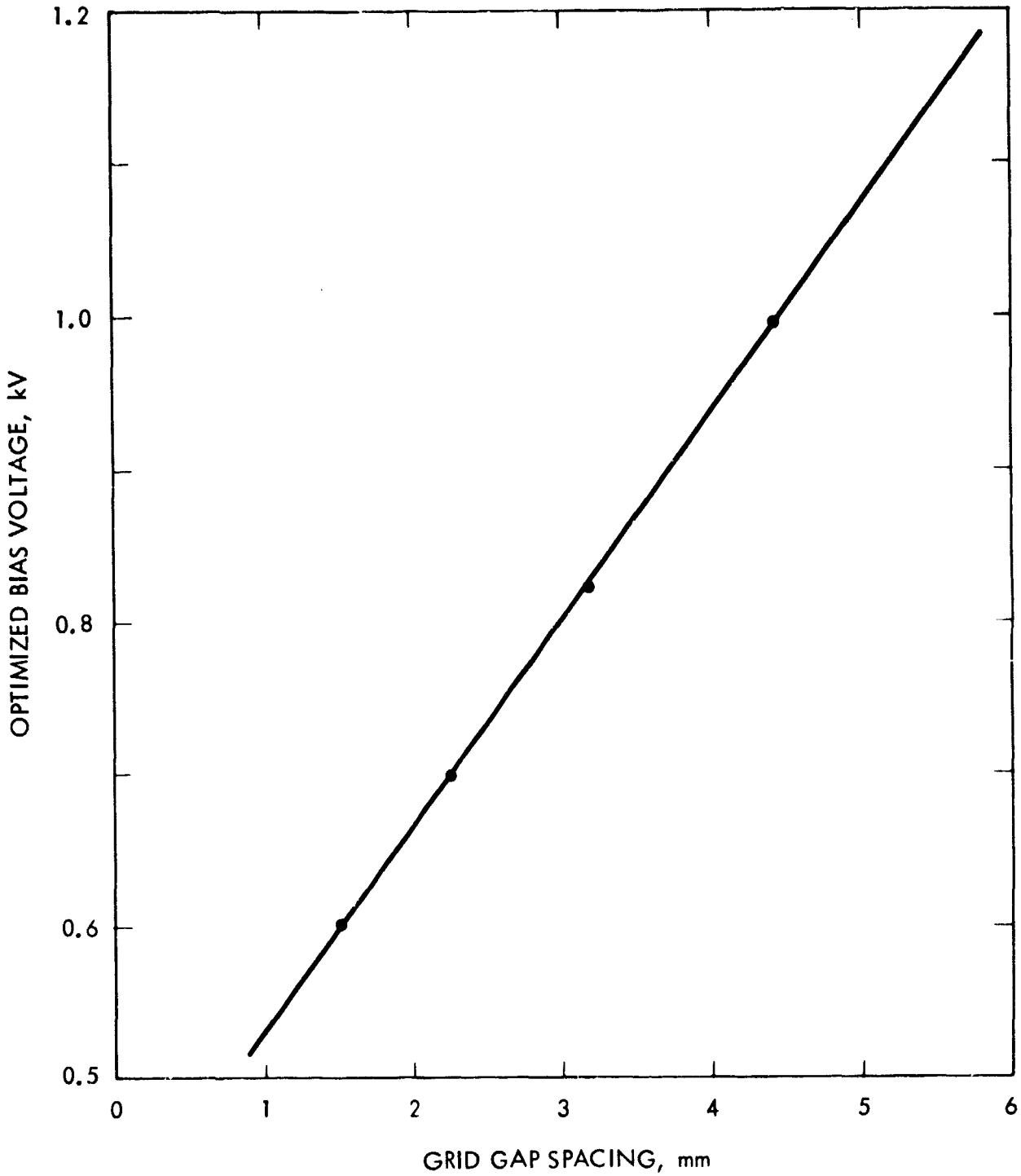

Fig. 30. Optimized Bias Voltage as a Function of Grid Spacing for the Strip-Electrode Grids

IX. DESCRIPTION OF HARDWARE

A. Grid

The construction of the grid is shown in a self-explanatory photograph in Figure 31. The strip electrodes were machined from 1.65 mm (0.065 in.) thick copper plates. They had step shoulders so that they could be pushed and registered in precise milled slots in the Micarta grid frame. One end of the plate had a small slotted tab to allow the soldering of bare copper wires to them to obtain the parallel voltage bias. All frames, except that for the No. 1 grid, were made from the Micarta. The No. 1 grid, due to its small electrode spacing, introduced considerable electrical conduction in the Micarta. The Micarta web spacer between the electrode plates formed by the slots had some porosity so that it could absorb considerable amounts of moisture and therefore created a leak current path between the electrodes biased at 500 V. Low insulation resistance (as low as 50 kΩ) was observed, which depended upon the humidity. This problem was resolved by using Teflon to fabricate the frame for the No. 1 grid. The fabrication procedure in this case was more involved, because Teflon is quite flexible and lacks mechanical stability.

It was also found that electrodes made from 1.65 mm (0.065 in.) thick copper plate were not very suitable for the fabrication of No. 1 grid. They created too much impedance to allow easy air flow through the grid-windbox assembly. Thinner copper plates of 0.5 mm (0.020 in.) thickness were used to fabricate the electrodes for this grid. A better flow rate through No. 1 grid was achieved this way.

B. Discharge Circuit

As explained previously, in order to minimize the inductance of the lead wires connecting the capacitor to the grid, the H.V. circuit has to be placed very close to the grid. The components of the circuit were contained in a small aluminum box in a very compact manner as shown in Figure 5. This approach allows one to directly attach the circuit onto the windbox. The circuit consisted of three 0.047 μF high-voltage capacitors (CDC PKM16S47, 1600 VDC rating) connected in parallel. The current limiting resistor was a 1 kΩ, 1 W Allen Bradley carbon resistor. It was chosen to act also as a safety component. In case the grid is short-circuited, i.e., by a fiber cluster, the continuous current passing through the resistor can cause the resistor to burn open, acting as a fuse. Thus, the charging of the discharge circuit will be terminated automatically.

The current shunt was made from a 0.1 Ω Delco precision resistor. It was connected to the PULSE-OUTPUT 50 Ω terminal via a 220 Ω precision resistor. The latter, combined with the 50 Ω load, formed a voltage divider, which reduced the output pulse amplitude by a factor of 270/50 = 5.4. The 220 Ω resistor can be replaced by a resistor of appropriate resistance, so that PULSE-OUTPUT amplitude can be modified to match the input requirement of a pulse integrator or other counting instrument. Under the designed arrangement, the amplitude of the pulse output was about -5 V for all five grids. These were appropriate for interfacing to the JPL pulse integrator.

The current shunt and the 200 Ω resistor were contained in a Pomona Electronics Model 2397 aluminum box. The purpose of this design was to isolate this part of the circuit from the main discharge circuit so that interference

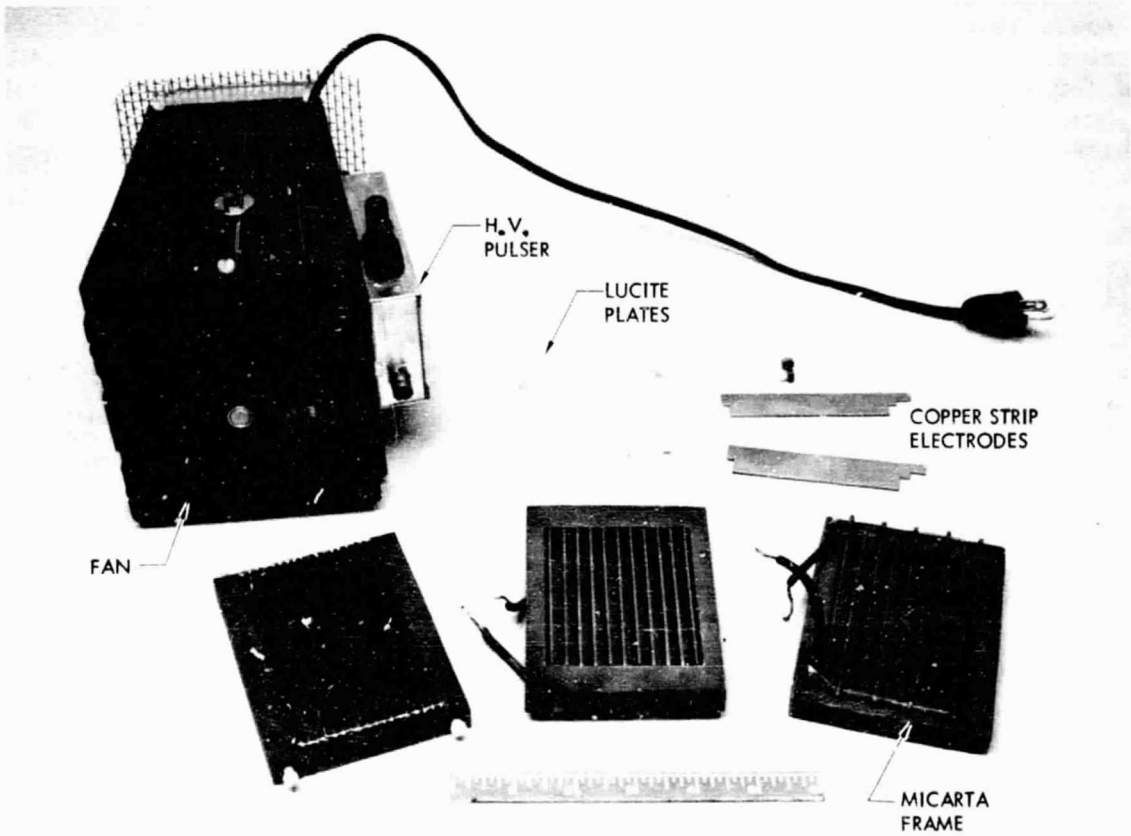

Fig. 31. The Design of the Grid and the Windbox

from the grid through a electromagnetic induction could be avoided. The pulse output amplitude so obtained has a quantitative meaning which can be used to calculate the discharge current in the spark.

C. Fan and Wind Speed

The fans used to construct the windbox were 14 watt Muffin fans manufactured by Rotron, Inc., and are commonly used for electronic equipment cooling. They had physical dimensions of 11.9 cm x 11.9 cm x 3.8 cm. The air flow speed in the windbox was measured by the technique described previously--by inserting a resistance flow rate probe (Hastings-Raydist Model AB-27) in the box as shown in Figure 10. The air flow speed as a function of Variac setting for the five grid-windbox assemblies is shown in Figure 32. These measurements were performed with negligible background air flow speeds. When there was a strong background air flow comparable to the zero background flow rate in the windbox, there was an add-on effect; i e., the apparent air flow speed in the windbox was increased. However, due to the impedance of the grid, the increases were much smaller than the direct arithmetical addition of these two speeds.

This is a good design feature of the JPL carbon fiber detection system. For small variations of the background air flow speed, the flow speed in the windbox can be considered constant. Some quantitative results are shown in Table 2.

A DC voltage-operated fan which has the identical physical dimensions as the AC Muffin fan is available commercially. It is manufactured by PAMOTOR, INC. and has a designation of Model 4124X. It has a 24 V rating and its rotational speed (therefore the air flow speed) is variable as controlled by the DC voltage. It can be handily used to replace the AC fan so that the system can be used in the field tests in which AC power is not available.

D. Pulse Integrator

Figure 33 shows the schematic diagram of the pulse integrator. It was fabricated on a single 10.1 cm x 10.1 cm printed circuit board. The letters X, Z, C, E, K and N correspond to the interface terminal locations on the board. The following is a brief description of the circuit features.

1) The incoming pulse signal from the H.V. discharge circuit is negative (-5 V, 0.5 μs). The function of the diode D_1 (1N5240B) is to eliminate any positive inputs and limit negative pulse amplitude to be not larger than -10 V in order to protect the IC CA555CG timer. The isolation capacitor C_1 further protects the IC from any DC voltages.

2) The timer IC CA555CG produces a +5 V positive square pulse upon receiving the trigger pulse, the spark signal. The duration of the square pulse is determined by the RC time of R_2 and C_2, the timing tank circuit. For the values of 9.1 kΩ and 0.01 μF shown in the figure, this duration was about 100 μs. Furthermore, the IC will ignore any trigger command during this period of time. The maximum pulse rate of the output under the arrangement is thus about 10^4 pulses per second. In this manner the IC acts as a pulse conditioner. Also, the longer pulse duration of the output pulse provides more electrical charge to increase the sensitivity of integration.

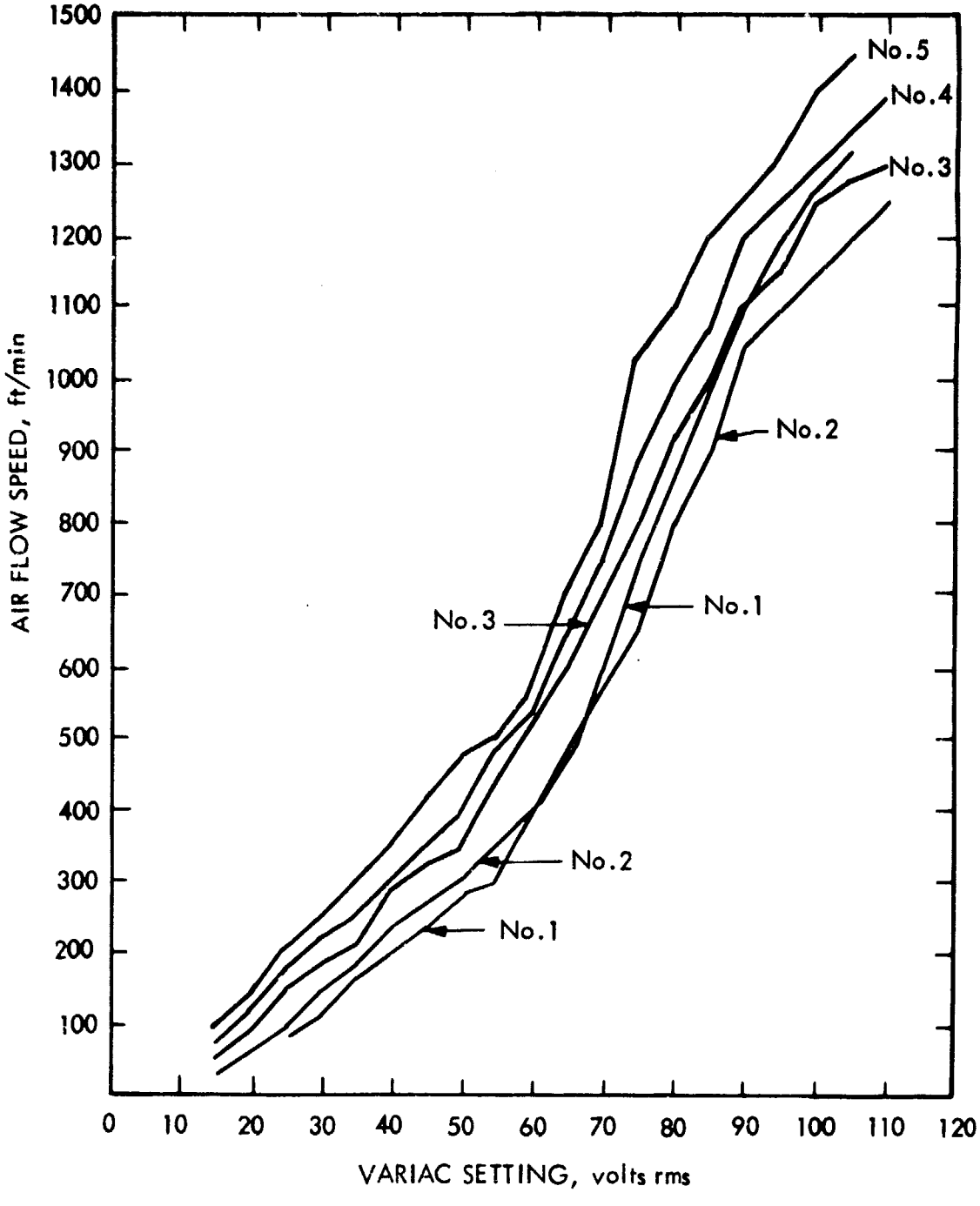

Fig. 32. Air Flow Speed as a Function of Variac Setting for the Five Prototype Strip-Electrode Grid-Windbox Assemblies

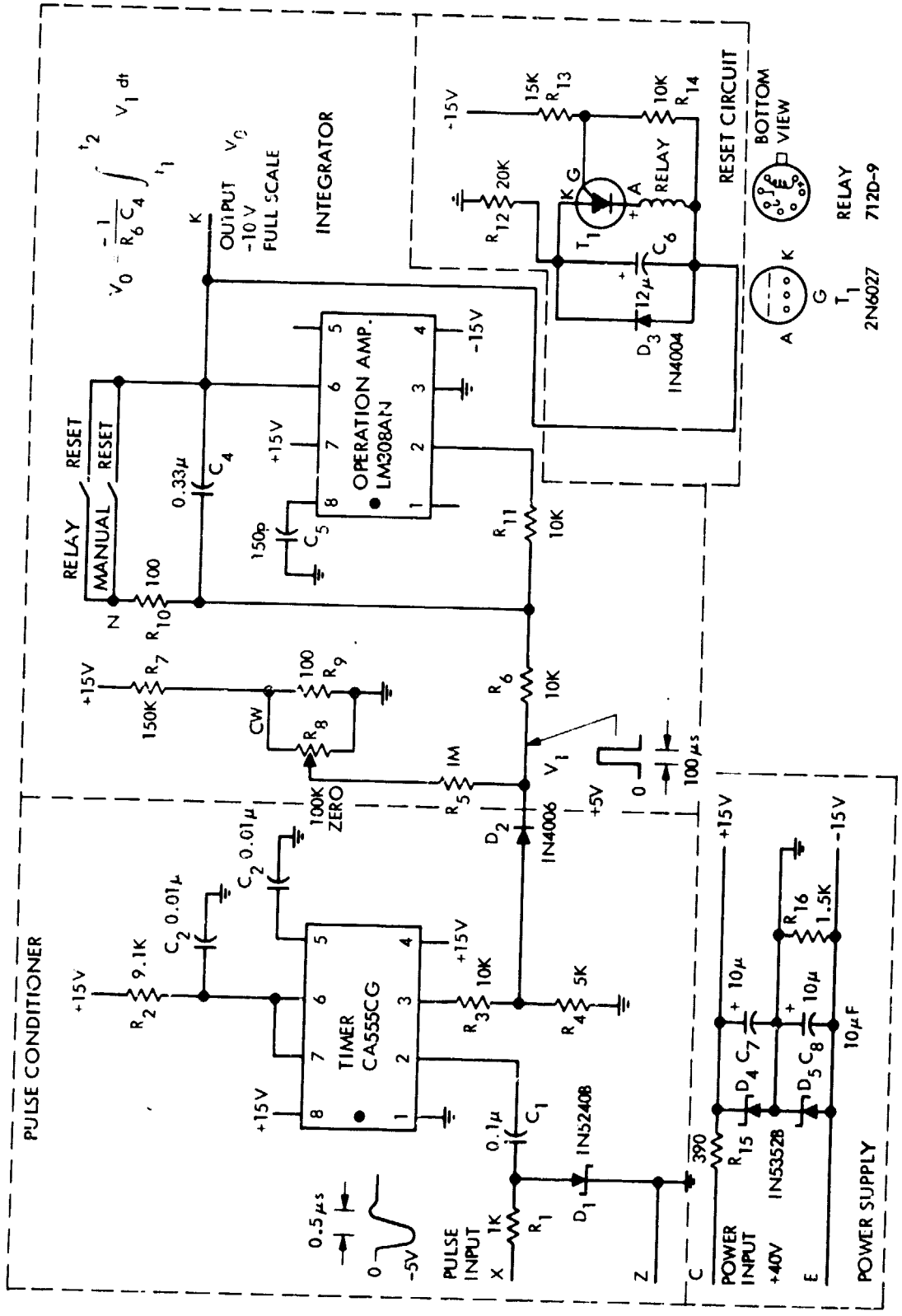

Fig. 33. Schematic Diagram of the Pulse Integrator

TABLE 2. Air Flow Speed in the Windbox (ft/min) as a Function of the Variac Setting and the Background Air Flow Speed

Grid No.	Variac Setting (Volts RMS)	Background Air Flow Speed (ft/min.) 0	100	150	200
1	0	-	5	20	40
	50	275	275	300	400
2	0	-	20	40	60
	50	300	310	340	450
3	0	-	45	60	100
	50	350	350	395	550
4	0	-	50	75	110
	50	390	390	450	550
5	0	-	55	85	120
	50	475	475	505	650

NOTES: 1) The small inconsistencies in this table are believed to be introduced by the poor resolution of the air flow meter readout.

2) Data shown in English units (rather than SI) because the flow probe reads only in these units.

3) The IC LM308AN is an operational amplifier. It integrates the output of the IC CA555CC timer and produces a negative output according to the following formula:

$$V_o = \frac{-1}{R_6 C_4} \int_{t_1}^{t_2} V_1 \, dt$$

The output can be nulled by either manually closing the push switch "RESET" which will discharge the integration capacitor C_4, or when the output reaches approximately -10 V. Then it will induce the avalanche conduction of the unijunction transistor T_1 (2N6027). This will in turn actuate the miniature relay Teledyne 712D-9 to discharge the integration capacitor C_4. The automatic reset voltage of -10 V was chosen in order to assure the linearity of the integration. The LM308AN was chosen over other similar operational amplifier IC's, such

as LM108AN, because it possesses a greater temperature stability and is readily available.

4) Severe drift of the integrator output normally exists due to the leakage in the IC CA555CG. The purpose of the diode D_2 (1N4006) is to isolate this effect from the integrator. The remaining minor drifts in the output, due to the current leakage through the diode D_2 and the LM308AN itself can be compensated for by a small controlled leak current provided by the potential divider formed by the resistors R_7 and R_9 and the 100 kΩ potentiometer R_8 via a high impedance resistor R_5 (1 MΩ). Depending upon the temperature environment, output drift can be alleviated by adjusting R_8, the "ZERO" adjustment. Output stability of the order of 0.1 V per hour can be achieved this way. The test setup for one grid is shown in Figure 34.

5) The isolated circuit showed in the lower-left corner of the circuit diagram (Figure 33) is a regulated DC power supply. The zener diodes D_4 and D_5 and the capacitors C_7 and C_8 convert the input DC voltage ranging from 35 V to 45 V into a regulated +/-15 V output, for the power source for the entire integrator circuit. This design allows for the use of a battery power supply for field tests in which AC power may not be available.

6) The sensitivity of the circuit, i.e., the output voltage increments per each occurrence of the input-pulsed trigger signal, was approximately -0.1 V/pulse. Since the maximum magnitude of the output voltage was about -10 V, this sensitivity gave about 100 input pulses for the full output range of the pulse integrator. The calibration can be easily performed by incorporating a pulse generator, which can provide a pulse of -5 V in amplitude and 0.05 μs to 0.5 μs in duration, to the input of the pulse integrator. The generator could be a low-repetition rate unit or even a manually commanded pulser. The sensitivity factor can be changed to other values suitable for the carbon fiber counting at different exposure rates. This can be accomplished by one of the following two simple modifications of the circuit: (1) Change the value of the capacitance of the integration capacitor C_4, or (2) change the RC time constant of the timing circuit of the IC CA555CG as described previously (i.e., change the value of R_2 and/or C_2). Experience has shown that with the designed 0.1 V sensitivity, the integrator is suitable for use for most tests in which counting of carbon fiber fragments is necessary.

7) The output power of the integrator is self-regulated. Therefore it can be used to interface with most recording instruments such as a chart recorder, an oscillograph, a Simpson meter or a vacuum tube voltmeter.

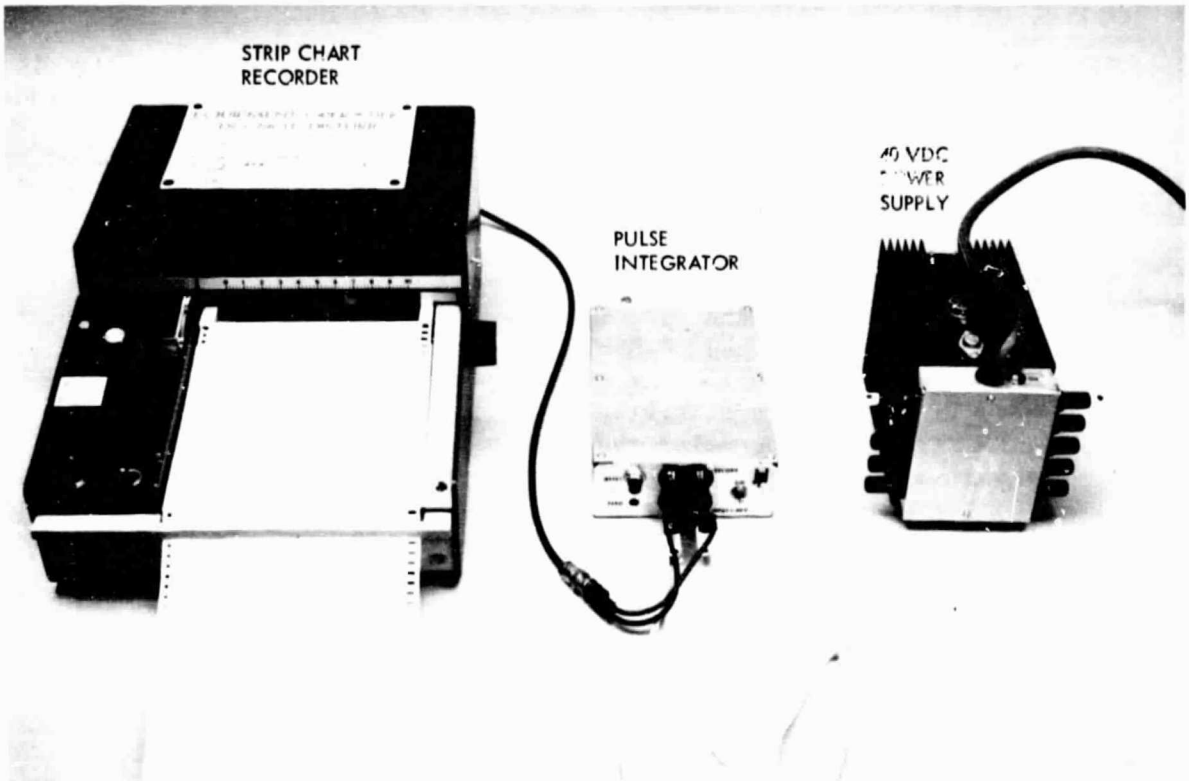

Fig. 34. Pulse Integrator Stability Test Setup

X. APPLICATIONS

A. JPL Chimney Test

Independent of the carbon fiber detection instrument developments, JPL also worked on carbon fiber gasification. The objective of the assignment from NASA HQ was to study the effect of catalysts on enhancing the consumption of carbon fibers in a fire of carbon fiber composites. The test method has been described previously, i.e., a small amount of carbon fiber composite fabricated from catalyst-treated carbon fibers was burned under a glass chimney with the aid of a propane flame. The composite piece was mounted on a mechanical vibrator which can generate agitation up to 100 Hz and about 1 g of peak acceleration. The H.V. grid was mounted on top of the chimney to detect the fiber fragments released from the fire as they were carried upstream by the convection of the hot air. Figure 35 shows the typical result. The untreated fiber composites had large fiber counts. The full scale was about 250 counts. On the other hand, catalyst (calcium acetate 2% to 10% wt)-treated fiber composites did not cause any significant fiber counts.

The H.V. grid detection system can be applied to many research projects in which fiber release or consumption mechanisms are being studied. The instrument can directly provide information on the fiber fragment release rate, therefore it is also beneficial to the understanding of the fiber release chemical reaction kinetics.

B. Ames Box Test

JPL has modified the widely used laboratory carbon fiber composite burner developed by the NASA Ames Research Center (Reference 6). A grid equipped with its associated H.V. discharge circuit was mounted in line with the vacuum exhaust of the box (see Figure 36). The system was used to test the gasification of carbon fiber with catalyst treatments. Results similar to the JPL chimney tests were verified. Later, it was used to obtain information on the capture efficiency of the sticky tape. Sticky tape cylinders (13 mm in diameter and 40 mm long, Reference 1) were mounted in front of the grid so that the exposure measured by both systems could be directly compared. Preliminary results indicated that the capture efficiency of the tape was low, ranging from 5% to 10% (depending upon the fiber length and the air flow rate) for nominal air flow rate of 0.5 to 2 m/s in the grid.

C. Dahlgren Shock Tube Test No. 52 (Aug. 22, 1979)

The description of this test and the test facility is included in References 1 and 2 . The tube was a 7.3 m (22 ft.) diameter, 244 m (800 ft.) long tunnel made from cast steel. The carbon composite, about 10 kg (22 lb.) in weight, was burned at the open end of the tube with the aid of about 302 liters (80 gallons) of jet fuel. The plume and carbon fiber fragments released from the fire were caused to flow toward the other end of the shock tube by the flow induced by a number of large fans installed at this end.

The flow pattern and the fiber flux field were relatively uniform in the center of the tube where electronic equipments were exposed to determine the critical failure exposure. In Test No. 52, the equipment under test was commercial audio amplifiers. They were placed on the left-hand side of a wooden platform across the center of the shock tube and at about 244 m downstream from

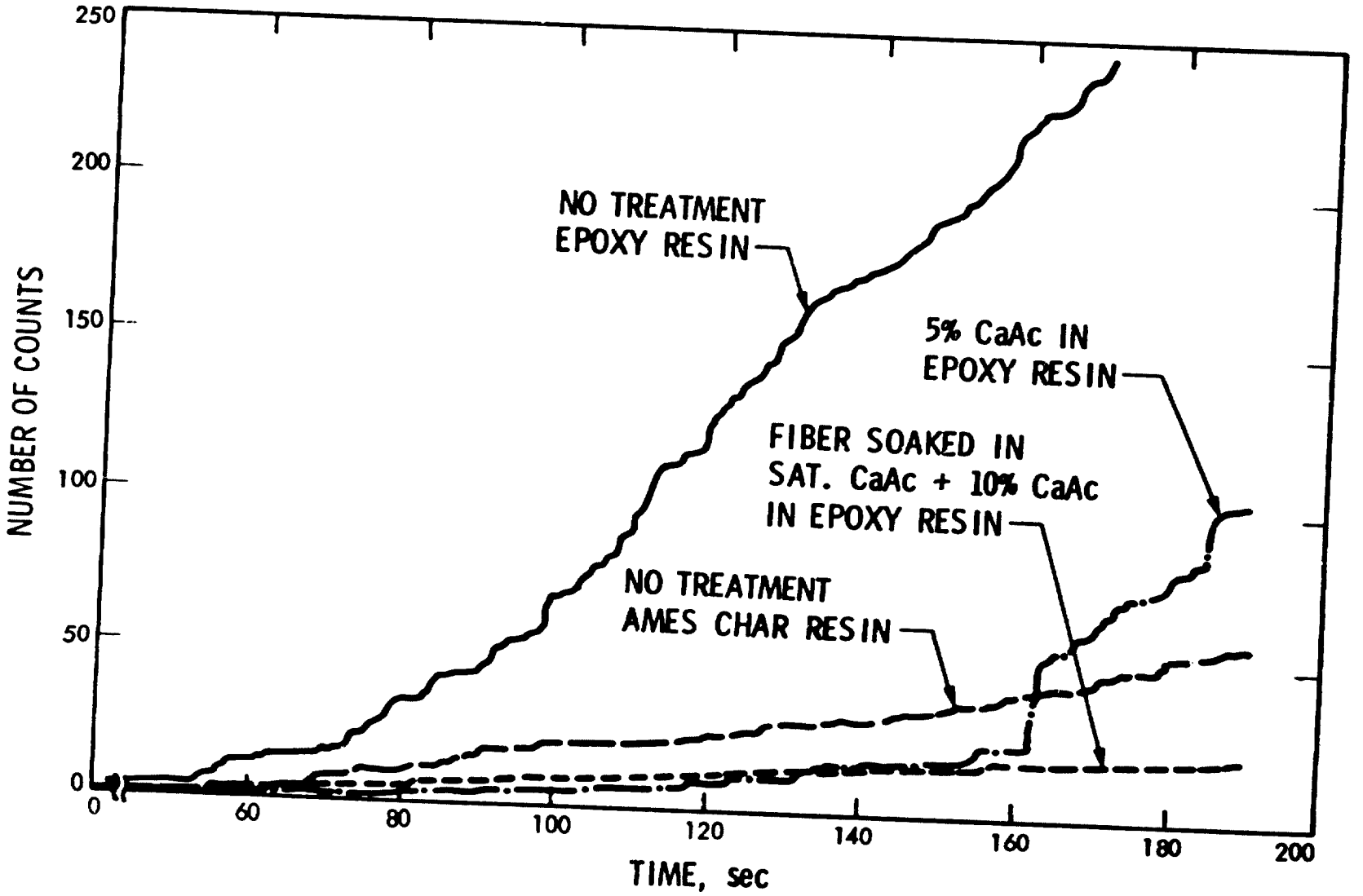

FIGURE 35. Typical Test Result of JPL Catalyst-Enhanced Carbon Fiber Gasification Project

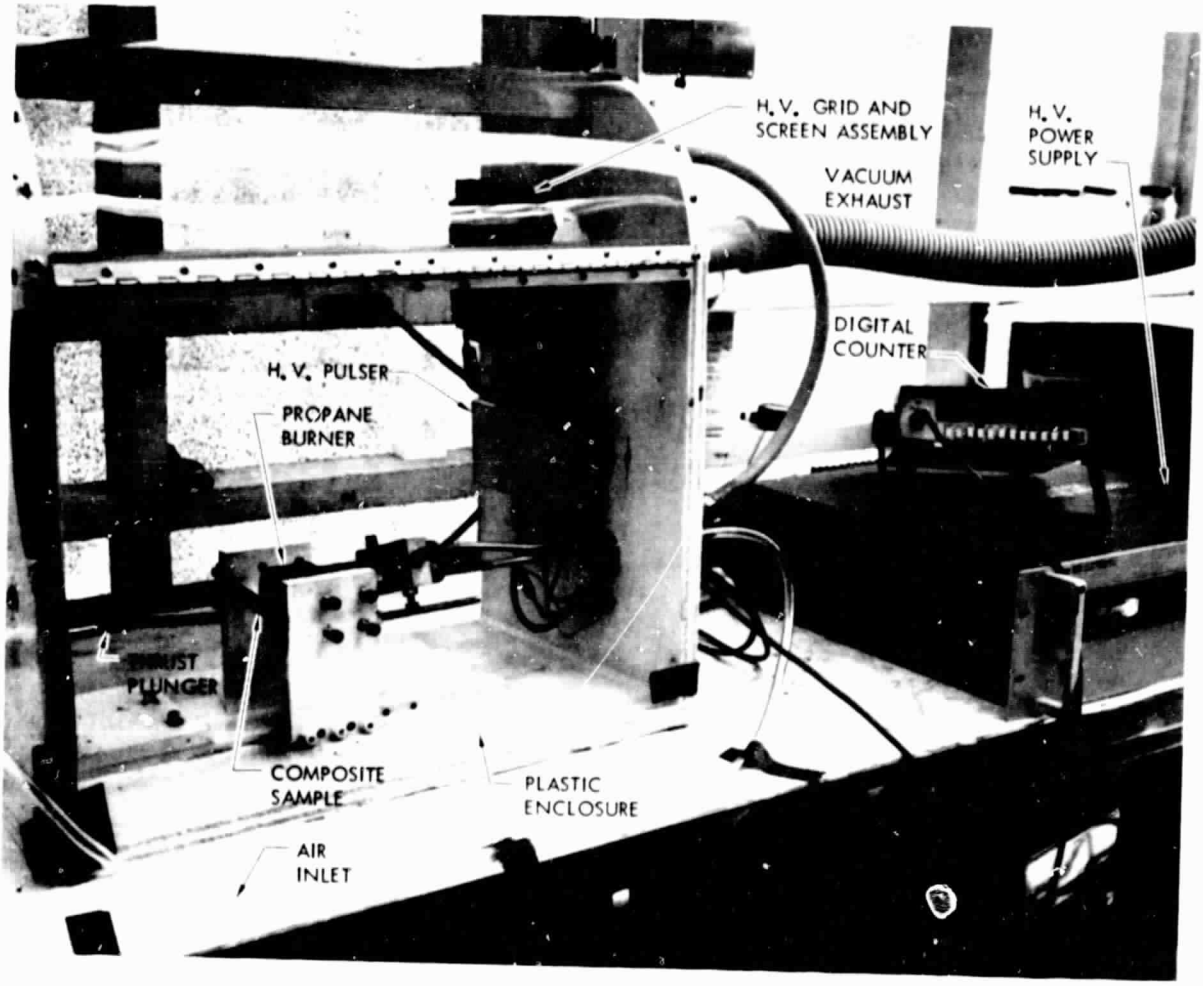

Fig. 36. Ames Carbon Fiber Burn Box Test Equipped with JPL H.V. Grid Fiber Counter

the fire. The JPL H.V. grid-windbox assemblies were placed on the right-hand side of the platform (Figure 37). Also seen in the same figure, in front of the platform, was a wooden stand upon which the Bionetics grid counter and the TRW optical counter were supported.

The top view of the layout of the JPL H.V. grid carbon fiber counters is shown in Figure 38. The five-channel output H.V. battery pack was connected to the five H.V. discharge circuits on the grid-windbox assemblies by insulated lead wires. The pulse signal output of the discharge circuits were conveyed by 26.6 m (80 ft) long RG58C transmission cables to an instrumentation trailer stationed outside the shock tube. The pulse integrators and recorders were stationed inside the trailer.

Figure 39 shows the raw data as recorded by several strip chart recorders. It plots the number of fiber counts received by each grid as a function of time. The time zero was the time when the fire was first established in the pile of carbon fiber composites. For a period of five to six minutes, no counts in the grids were observed. This was an indication that the air flow speed in the shock tube was of the order of 0.6 to 0.76 m/s (120 to 150 ft/min), because the distance between the fire and the grids was about 244 m (800 ft).

The total counts increased rapidly with the time at nearly constant rates. The count rates slowed down between the 17th and 27th minutes. At the later time, a mishap occurred: the rotary metal basket in which the carbon fiber composites were held broke loose from its axis of rotation. It fell down on the floor of the shock tube. This induced a fast fiber release in the time period of 27th to 37th minutes. After that, the count rate slowed down once again. The test was terminated at the 45th minute. Continuous counting after that time showed a very small number of fiber counts.

The data reduction proceeded as follows:

1) Convert the counts f_i obtained by the grid number i to the exposure e_i by using the formula which defines e_i:

$$e_i = \frac{f_i/A_i}{v_i}$$

where

A_i = the area of effective aperture of the grid number i (m^2)

v_i = the air flow rate in the windbox number i (m/s)

The zero background air flow speeds at 50 V rms drive voltage for the fan are listed in Table 1. Flow speeds for Variac settings other than 50 V rms are shown in Figure 32. To account for the add-on effect of the background air flow speed, values of the flow speeds extrapolated from Table 2 were used.

2) The next step is to perform some simple arithmetical manipulations to account for the multiple counting effect due to long fibers. Obviously, if a fiber is much longer than the grid spacing upon which it landed, then several spark counts will be generated by the same

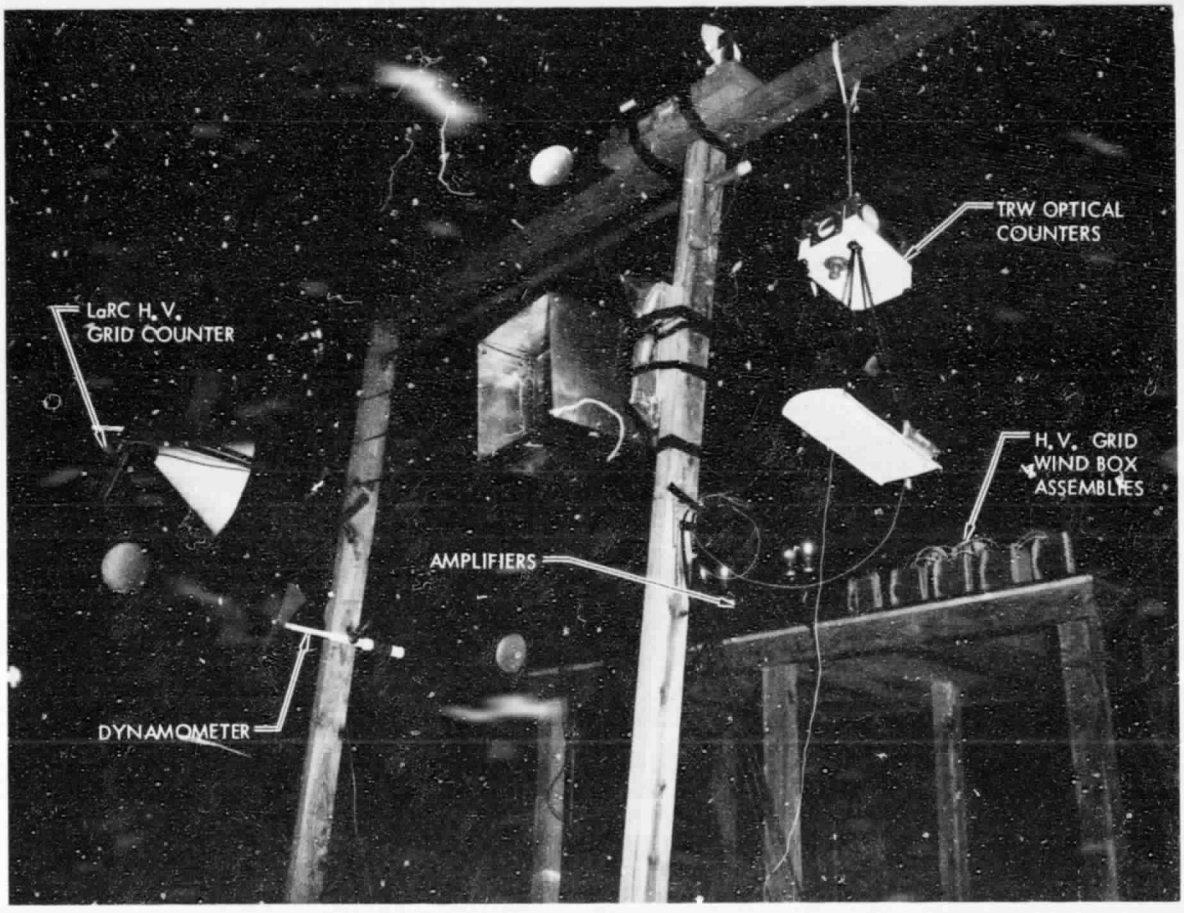

Fig. 37. JPL H.V. Grid Spark Carbon Fiber Counters Layout on the Test Platform in the Dahlgren Shock Tube Test No. 52

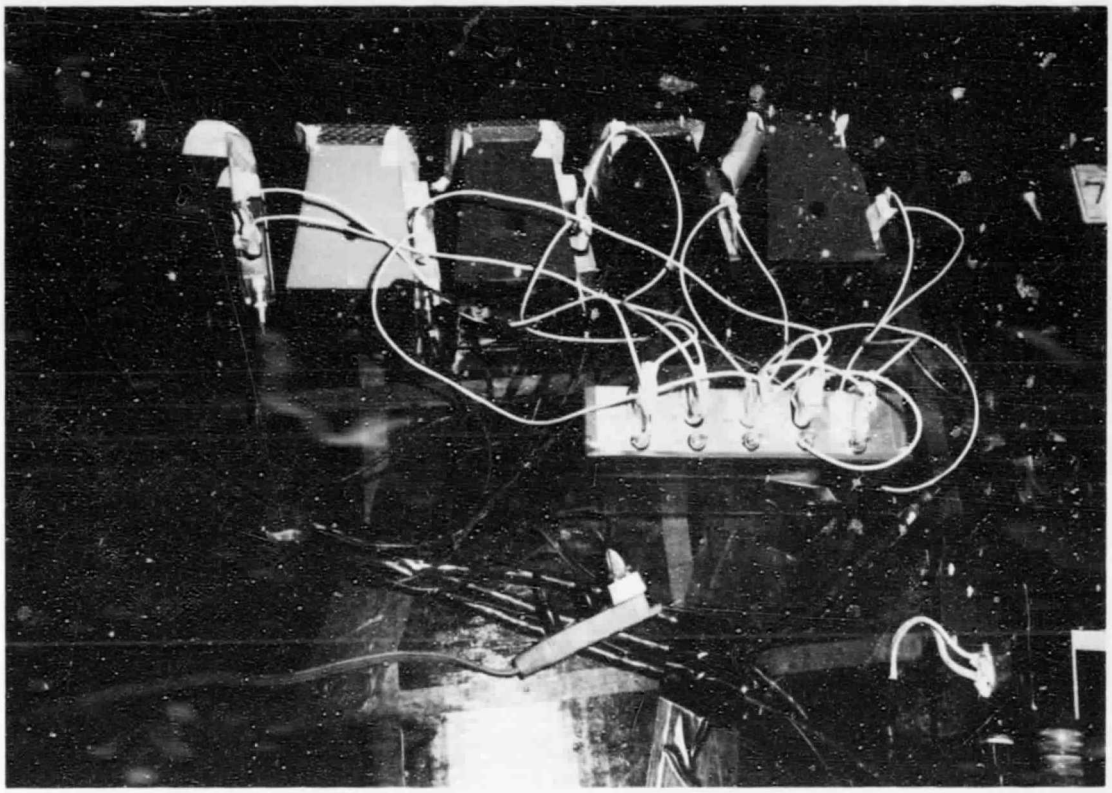

Fig. 38. Top View of the Layout of JPL Spark Carbon Fiber Counters in the Dahlgren Shock Tube Test No. 52

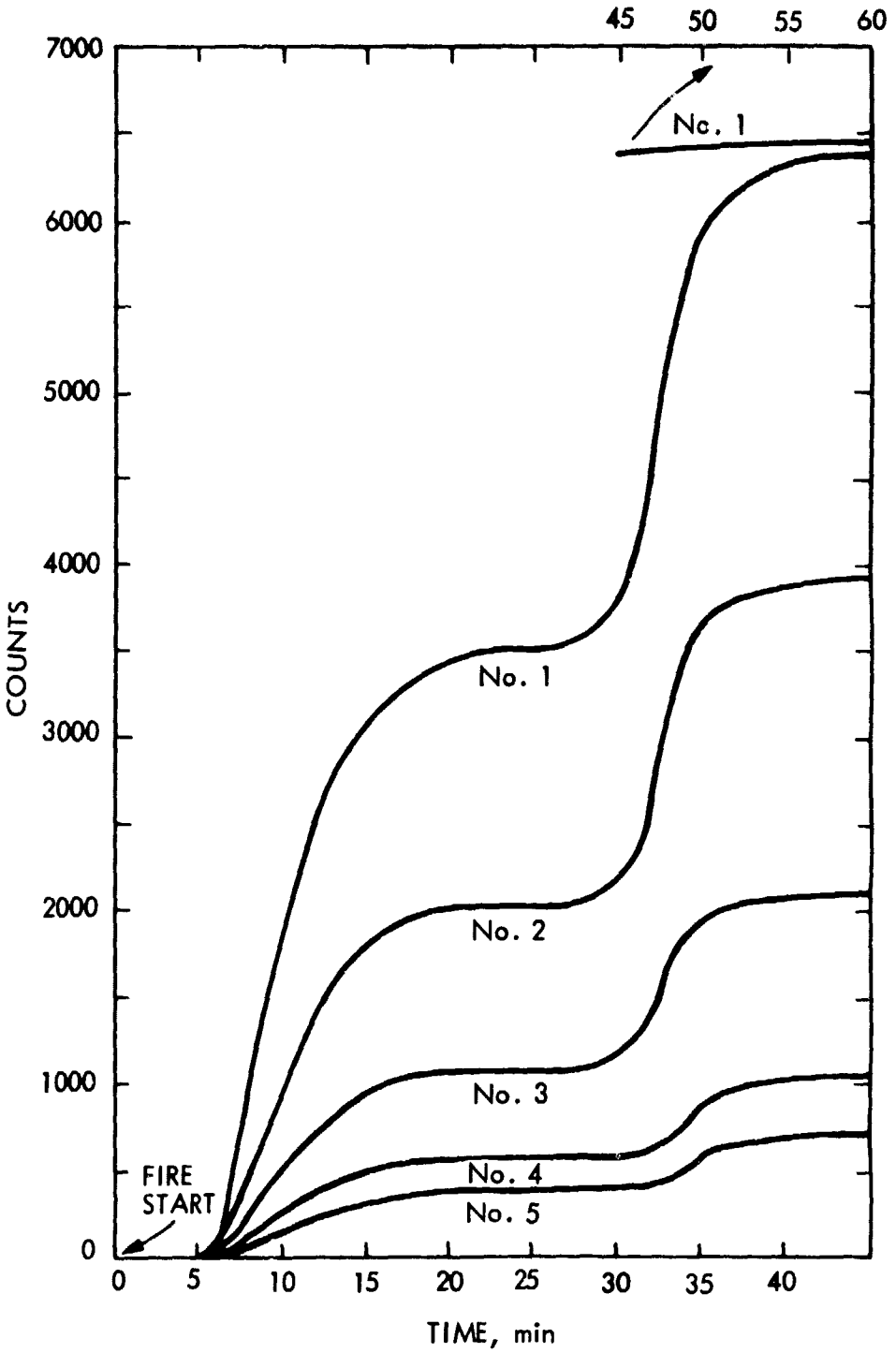

Fig. 39. Dahlgren Shock Tube Test No. 52 Results as Recorded by the JPL H.V. Grid Spark Carbon Fiber Counters: Total Counts as a Function of Time

fiber. With prescreens installed in front of the grids to reduce the chance of fiber clusters as well as long fibers from reaching the grid, the manipulations proceed as follows:

E_5 = exposure due to fibers 5 mm tc 10 mm in length
$= e_5$
E_4 = exposure due to fibers 4 mm to 5 mm in length
$= e_4 - e_5$
E_3 = exposure due to fibers 3 mm to 4 mm in length
$= e_3 - e_4$
E_2 = exposure due to fibers 2 mm to 3 mm in length
$= e_2 - E_3 - 2e_4$
E_1 = exposure due to fibers 1 mm to 2 mm in length
$= e_1 - E_2 - 2E_3$

The multiplication coefficients were determined empirically from the experiments. For instance, when a fiber 4 mm to 10 mm in length was injected into the grid No. 2 with the prescreen installed in front of it, usually an average of two counts was recorded. A fiber 3 mm to 4 mm long usually will cause two counts in the No. 1 grid. A simple computer program included in Appendix B can be used to perform these calculations and plot the results.

The test data of the Dahlgren shock tube test No. 52 after this data reduction procedure are shown in Figure 40. These values of exposure were about one order in magnitude higher than those measured by the sticky tape used in the same test which was placed near the wooden platform. Later, as has been mentioned previously, it was found that the tape has very poor fiber capture efficiency, of only about 5% to 10% at the air flow speed of several meters per second. Our data were essentially in agreement with the Bionetics grid system, if a corrected air flow speed is used in the data reduction of the latter results.

D. Soot Effects on the Grid Counting - Dahlgren Shock Tube Test No. 54 (Sept. 26, 1979)

In a simulated aircraft fire test in which carbon fiber composite is being consumed by a jet fuel fire, a large amount of soot is produced by the fuel as well as by the epoxy resin in the composite. The soot seriously impacts the accuracy of an optical fiber counting system since the cross section of a soot particle may be much larger than that of a fiber fragment. It was wondered what would be the effect of soot on the H.V. grid fiber counting system.

In the laboratory, it was soon found that soot produced by a propane or kerosene flame did not generate spark counts in the H.V. biased grid. One can observe this by directly impinging a propane or kerosene flame onto the grid (Figure 41). The soot produced by the epoxy can initiate some spark counts in the grids with small grid spacing, especially the No. 1 grid (Figure 42). Small-scale burn tests of glass fiber composite made from epoxy, performed in the Ames box equipped with H.V. grid, have shown that the soot-induced counts were less than 1% as compared to the counts due to carbon fibers released from a carbon fiber composite of the same resin/fiber ratio composite.

Apparently, the soot particles produced by the epoxy had poor electrical conductivity, therefore they were very inefficient to initiate sparks in the

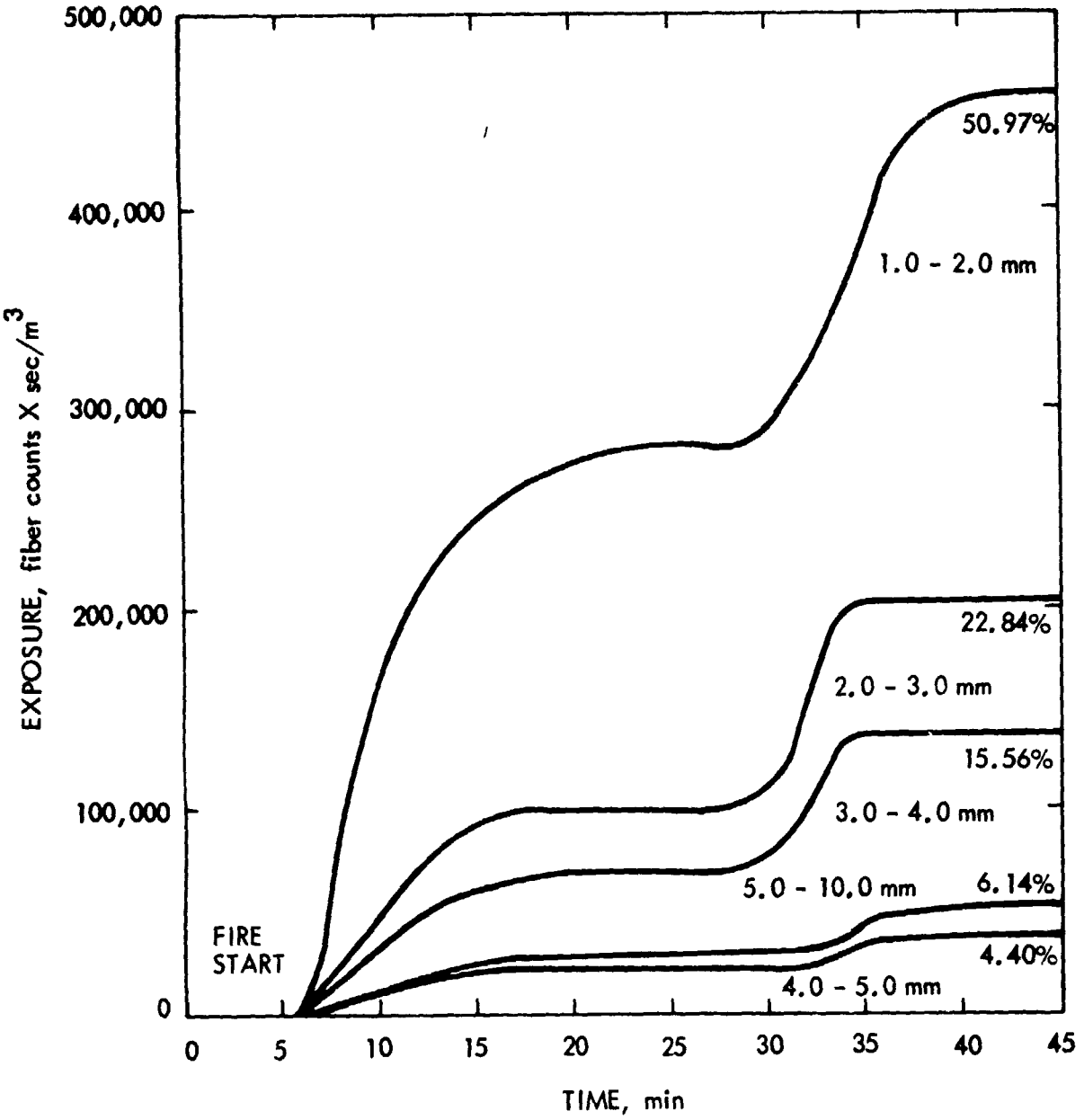

Fig. 40. Dahlgren Shock Tube Test No. 52 Results as Generated by the JPL H.V. Grid Spark Carbon Fiber Counters Data: Exposure as a Function of Time

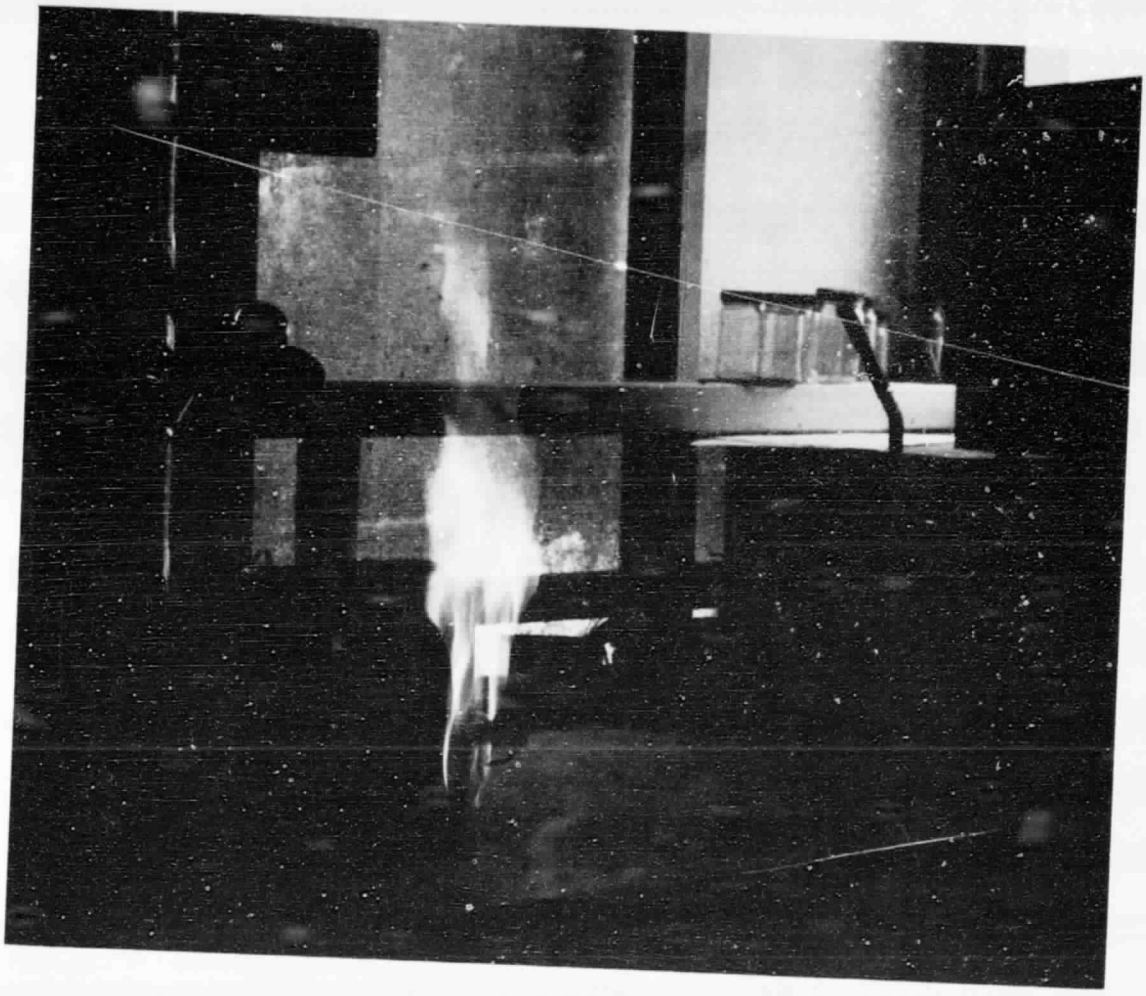

Fig. 41. Soot Effect on the JPL H.V. Grid Spark Carbon Fiber Counter, Tested by a Kerosene Flame

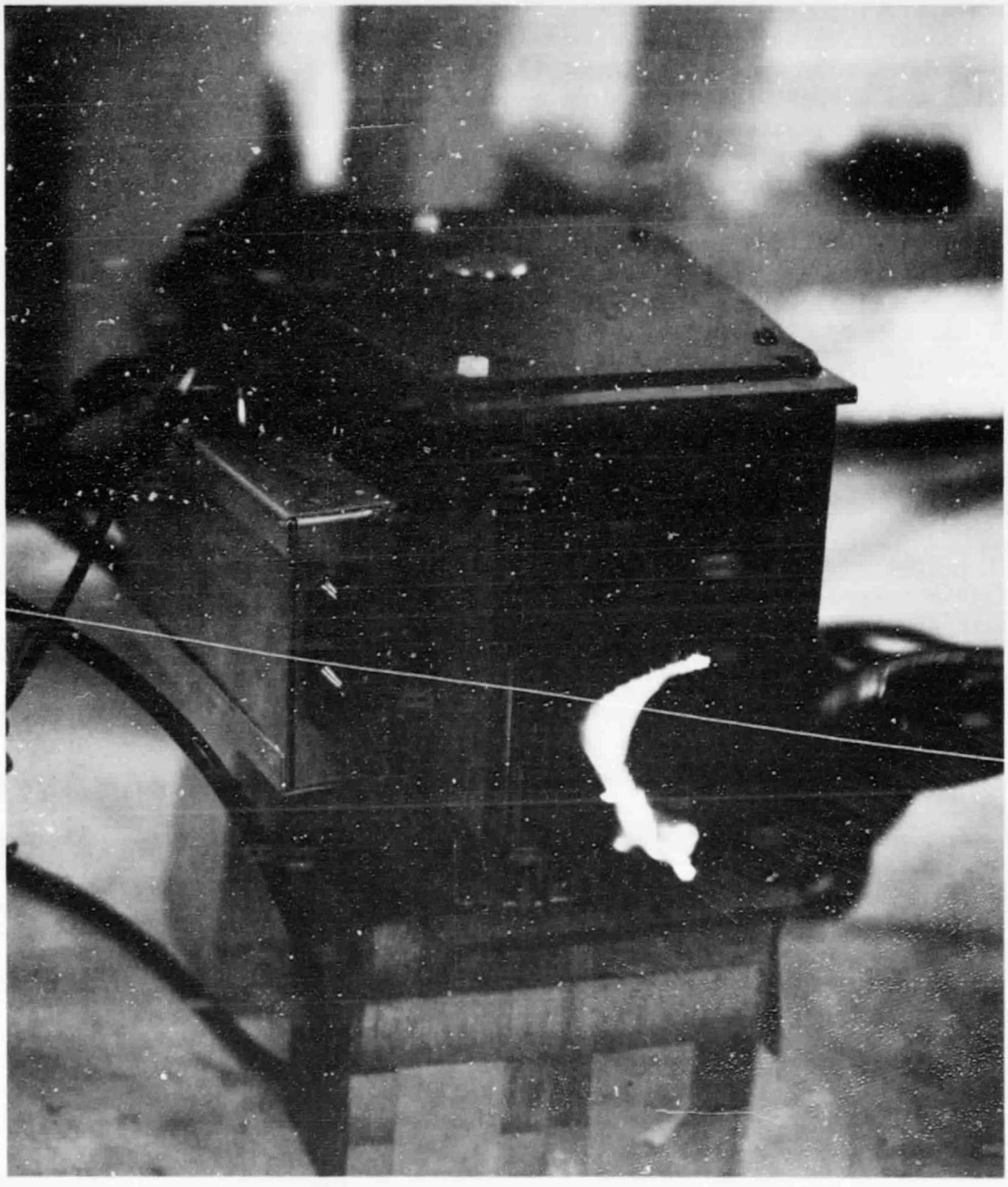

Fig. 42. Soot Effect on the JPL H.V. Grid Spark Carbon Fiber Counter, Tested by an Epoxy Resin Flame

grid. Larger soot particles were more potent in the initiation of sparks. The ability of a soot particle to initiate the spark was a random phenomenon. After the soot was collected for about 15 minutes and then fed through the grid, its ability to generate sparks in the grid decreased drastically, possibly due to the loss of water content from the soot particle.

In order to clarify these uncertainties, a test was performed in the Dahlgren shock tube facility. About 13.6 kg (30 pounds) of fiberglass epoxy composite was burned with the aid of a jet fuel. The test configuration for the grid system was the same as in the Test No. 52 (Figure 43). Figure 44 shows the test results. It can be seen that grid No. 1 (the 1 mm grid) had the highest soot count registrations. Grids No. 2 and 3 had minor soot counts. Grids No. 4 and No. 5 had no counts at all, therefore no data are shown in the figure. Comparing this with the Test No. 52 data shown in Figure 39, one can conclude that the interference of the soot on the H.V. grid count accuracy was less than 1%. One should also note that Test No. 52 burned for only 45 minutes while Test No. 54 had a burn time of 105 minutes.

Post-test examination of the grid from both Dahlgren tests showed heavy soot deposits (coatings). However the grid bias voltages used, ranging from 510 V to 1200 V, depending on the grid spacing, were sufficiently high to overcome the contact resistance problem. Thus, spark and counting could be reliably initiated by the carbon fiber fragments.

A better understanding of the air flow speed in the shock tube was obtained. The Hastings-Raydist air flow gage (Model AB-27) was used to measure the flow speed in the tube. The gauge was located near the main downstream view port of the shock tube and was about 0.6 m (2 ft.) away from the wall of the tube as shown in Figure 45. The air flow speed history during the test was as follows:

TIME (min)	FLOW RATE (ft/min)
-5	120
0	180
9	100
30	110
39	130
54	120
79	145
93	130
102	130
135	185

Therefore during the major part of the test the air flow speed in the shock tube was about 0.6 m/s (120 ft/min).

Fig. 43. Dahlgren Shock Tube Test No. 54, Test Layout of JPL H.V. Spark Carbon Fiber Counters

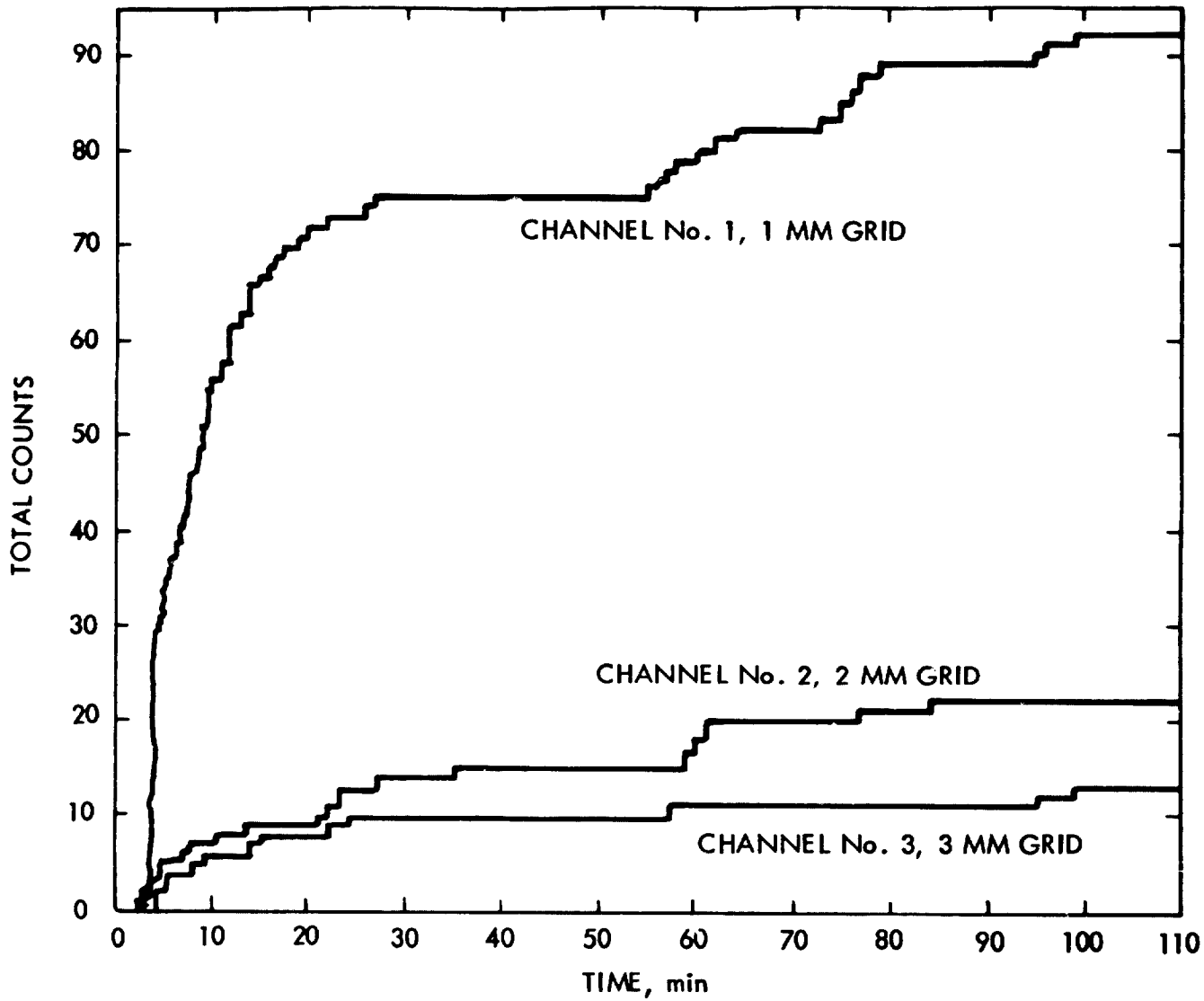

Fig. 44. Dahlgren Shock Tube Test No. 54, Counts Generated by the Soot as Recorded by the JPL H.V. Grid Spark Carbon Fiber Counters

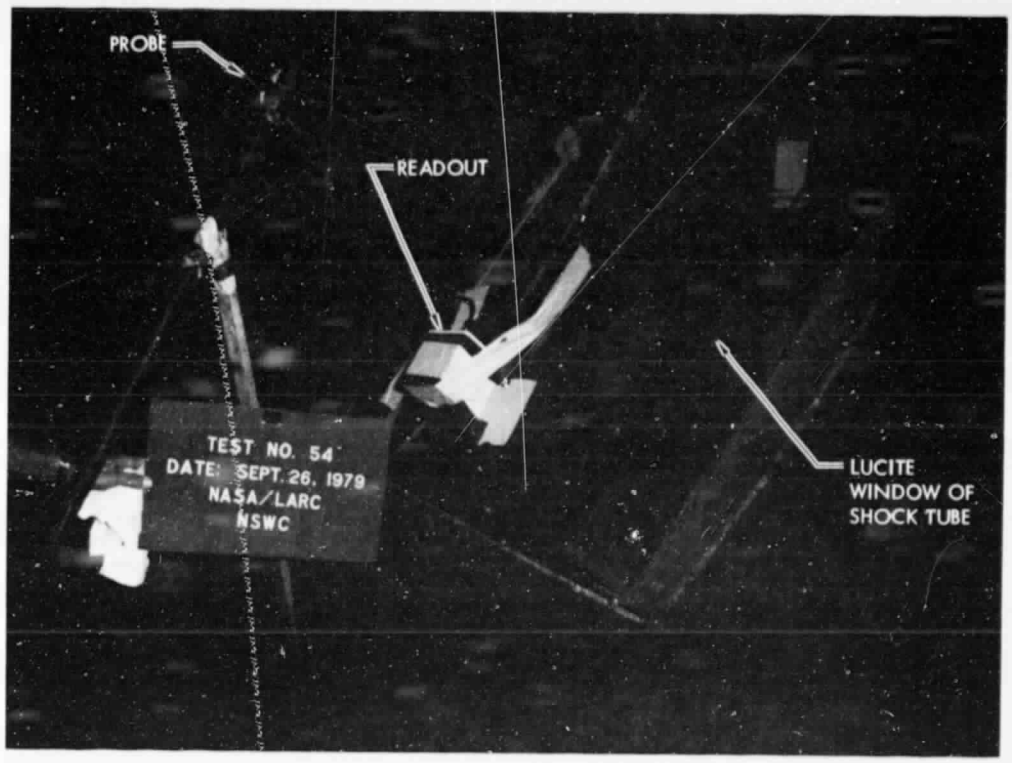

Fig. 45. Test Setup of Hastings-Raydist Air Flow Gauge (Model AB-27) in Dahlgren Shock Tube Test No. 54

XI. CONCLUDING REMARKS

In this project we have successfully accomplished the following tasks:

1) We have achieved a general understanding of the carbon fiber-initiated spark phenomenon across a H.V. biased grid.

2) We have obtained sufficient data for the optimized design of a H.V. spark carbon fiber counting and sizing system.

3) We have developed prototype hardware and demonstrated their satisfactory performance in a number of laboratory and field tests.

The current system is suitable for the majority of test needs of interest to NASA, i.e., for monitoring the fiber exposure from a simulated fire of carbon composites due to the crash of an aircraft that is fabricated from parts made of carbon fiber composites. It can also be used for military applications, e.g., to monitor carbon fiber release around the crash site of a military aircraft. In this case, higher portability of the detection system is needed and the system should be further miniaturized. The system can be modified and further developed for a number of special applications. Two examples are given below:

1) If the grid is made from high-temperature resistant materials, it can be used as an in-situ grid; i.e, it can be put into the fire of a carbon fiber composite. Information on total fiber release by a given carbon fiber source can thus be determined.

2) The system can be modified to detect submillimeter fiber fragments. Normally, fires of carbon fiber composite do release a large percentage of fiber fragments in this length range. In a composite fabrication location, due to machining processes, short fiber fragments will similarly be released in large quantities. These fibers possess much lower electrical resistance and higher mobility. Therefore they can pose a serious threat to microelectronics. There is indeed a need to further develop the system for detecting these short fiber fragments.

REFERENCES

1. "Carbon Fiber Risk Analysis," NASA Conference Publication 2074, an industry/government briefing held at Langley Research Center, Hampton, Virginia, October 31 - November 1, 1978.

2. "Carbon Fiber Hazard," NASA Conference Publication No. 2119, An industry/government briefing held at Langley Research Center, Hampton, December 4-5, 1979.

3. T. C. Babinsky and K. A. Musselman, "Burn/Blast Tests of Aircraft Structure Elements," NSWC/DL, TR-3897, December 1978.

4. J. A. Morrisey, W. I. Brannan and S. C. Thompson, "Calibration of BRL Ball and Sticky Cylinder Detector Systems," Technical Report, ARBRL-TR-02079, June 1978.

5. Samuel P. Feinstein and Michael A. Girard, "Feasibility Evaluation of an Image Processing Approach to Graphite Filament Counting," Jet Propulsion Laboratory, Internal Document, July 1979.

6. W. J. Cilwel, Jr. and R. H. Fish, "Small Scale Test for Fiber Released from Carbon Composite," NASA Ames Research Laboratory, TM-81179 (1979).

APPENDIX A

OPERATING PROCEDURES

The following operating procedures should be observed:

1) Beware of the exposed high voltage in the system, handle it with the precautions used for any high voltage device.

2) Check grid insulation by connecting a Simpson or other multimeter across the lead wires of the grid. On the x10,000Ω scale, the insulation resistance should be larger than 2 MΩ.

3) With all power off, assemble the prescreens in front of the grids. Use nylon straps to tie down the screen from the top Lucite insulation plate which has two holes for this purpose. Tape the edge of the screen with masking tape so that the grids are sealed behind the screen.

4) Verify that the lead wires of the grid are securely locked in the H.V. OUTPUT banana terminal on the H.V. discharge circuit.

5) Place the grid-windbox assemblies on a supporting platform with the grids facing perpendicular to the air flow.

6) Connect the H.V. lead wires from the H.V. power supply to the H.V. INPUT terminal on the H.V. Pulser. Make sure that the H.V. power supply is off before performing this procedure. It is preferable to place the H.V. power supply close to the grid-windboxes.

7) Connect a BNC Cable (RG58C) from the PULSE OUTPUT of the H.V. discharge circuit on the windbox to the SIGNAL INPUT on the pulse integrator. The length of the cable can be as long as 33 meters.

8) Connect the 40 VDC power supply to the DC INPUT terminal on the pulse integrator. (Power On-Off switch in the OFF position.)

9) Connect the DC signal (RECORD) on the pulse integrator to the recording system. The latter should have a range of 0 to -20 V.

10) Turn the ON-OFF switch to ON position. A clicking noise should be audible from the pulse integrator. This is due to the relay in the pulse integrator which automatically resets signals generated by transient response in the system. Wait for about half a minute, the noise should go away and normally the recorder should indicate a near zero reading.

11) If the recorder is not indicating zero, push the RESET button to achieve the zero reading.

12) If the discharge of the H.V. pulser is not actuated, the integrator will not receive any trigger signal, and the recorder should remain at its zero reading. The long-term zero drift recorded on the recorder should not exceed 0.1 V/hr.

13) In case the drift is large, uncover the button metal cap labelled ZERO. Using a small jewelers screwdriver, turn the miniature potentiometer and notice the improvement on the stability. Do it in 1/8 of a turn increments.

14) Connect the AC power cords of the fans in the grid-windbox assemblies to a Variac set at 50 V rms. A single Variac can be used for all fans. Verify that the fans are working.

15) A calibration of air flow speed can be performed at this point. Remove the metal cap on top of the windbox. Insert a Hastings-Raydist air flow probe into the box, and make sure that the sensing element of the probe is centered in the box (Figure 10). Read the flow speed on the readout console of the gauge. Also one should measure the background air flow speed outside the windbox as a reference.

16) Actuate the H.V. power supply. In this process, a few sparks could be generated in the grid due to some residual carbon fibers collected from the previous test that were not completely cleaned out.

17) A system check-out can be performed at this point. A carbon fiber brush is useful for the check-out. It can be made by attaching to one end of a 15 cm (6-in) wooden stick, a carbon fiber tow or bundle with pressure- sensitive tape. By inserting the brush into the prescreen and touching the grid electrodes, sparks will be generated. The recorder should register a negative voltage increase, indicating that the counting and integration circuits are working properly.

18) The system is then ready for live action. One may turn off the H.V. power supply and turn it on just prior to the live test.

19) Select a convenient chart speed on the recorder; the total counts will be recorded automatically, since the relay circuit in the pulse integrator will automatically reset the recorder for about every 100 counts.

20) After the test, turn off all power to the system. Disassemble the system in the reverse order of that described above.

21) Disassemble the grids from the windboxes by removing the nylon screws. Clean them by air jet, acetone or minor grit blasting as necessary.

22) Wipe clean the rest of the system with acetone or similar solvent.

23) Reassemble the grids onto the windboxes.

24) In case of emergency, the first step of system shutdown is to turn off all power switches. Discharge the H.V. pulser by touching the grid with the carbon fiber brush before disassembling and diagnosis.

APPENDIX B

A computer program has been developed to read in five sets of data, perform a set of calculations and plot the results. The program consists of five subroutines in addition to the main program and uses two in-house library routines. The main program is primarily a calling routine; only one calculation is performed in it.

The first routine called is named SETUP; it is called only once. This routine reads in the data and establishes the basic parameters. The first two arguments represent the dependent and independent variable arrays respectively and the last argument is the number of points in these arrays. The next routine called is BGNPLT. It initializes the plotter and must appear before the first call to PLT, the plotting routine. The next set of routines are always called together with the same arguments but may be called separately if desired. The first argument represents an array containing the values of the dependent variable and the second argument represents an array containing the values of the independent variable. The third argument represents the number of points to be plotted or printed, and the final argument is a flag for the titles. PLT uses many routines from the JPL library. CAL is the data reduction routine. The first argument of this subroutine is the array of raw data and the second is the array of reduced data. The final argument represents the total number of data points. A smoothing routine, SMTH, has been included to adjust the curves of the reduced data. The first and second arguments are the arrays containing the values of the dependent and independent variables respectively. The last argument represents the number of points in these variable arrays. The values of the independent and dependent variables are altered in the subroutine. SMTH uses an IMSL (International Mathematical and Statistical Libraries) routine called IQHSCU. This routine smooths the curves by using three points to fit a straight line. IQHSCU generates the coefficients for the straight lines through each point, and then values for the dependent variable may be determined for new values of the independent variable. The final subroutine called is ENDPLT; this routine closes the graphic package.

Several cards must follow the @MAP card prior to the @XQT in order to use the IMSL routine and the graphics routines. Each line starts in column one.

```
LIB LIB*IMSL$
LIB LIB*JPL$
CLASS P
LIB PLOT*PLOT, VECTOR*VECTOR, LIB*CLIB$
@SYM,P PUNCH$,,G9PLTL
```

Some of these cards may have to be changed for other systems.

The data cards must be organized in the following way. The first card sets the number of points read into the variable arrays. This card is formatted by I3. The maximum number of points that may be read is 61. The next three cards contain the alphanumerics for the data table titles and the plot titles. Each title may be up to 80 characters; the values in the first 18 columns of each title are used as the y-axis labels for the graphs. After the title cards come the values for the areas (m^2) and the wind speeds (m/s) for the five different grids. Only one card is necessary to describe each grid, totaling five cards. The area is always listed first and the format specification is E10.2, F5.2. The remaining cards contain the raw data for each of the five grids. The format specification is 10F8.1. If the number of points is greater than ten, the values may be continued on subsequent cards until the data set is complete.

```
@FOR,SI MAIN
FOR 810A=H  01/18/80  19108152  (=0)  MAIN

   MAIN PROGRAM

   STORAGE USED: CODE(1) 000144: DATA(0) 001735: BLANK COMMON(2) 000000

    COMMON BLOCKS:

    0003    A       000052
    0004    B       000012


   EXTERNAL REFERENCES (BLOCK, NAME)

    0005    SETUP
    0006    BGNPLT
    0007    OUT
    0010    PLT
    0011    CAL
    0012    SMTH
    0013    ENDPLT
    0014    NINTRS
    0015    NSTOPS


   STORAGE ASSIGNMENT  (BLOCK, TYPE, RELATIVE LOCATION, NAME)

    0001    000021 107G       0001    000025 112G       0004 R 000000 A          0000 R 001142 E          0000 I 001721 I
    0000 I 001722 J           0000 I 001720 NPT         0000 R 001623 T          0003 R 000000 TITLE      0004 R 000005 V
    0000 R 000000 Y           0000 R 000461 YN

77


00101      1*            DIMENSION Y(5,61),YN(5,61),E(5,61),T(61)
00103      2*            COMMON/A/ TITLE(42)
00104      3*            COMMON/B/ A(5),V(5)
00104      4*      C
00104      5*      C    THE MAXIMUM NUMBER OF DATA POINTS ALLOWED IS 61
00104      6*      C    INPUT CONSISTS OF THE FOLLOWING (FORMAT SPECIFICATION IS SHOWN IN
00104      7*      C    PARENTHESIS):
00104      8*      C         N  (I3) = THE NUMBER OF POINTS TO BE PLOTTED PER CURVE
00104      9*      C         A(J),V(J), J=1,5  (E10.2,F5.2) = TOTAL APERATURE, WIND SPEED
00104     10*      C         FOR A CHANNEL (J CORRESPONDS TO THE 5 DIFFERENT CHANNELS)
00104     11*      C         TITLE(J), J=1,42  (13A6,A2) = THE ALPHANUMERIC ARRAY CONTAINING
00104     12*      C         THE TITLES FOR THE GRAPHS.  EACH TITLE MAY HAVE UP TO AND
00104     13*      C         INCLUDING 80 CHARACTERS.  THE FIRST 18 CHARACTERS ARE USED AS
00104     14*      C         THE Y-AXIS LABEL.  THIS VARIABLE MUST BE ON 3 SEPARATE CARDS.
00104     15*      C         Y(I,J), J=1,N, I=1,5  (10F8.1) = THE NUMBER OF RAW COUNTS AT
00104     16*      C         SPECIFIC TIMES WHICH DEFINE A SEPARATE CURVE FOR EACH CHANNEL.
00104     17*      C         (HERE I CORRESPONDS TO THE 5 DIFFERENT CHANNELS).
00104     18*      C
00105     19*            CALL SETUP (Y,T,NPT)
00106     20*            DO 50 I=1,5
00111     21*                DO 40 J=1,NPT
00114     22*                    E(I,J) = Y(I,J)/(A(I)*V(I))
```

```
00115      23*          40     CONTINUE
00117      24*          50 CONTINUE
00121      25*             CALL BGNPLT
00122      26*             CALL OUT (Y,T,NPT,1)
00123      27*             CALL PLT (Y,T,NPT,1)
00124      28*             CALL OUT (E,T,NPT,15)
00125      29*             CALL PLT (E,T,NPT,15)
00126      30*             CALL CAL (E,YN,NPT)
00127      31*             CALL OUT (YN,T,NPT,29)
00130      32*             CALL PLT (YN,T,NPT,29)
00131      33*             IF (NPT.EQ.61) STOP
00133      34*             CALL SMTH (YN,T,NPT)
00134      35*             CALL OUT (YN,T,61,29)
00135      36*             CALL PLT (YN,T,61,29)
00136      37*             CALL ENDPLT
00137      38*             END

      END OF COMPILATION:        NO  DIAGNOSTICS.
CPU:.238   CTP:.028   SUPS:2.547
```

```
$FOR,SI SETUP
FOR $10A.M  01/18/80  19:06:55  (.0)  SETUP

   SUBROUTINE SETUP     ENTRY POINT 000126

   STORAGE USED: CODE(1) 000151; DATA(0) 000045; BLANK COMMON(2) 000000

    COMMON BLOCKS:

    0003   A       000052
    0004   B       000012

   EXTERNAL REFERENCES (BLOCK, NAME)

    0005   NRDUS
    0006   NIO2S
    0007   NIO1S
    0010   NERR3S

   STORAGE ASSIGNMENT  (BLOCK, TYPE, RELATIVE LOCATION, NAME)

    0000   000004 100F       0000   000005 110F       0001   000032 113G       0000   000007 120F       0001   000044 121G
    0000   000011 130F       0001   000064 131G       0001   000073 137G       0001   000100 143G       0000 I 000003 I
    0000   000021 INJPS      0000 I 000000 J          0000 I 000001 K          0003 R 00000C TITLE      0000 R 000002 XINC
    0004 R 000000 X2         0004 R 000005 X3

00101      1*            SUBROUTINE SETUP (X1,X4,N)
00103      2*            DIMENSION X1(5,61),X4(61)
00104      3*            COMMON/A/ TITLE(42)
00105      4*            COMMON/B/ X2(5),X3(5)
00106      5*            READ (5,100) N
00111      6*            READ (5,130) (TITLE(J),J=1,42)
00117      7*            READ (5,110) (X2(K),X3(K),K=1,5)
00126      8*            X4(1) = 0.
00127      9*            XINC = 60./(FLOAT(N) - 1.)
00130     10*            DO 30 I=2,N
00133     11*                X4(I) = X4(I-1) + XINC
00134     12*         30 CONTINUE
00136     13*            DO 50 I=1,5
00141     14*                READ (5,120) (X1(I,J),J=1,N)
00147     15*         50 CONTINUE
00151     16*            RETURN
00152     17*        100 FORMAT (I3)
00153     18*        110 FORMAT (E10.2,F5.2)
00154     19*        120 FORMAT (10F8.1)
00155     20*        130 FORMAT (13A6,A2)
00156     21*            END

      END OF COMPILATION:        NO  DIAGNOSTICS.
```

```
*FOR,SI CAL
FOR $10A.HB  01/18/80  19:08:57  (.0)  CAL

   SUBROUTINE CAL       ENTRY POINT 000045

   STORAGE USED: CODE(1) 000056: DATA(0) 000015: BLANK COMMON(2) 000000

   EXTERNAL REFERENCES (BLOCK, NAME)

    0003   .ERR3S

   STORAGE ASSIGNMENT  (BLOCK, TYPE, RELATIVE LOCATION, NAME)

    0001   000010 105G      0000   000003 INJP$     0000 I 000000 J



00101      1*            SUBROUTINE CAL (YOLD,YNEW,N)
00103      2*            DIMENSION YOLD(5,61),YNEW(5,61)
00104      3*            DO 50 J=1,N
00107      4*                YNEW(5,J) = YOLD(5,J)
00110      5*                YNEW(4,J) = YOLD(4,J) + YOLD(5,J)
00111      6*                YNEW(3,J) = YOLD(3,J) + YOLD(4,J)
00112      7*                YNEW(2,J) = YOLD(2,J) + YNEW(3,J) + 2.*YOLD(4,J)
00113      8*                YNEW(1,J) = YOLD(1,J) + YNEW(2,J) + 2.*YNEW(3,J)
00114      9*         50 CONTINUE
00116     10*            RETURN
00117     11*            END

      END OF COMPILATION:       NO  DIAGNOSTICS.
CPU:.180   CTP:.028   SUP:12.387
```

```
$FOR,SI SMTH
FOR B10A=M  01/18/80  19:09:00  (,0)  SMTH

   SUBROUTINE SMTH      ENTRY POINT 000226

   STORAGE USED: CODE(1) 000255 DATA(0) 000540 BLANK COMMON(2) 000000

   EXTERNAL REFERENCES (BLOCK, NAME)

    0003   IGMSCU
    0004   MERR3S

   STORAGE ASSIGNMENT  (BLOCK, TYPE, RELATIVE LOCATION, NAME)

    0001   000145 100L      0001   000032 105G      0001   000041 110G      0001   000077 123G      0001   000110 131G
    0001   000114 134G      0001   000175 160G      0001   000125 90L       0000 R 000000 C         0000 R 000467 D
    000C I 000461 I         0000 I 000465 IER       0000   000477 INJPS     0000 I 000462 J         0000 I 000466 K
    0000 I 000463 L         0000 I 000470 M         0000 I 000464 NDM       0000 R 000364 W         0000 R 000267 ZD


00101      1*            SUBROUTINE SMTH (YN,T,NPT)
00103      2*            DIMENSION YN(5,61),T(61),C(61,3),ZD(61),W(61)
00104      3*            DO 120 I=1,5
00107      4*                DO 60 J=1,NPT
00112      5*                    IF (YN(I,J).EQ.0.0) L = J
00114      6*                    ZD(J) = YN(I,J)
00115      7*          60    CONTINUE
00117      8*                NDM = NPT - L
00120      9*                CALL IGMSCU (T(L+1),ZD(L+1),NDM,C,61,IER)
00121     10*                W(1) = 0.0
00122     11*                DO 70 J=2,61
00125     12*                    W(J) = W(J-1) + 1.0
00126     13*          70    CONTINUE
00130     14*                DO 110 K=1,60
00133     15*                    DO 80 J=1,NPT
00136     16*                        IF (W(K).LT.T(J)) GO TO 90
00140     17*          80        CONTINUE
00142     18*          90        J = J - 1
00143     19*                    C = W(K) - T(J)
00144     20*                    M = J - L
00145     21*                    IF (M.GT.0) GO TO 100
00147     22*                    C = 0.0
00150     23*                    M = 1
00151     24*         100        YN(I,K) = ((C(M,3)*D + C(M,2))*D + C(M,1))*D + ZD(J)
00152     25*         110    CONTINUE
00154     26*                YN(I,61) = ZD(NPT)
00155     27*         120 CONTINUE
00157     28*                DO 130 J=1,61
00162     29*                    T(J) = W(J)
00163     30*         130 CONTINUE
00165     31*                RETURN
```

```
00166      32*            END

       END OF COMPILATION:        NO  DIAGNOSTICS.
CPU:1.387    CTP:1.028   SUPS:2.032
```

```
@FOR,SI PLT
FOR 810A-HN  01/18/80  19:09:04  (.0)  PLT

   SUBROUTINE PLT       ENTRY POINT 000217

   STORAGE USED: CODE(1) 000241; DATA(0) 000157; BLANK COMMON(2) 000000

    COMMON BLOCKS:

    0003   A       000052
    0004   PLOTER  000003

   EXTERNAL REFERENCES (BLOCK, NAME)

    0005   PLFORM
    0006   PLSCAL
    0007   PLABEL
    0010   PLGRAF
    0011   PLCURV
    0012   PLTEXT
    0013   ADVPLT
    0014   NERR38

   STORAGE ASSIGNMENT  (BLOCK, TYPE, RELATIVE LOCATION, NAME)

    0001   000044 110G      0001   000060 117G      0000 I 000076 I         0000   000141 INJPS     0000 I 000077 J
    0000 I 000075 N         0004 R 000000 PEN       0003 R 000000 TITLE     0000 R 0001CC M         0004 R 000001 NHERE
    0000 R 000000 Z


00101      1*           SUBROUTINE PLT (Y,X,M,K)
00103      2*           DIMENSION Y(5,61),X(61),Z(61)
00104      3*           COMMON/A/ TITLE(42)
00105      4*           COMMON/PLOTER/PEN,NHERE(2)
00106      5*           CALL PLFORM ('LINLIN',10.,8.)
00107      6*           N = 5*M
00110      7*           CALL PLSCAL (X,M,2,Y,N,2)
00111      8*           CALL PLABEL (TITLE(K),80,'TIME (MIN)',10,TITLE(K),18)
00112      9*           CALL PLGRAF
00113     10*           DO 50 I=1,5
00116     11*               DO 40 J=1,M
00121     12*                   Z(J) = Y(I,J)
00122     13*        40     CONTINUE
00124     14*               CALL PLCURV (X,Z,M,0,'*')
00125     15*               M = NHERE(2) + 0.05
00126     16*               IF (I.EQ.1) CALL PLTEXT (9.0,M,.08,0.,'NO. 1',5,1)
00130     17*               IF (I.EQ.2) CALL PLTEXT (9.0,M,.08,0.,'NO. 2',5,1)
00132     18*               IF (I.EQ.3) CALL PLTEXT (9.0,M,.08,0.,'NO. 3',5,1)
00134     19*               IF (I.EQ.4) CALL PLTEXT (9.0,M,.08,0.,'NO. 4',5,1)
00136     20*               IF (I.EQ.5) CALL PLTEXT (9.0,M,.08,0.,'NO. 5',5,1)
00140     21*        50 CONTINUE
```

```
00142      22*            CALL ADVPLT
00143      23*            RETURN
00144      24*            END

      END OF COMPILATION:        NO  DIAGNOSTICS.
CPU1.293   CTP1.028   SUPS12.571
```

```
$FOR,SI OUT
FOR 810A** 01/18/80  19:09:06  (,0)  OUT

   SUBROUTINE OUT       ENTRY POINT 000122

   STORAGE USED: CODE(1) 000137: DATA(0) 000106: BLANK COMMON(2) 000000

    COMMON BLOCKS:

    0003   A       000052
    0004   B       000012

   EXTERNAL REFERENCES (BLOCK, NAME)

    0005   ^^DUS
    0006   ^IO2S
    0007   ^IO1S
    0010   ^ERR3S

   STORAGE ASSIGNMENT  (BLOCK, TYPE, RELATIVE LOCATION, NAME)

    0000   000004 100F      0000   000026 110F      0001   000034 115G      0000   000034 120F      0001   000055 125G
    0000   000037 130F      0001   000072 134G      0000   000060 140F      0001   000100 141G      0004 R 000000 A
    0000 I 000001 I         0000   000067 INJPS     0000 I 000003 J         0000 I 000002 M         0000 I 000000 N
    0004 R 000005 V         0003 R 000000 XLABEL


00101      1*            SUBROUTINE OUT (Y,T,M,L)
00103      2*            DIMENSION Y(5,61),T(61)
00104      3*            COMMON/A/ XLABEL(42)
00105      4*            COMMON/B/ A(5),V(5)
00106      5*            N = L + 2
00107      6*            IF (L.EQ.1) WRITE(6,130)
00112      7*            IF (L.EQ.1) WRITE(6,140) (I,A(I),V(I),I=1,5)
00123      8*            WRITE (6,120) (XLABEL(K),K=L,N)
00131      9*            WRITE (6,100)
00133     10*            DO 50 J=1,M
00136     11*                WRITE (6,110) T(J),(Y(I,J),I=1,5)
00145     12*         50 CONTINUE
00147     13*            RETURN
00150     14*        100 FORMAT (2ex,'TIME',12x,'Y(1,J)', 9x,'Y(2,J)', 9x,'Y(3,J)', 9x,
00150     15*           $        'Y(4,J)', 9x,'Y(5,J)',/,26x,'(MIN)',/,/)
00151     16*        110 FORMAT (2ex,F5.1,FX,1PE10.3,4(5x,E10.3))
00152     17*        120 FORMAT (1H1,35x,3A6,/,/)
00153     18*        130 FORMAT (1H1,25(/),45x,'CHANNEL NO.',5x,'APENATURE',5x,
00153     19*           $        'WIND SPEED',/,63x,'(M**2)',10x,'(M/S)',/,/)
00154     20*        140 FORMAT (49x,I2,10x,1PE8.2,8x,0PF5.2)
00155     21*            END

      END OF COMPILATION:        NO  DIAGNOSTICS.
```